Summer 2017

# COMPARING DISTRIBUTED ACOUSTIC SENSING TO THREE-COMPONENT GEOPHONES IN AN UNDERGROUND MINE

Nikolas Nesladek
*Montana Tech*

# COMPARING DISTRIBUTED ACOUSTIC SENSING TO THREE-COMPONENT GEOPHONES IN AN UNDERGROUND MINE

by

Nikolas Nesladek

A thesis submitted in partial fulfillment of the
requirements for the degree of

Master of Science in Geoscience: Geophysical Engineering

Montana Tech

2017

## Abstract

Geophones have become the industry standard for seismic data collection. However, a relatively new method is gaining popularity called Distributed Acoustic Sensing (DAS). DAS uses changes in backscattered light of a fiber-optic cable to detect strain from acoustic energy. The purpose of this project was to make a direct comparison between DAS and three component geophones, specifically in a mining setting. Experiments were done in the Underground Education Mining Center on the campus of Montana Tech. The sources used for this project were vertical sledgehammer shots, oriented shear sledgehammer shots, and blasting caps set off in both unstemmed and stemmed drillholes. Although the explosives performed the best for the geophones, the large amount of energy and its close distance from the fiber seemed to compromise the entire fiber loop. In a one to one comparison, the underground hammer shots seemed to produce data that was a rough match between the DAS traces and the geophone traces. However, the shots on the surface of the mine, specifically the shots oriented inline with the cable, seemed be close to an exact match between trace of the fiber and traces of the geophones. The data suggest that DAS is most useful when the fiber can be oriented in the same direction as particle motion from whatever source is used, whereas the three component geophones can accurately capture data from all sources.

Keywords: Geophones, Distributed Acoustic Sensing, DAS, Mining

## Dedication

I wish to dedicate this project to my family for their continued support throughout my academic career.

## Acknowledgements

I would like to thank my adviser, Marvin Speece, for all of his help and guidance throughout this entire project.

I thank my entire thesis committee of Mary MacLaughlin, Scott Rosenthal, and Khalid Miah for taking time out of their schedules to work with me.

I also need to thank my fellow graduate students, Calvin Kammerer, Brad Rutherford, and Akpofure Orubu for lending a hand during our many mine trips. Thank you as well to the Senior Design Team for their original work in this mine.

I would like to thank Thomas Coleman and Silixa for all their help operating the DAS system and provided help with data processing.

I would like to thank Neal Lord, Herb Wang, and Pete Swanson for helping with the many questions I had for them.

Funding for this project was provided by NIOSH Contract : CDC – NIOSH – OFFICE OF MINE SAFETY AND HEALTH RESEARCH Contract Number 211-2014-59580. Project Title: Demonstration of the Ability of Distributed Fiber Optic Sensing Technologies to Enhance Mine Safety through Distributed Monitoring of Ground Deformation, Temperature, & Dynamic Events.

# Table of Contents

## List of Tables

## List of Figures

## List of Equations

# 1. Introduction

The most common instruments currently used to gather elastic data in industry are geophones. Geophones work by having a mass on a spring inside a coil of wire. When elastic energy interacts with the geophone, the mass moves and produces a voltage in the wire that can be recorded. For a given survey, an array of geophones is set up to gather information at various locations. In order to improve the quality of data for a survey and increase the amount of interpretation that can be done, geophones can be manufactured to record three components. Three components can be oriented in any desired direction, but are most often oriented to record vertical, North-South, and East-West data.

While three component geophones have improved the quality of seismic data recording, a new method using fiber-optic cables has been introduced to gather seismic data. The method of using fiber-optic cables to record acoustic data is called Distributed Acoustic Sensing (DAS). While this method is relatively new to the field of geophysics, the method has the potential to provide better real time monitoring of areas of geologic interest. In order to record acoustic energy, DAS equipment sends pulses of light down a strand of fiber-optic cable. Light is continuously backscattered throughout the cable, and strain in the cable will cause a change in the backscattered light (Cannon and Aminzadeh, 2013). Certain companies have methods of processing this backscattered light to observe the strain rate at different locations along the cable at given time steps. Most of these processing methods are kept proprietary due to the relative young age of the method. For this project, we worked with Silixa, a company that specializes in distributed sensing using fiber optics.

The purpose of this experiment was to make a direct comparison between three component geophones and DAS in a mining setting. All sources in this project were triggered

sources, such as a swing of a hammer or explosive blasts using blasting caps and boosters. We collected all of the data for this study at the Underground Mining Education Center (UMEC), an educational facility on campus at Montana Tech.

The objective of this study was to make a direct comparison of data collected using three component geophones with data collected using DAS. All geophones were three-component Geospace 20DM geophones. For the DAS data, fiber-optic cables manufactured by Brugg and Optical Cable Corporation were used. I compared the performance of cables to each other to see if significant difference exists between types of cables. I used a variety of sources in order to determine if different sources affected the data. Another objective was to see if DAS would be a suitable method to monitor activity in a mining setting.

# 2. Previous Work

## 2.1. Previous Related Work in the UMEC

Montana Tech undergraduate students performed an initial study to test the effectiveness of geophones in the UMEC facility as part of a senior design project. This study determined the best method for installing geophones in the UMEC. The senior design team tested a metal bracket mount for geophones; however, the resonant frequency of the metal mount dominated the data. The conclusion of the design report was that the most effective method of geophone mounting was to drill a hole in the rock face, and secure the geophones inside the hole using Plaster of Paris.

As part of the report, the students gathered several rock samples in order to determine acoustic velocities of the geology in the mine. The senior design team first used cores from the mine to test the velocity of the samples in a lab setting. They drilled ten sample cores and used an Ult-100 to test the P- and S-wave velocities of the samples. The Ult-100 is a device that sends compressional or shear waves through a sample between two metal plates placed adjacent to the ends of the sample, to determine the velocities of a sample. The laboratory tests were used to find average P- and S-wave velocity values of weathered and unweathered samples. The students also used data from the geophone testing as a second way to determine the velocity of the rock in the mine. The team picked first break times of P- and S-waves from the hammer and weight drop test shots conducted at different locations, and used the data to determine the P- and S-wave velocity of the in-situ rock. The velocity values are seen in Table I.

**Table I: Senior Design Velocity Values**

| Sample | P Velocity (m/s) | S Velocity (m/s) |
|---|---|---|
| Laboratory Weathered Samples | 2137 ± 417 | 1358 ± 246 |
| Laboratory Unweathered Samples | 4189 ± 234 | 2524 ± 247 |
| Sledgehammer First Break Data | 2088 ± 399 | N/A |
| Vertical Weight Drop First Break Data | 1145 ± 70 | N/A |
| North-South Weight Drop First Break Data | N/A | 585 ± 23 |
| East-West Weight Drop First Break Data | N/A | 659 ± 28 |

The sledgehammer first break data used a standard sledgehammer to strike a metal plate on the ground. The Vertical weight drop used a 45 kg accelerated weight drop on a steel plate. The North-South Weight Drop used a 45 kg accelerated weight drop in S-wave mode, with the source oriented in the North-South direction. The East-West weight drop used a 45 kg accelerated weight drop in S-wave mode, with the source oriented in the East-West direction.

A conclusion of the senior design report was that the geophones in the mine could accurately determine a P-wave velocity that was comparable to laboratory values. The S-waves measured using the geophones were slightly lower in comparison to the laboratory values, which could be due to the location and size of the rock samples. The geophone data also showed a difference in North-South and East-West S-wave values. The difference in S-wave velocities could suggest anisotropy in the area, which could be due to the East-West oriented fracture sets or ore veins in the mine.

## 2.2. Previous DAS Field Work

Work has been done to compare geophones with DAS in different settings. One example compared borehole seismic data using geophones to DAS (Daley et al., 2013). Three boreholes were tested, and the study determined that while DAS did seem to accurately capture most of the seismic data. However, DAS had lower sensitivity in comparison to the geophones. One of the large advantages found in this study was that the DAS system could be deployed permanently for continued data collection. DAS has been shown to be able to provide long term, repeatable

results when placed in a proper coupling system (Hornby, 2004). Having the fiber-optic cable well coupled to the area of interest is extremely important in order to produce high quality data. A study that tested different types of coupling methods showed that DAS was extremely sensitive to noise when the coupling of the fiber-optic cable was poor (Hornby, 2004).

An area where DAS excels is Vertical Seismic Profiling (VSP). This method is used in oil production to monitor wells. A fiber-optic cable is cemented in a borehole, and can provide real-time updates on the production of the well. DAS is thought to be simpler than geophones for a VSP because an entire well can be covered in one shot (Mestayer, 2011). For a VSP survey using geophones, often an array of geophones covers a small portion of the borehole, and the entire survey is taken in multiple shots as the array is moved to different depths in the borehole. However, using DAS, a length of fiber-optic cable can cover the entire borehole, which allows a single shot to provide data for the entire borehole. DAS has also been used in VSP surveys in a marine environment. In 2012, DAS was used to collect 3D VSP data in two wells in the Gulf of Mexico (Wu, 2015). The study showed that DAS VSP data could be used to produce high quality 3D images of deepwater reservoirs. The study showed one of the reasons DAS excels is due to the large number of evenly sampled shots present in a DAS survey. The data collected using DAS allowed for clear first break picking and accurate data for reservoir modeling. DAS can be used in conjunction with current VSP survey techniques in order to quality control or optimize surveys in real time (Barfoot, 2013).

In the fall of 2012, field tests were performed in Manitoba, Canada, to compare DAS to surface-placed as well as trenched geophones. In this test, both methods were able to show clear reflection and refraction of waves (Kendall, 2014). However, an area of difficulty for this study was separating different modes of the wave based on particle motion. The study used event

velocities to stack data rather than using particle velocities. They determined that not being able to differentiate different elastic modes in datasets led to comparable, but not identical, data sections between geophones and fiber-optic cable.

DAS has also seen use outside of exploration geophysics. Since fiber-optic cable can be deployed over a large area, DAS has been used for perimeter security detection, as well as intrusion detection (Liu, 2016). DAS can also be used to detect pipeline leaks (Tanimola, 2009). Detecting leaks in a pipeline is an example of DAS being used for continuous monitoring rather than a triggered exploration survey. DAS has been used for continuous pipeline health monitoring, including the monitoring of small pieces like specific nozzles of a larger pipeline (Carpenter, 2017). Real-time imaging has also been done using DAS in order to image near-surface geology, as well as monitor vehicle traffic over a large amount of time (Lancelle, 2016). DAS has the potential for constant monitoring over large areas with relatively low cost.

## 3. Distributed Acoustic Sensing Theory

Distributed acoustic sensing is a method that uses a fiber-optic cable as a sensor for seismic data. In order to record seismic data, DAS sends a pulse of light into the optical fiber that scatters in the glass fiber within the cable. Acoustic signal deforms the fiber and causes the pulse of light to change, which is monitored by a recording device. The basic concept of DAS can be seen in Figure 1. The recording device used by Silixa uses the scattered light to determine changes in axial strain in line with the fiber. The recording device is able to use the arrival time of the scattered light to determine the location of strain along the fiber. The system fires pulses throughout the survey to generate a time record of strain for a given survey (Parker, 2014).

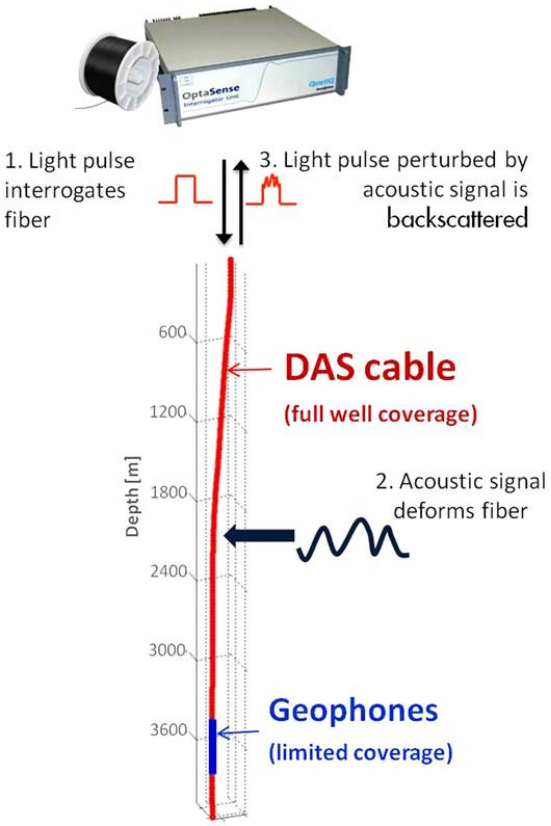


**Figure 1: Basic concept of DAS**. Light pulses are sent down the fiber. When the fiber is deformed by acoustic signal, the light pulse is perturbed and backscattered, which can be monitored by a recording device (Mateeva, 2012).

A cable must be calibrated in order to serve as a recording device for any survey. The backscattering of light in a fiber is random; however, the backscatter will be constant if the fiber is not under any strain. The difference in backscattering when the fiber is not under strain and when it is under strain during a survey is used to determine the acoustic signal (Poczesny, 2011). The distributed term in the name of the method comes from the fact that measurements are distributed over some distance. Backscattered signal has a nonlinear transfer function, which means the output cannot be easily related to the input. A nonlinear transfer function is not useful for seismic applications because the difference between the input and output signal is important for determining subsurface characteristics. Instead, the phase difference in backscattered light is taken between two points. Using the difference between two physical points allows the data to be better suited for seismic surveys. The term for the distance between the points used in a survey is the gauge length (Dean, 2016). Gauge length is determined by the distance between the Gaussian envelope of the laser pulse, shown in Figure 2.

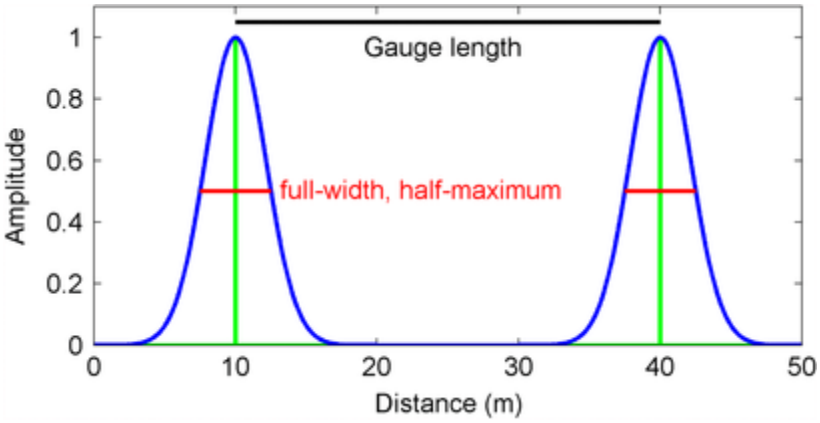


**Figure 2: The relationship between the pulsewidth of the laser and the gauge length (Dean, 2016).** The full-width half maximum is shown to demonstrate the laser pulses are Gaussian, with the red line being at half of the maximum amplitude.

The gauge length operates similar to a moving average filter. For example, the gauge length could be 10 meters, but the station spacing could still be 1 meter by overlapping gauge

length between data points. Smaller gauge length leads to better resolution due to less overlap between data points; however, if the gauge length is too small, the signal to noise ratio will be negatively affected (Dean, 2016). For a given survey, the gauge length is constant across the entire fiber, and is not affected by source and receiver distance.

The changes in the light pulses for DAS occur when the fiber stretches or compresses. The glass fiber inside of the cable is straight and rigid, which is one of the reasons DAS is not sensitive to broadside compressional waves. Instead, DAS records data from waves where the particle motion is inline with the fiber. A solution used in field tests has been to wrap a cable helically around an area of interest, in order to record data from waves of all orientations (Kuvshinov, 2016). The introduction of a helically wrapped cable allows for better collection of data, but adds complexity due to the changing direction of the fiber. In addition, along with direction of the fiber, better coupling between the fiber and the target improves the quality of data recorded (Castongia, 2017).

The data collected by DAS is in terms of a localized strain rate, localized over one gauge length. The final data are reported as the strain rate at some desired spacing. However, geophones do not record a strain rate. Instead, they record a voltage in the coil of wire, which is proportional to particle velocity. In order to compare these two methods, the strain rate of the fiber can be converted to strain (Daley et al., 2015). A study by Stanford University researchers showed that once strain rate is converted to strain, the data are proportional to particle velocity (Feigl, 2017). With the strain of the fiber and the voltage of the geophone both being proportional to particle velocity, a one to one comparison can be made between the two methods. Although the amplitude of fiber strain and geophone voltage will be different, the two methods will be in phase and can be used to make time picks for a dataset.

# 4. Experimental Design and Data Collection

## 4.1. UMEC Geology

All data for the comparison between DAS and geophones were collected in the UMEC during November 2016. Although the UMEC was previously an active mine, referred to as the Orphan Boy mine, it is now a controlled environment used for mining education purposes. The minerals mined out of this area were lead, zinc and silver. The geology of this area consists of primarily granite rock that is slightly weathered, or grade II weathering (Rose, 2017). A weathering grade of II indicates that small fractures exist in the rock, but the rock is mostly intact. The rock may have microfissures that are spaced more than one cm apart with tightly bonded grain boundaries (Goodman, 1993). Although the average weathering in the mine is grade II, some zones of extreme weathering are present. In addition, many of the old mining tunnels have collapsed near the area of study for this project.

Geophones and fiber-optic cable were placed around the pillar highlighted in Figure 3, which consisted of solid granite with few fractures. The pillar area is roughly 30 m below the ground surface. Two boreholes were drilled through the pillar to place fiber-optic cables. No geophones were placed in the boreholes. Geophones and fiber-optic cables were placed in a loop around the pillar, as well as in a triangular loop on the ground surface almost directly above the pillar area.

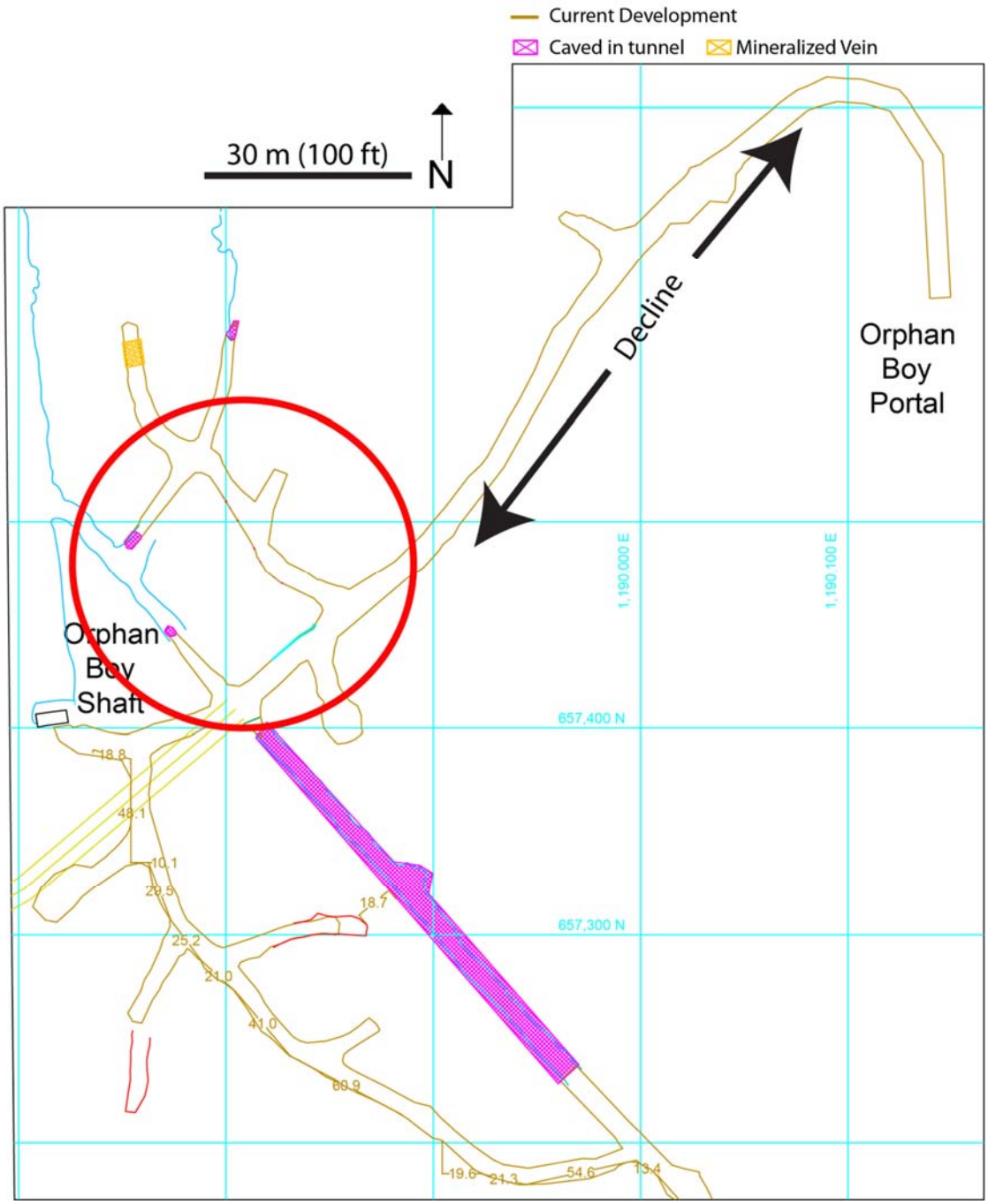


**Figure 3: Map view of UMEC facility**. The red circle highlights the pillar of the mineshaft, which served as the area of interest for this study. From the entrance of the mine at the Orphan Boy Portal, the passageway descends roughly 30 meters to the area of interest (called Decline on the figure).The pink hatching highlights collapsed areas of the mine.

## 4.2. Survey Layout

For this survey, we used geophones both in the mine and on the ground surface. Figures 4 and 5 show the layout of the geophones. We placed 19 geophones underground at a depth of approximately 30 m, and 21 geophones on the surface.

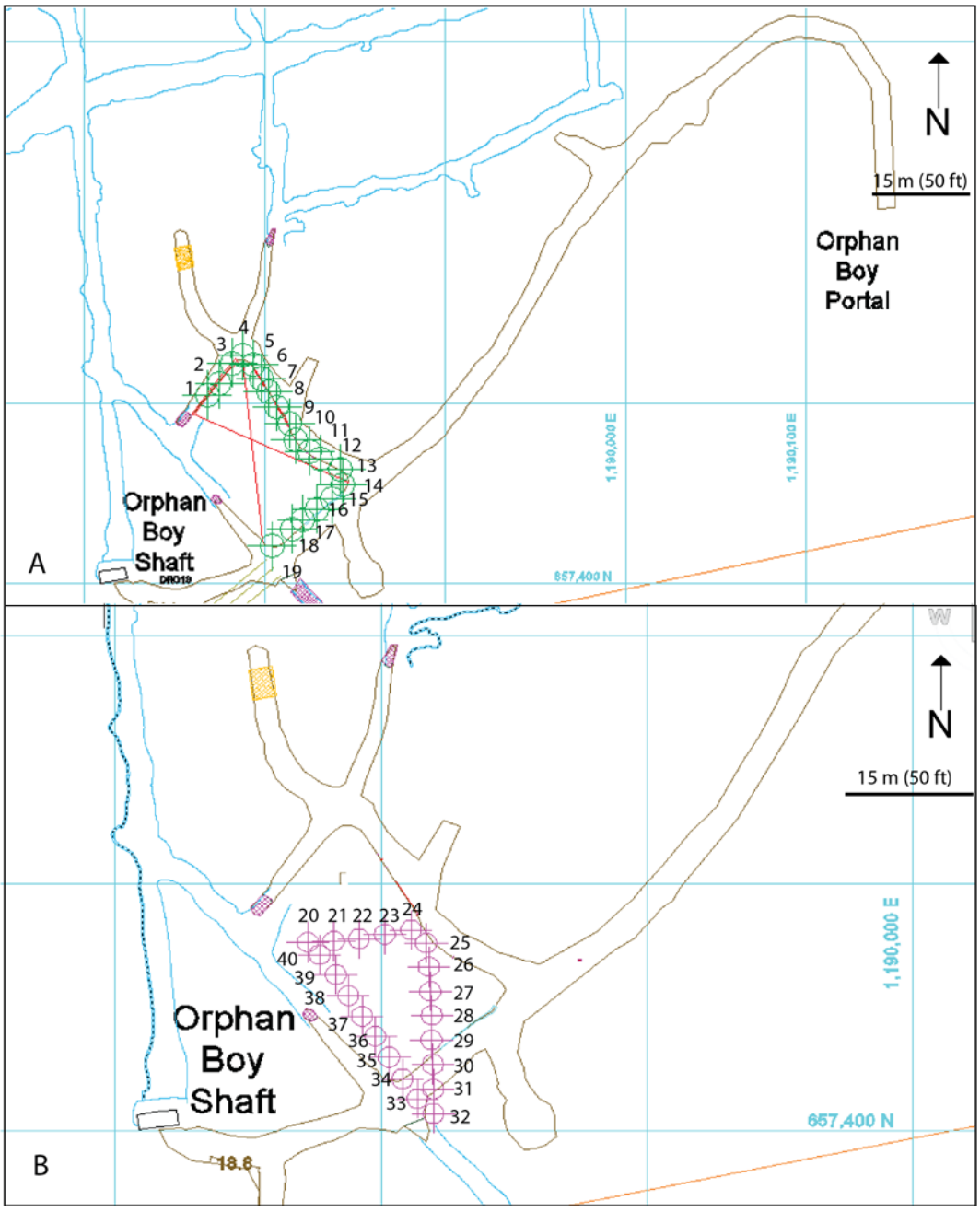


**Figure 4: Plan view of geophone layout.** (A) shows the underground geophones at a depth of approximately 30 m and (B) shows the surface geophones. The station labels that were used during the survey are displayed for all geophones.

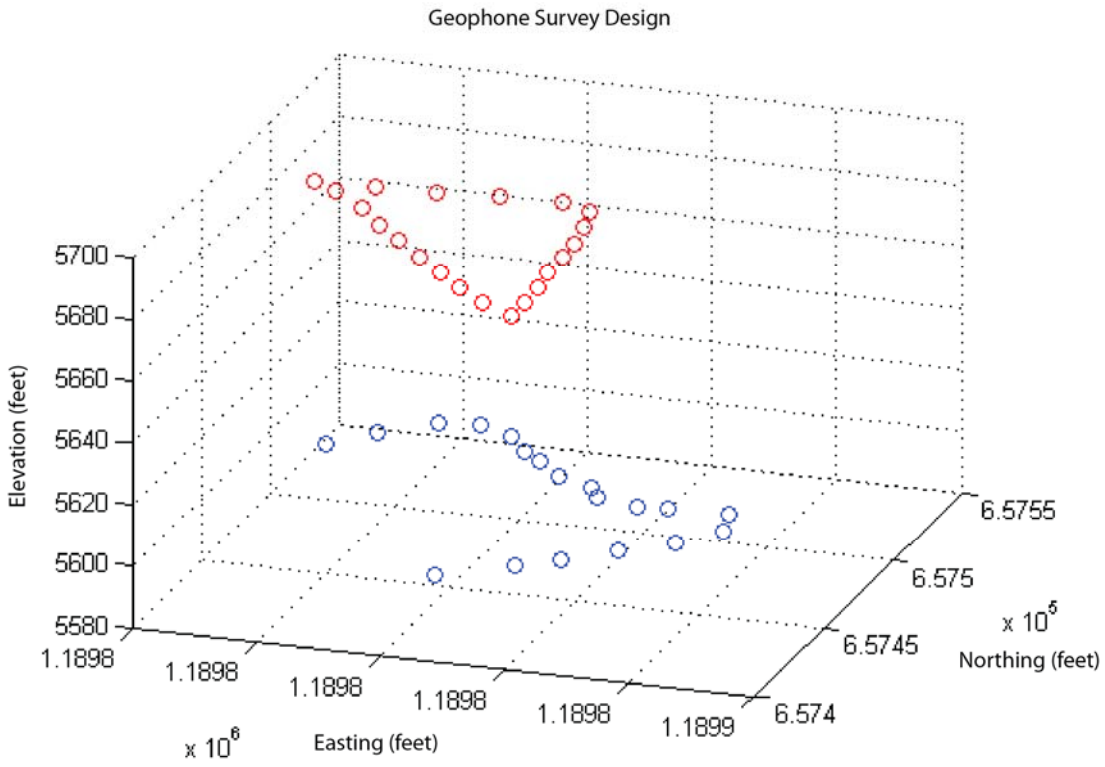


**Figure 5: Three-dimensional view of the station locations for the geophones**. The red points are geophone locations on the surface of the mine, and the blue points are the locations of geophones that are secured to the pillar inside of the mine.

We also had a single loop of fiber on the surface in the same location as the geophones. Geological engineering graduate student Calvin Kammerer dug a roughly 0.5 m deep trench on the surface in the shape of a triangle. The East-West side was 12 m long, the North-South side was 21 m long, and the third diagonal side was 27 m long. The surface loop path can be seen in Figure 6. Although the geophone stations on the surface were numbered 20 to 40 in a clockwise direction, the fiber optic cables in the surface loop were connected such that they followed a counterclockwise path. Consequently, in the dataset, the traces associated with the stations are found in reverse numerical order (ie, station 20 is associated with trace 306 and station 40 is associated with trace 246). Inside of the mine, a Brugg temperature cable, a Brugg strain cable,

and an OCC strain cable were wrapped around the pillar in the configuration seen in Figure 7. For the loops of cables in the mine, UMEC personnel drilled two boreholes diagonally through the pillar. The Brugg temperature and OCC strain cables followed a loop that went from the control room to borehole 1, through borehole 1 from Northeast to Southwest, around the pillar in a counter-clockwise path, through borehole 2 from Northwest to Southeast, and back to the control room. The ends of the Brugg strain cable were reversed when they were hooked up, so the Brugg strain cable went from the control room to borehole 2, through borehole 2 from Southeast to Northwest, around the pillar in a clockwise motion, through borehole 1 from Southwest to Northeast, and back to the control room.


**Figure 6: Surface image showing the path of the fiber on the surface**. The red line shows where the fiber-optic cable came out and back in to the mineshaft. The cable was not buried on the red path. The blue arrows show the path of the buried cable. The blue triangle is in the same location as the surface geophones, seen in Figure 4b.

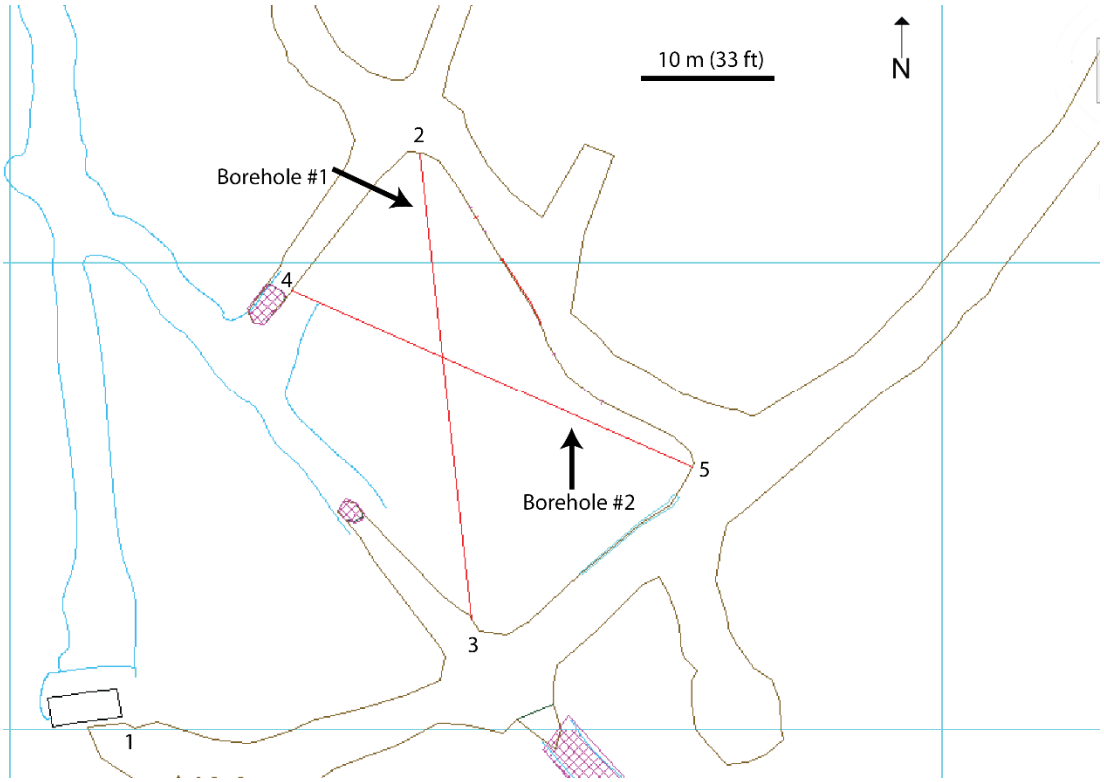


**Figure 7: Map of the underground cable network**. The Brugg temperature cable had a lead in cable from point 1 to point 2, then went through borehole 1 and came out at point 3. The cable then wrapped around the pillar and entered borehole 2 at point 4 and exited at point 5 and returned to the control room. The OCC strain cable followed the same path, and the Brugg strain cable followed the path in reverse order.

## 4.3 Geophones

All geophones used for this study were Geospace 20DM three-component geophones. The 20DM geophone has a natural frequency of 40 Hz and resistance of 720 Ohm. For the subsurface geophone placement, we drilled a hole in the face of the pillar, and secured the geophones to the rock using Plaster of Paris, which is shown in Figure 8a. The Plaster of Paris was used to increase the coupling to the rock and improve signal to noise ratio. We used 19 geophones underground, and secured all of them using this method. We placed 21 geophones on the surface 30 m above the pillar. The spacing for the geophones was three meters, both above and below the surface. We secured the surface geophones by pressing a 10 cm spike in the dirt on the surface to improve their coupling, seen in Figure 8b.

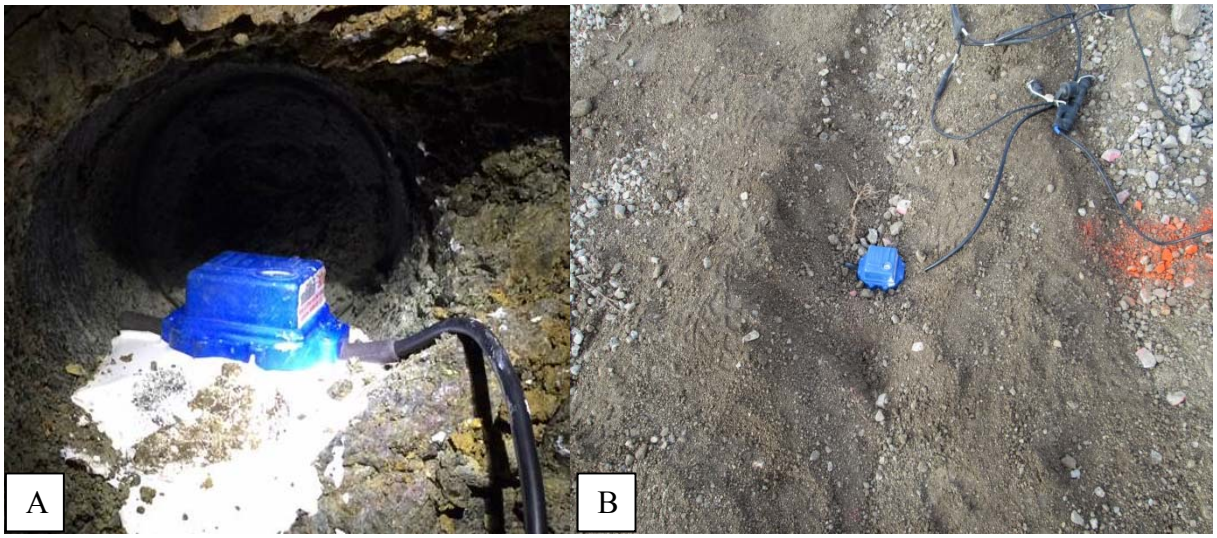


**Figure 8: Mounting of subsurface and surface geophones.**
(A) Geophone mounted inside of a drilled hole using plaster of Paris.
(B) Geophone with spike secured into the dirt on the ground surface.

## 4.4 Fiber-Optic Cables

Table 2 shows field measurements for the different lengths of cable to locations seen in Figure 7. The path around the pillar was roughly 200 m. The gaps between cables came from extra cable or connections that had to be added to the system. Although we used four cables total, they were all connected to the same recording device to form one continuous loop that covered roughly 1500 m. An example of a full shot record can be seen in Figure 9. We used the measurements in Table II to parse out individual cables from the full shot.

**Table II: Cable Distances**

| Cable Distance (m) | Cable Type | Coupling Notes |
|---|---|---|
| 0-205 | Brugg Strain | From control room up escape shaft |
| 205-245 | Brugg Strain | On surface, not buried |
| 245-305 | Brugg Strain | Surface loop, buried |
| 305-340 | Brugg Strain | On surface, not buried |
| 340-405 | Brugg Strain | Down escape shaft, extra cable |
| 405-415 | Corning lead in cable | Control room to pillar, uncoupled |
| 415-475 | Corning lead in cable | Uncoupled along the pillar |
| 475-505 | Brugg Temp | Borehole #1 |
| 505-550 | Brugg Temp | Poor/Uncoupled |
| 550-560 | Brugg Temp | Tightly coupled, Northwest wall |
| 560-590 | Brugg Temp | Borehole #2 |
| 590-650 | Corning lead in cable | Uncoupled, returning to control room |
| 650-865 | Corning lead in cable | Extra cable |
| 865-885 | OCC Strain | Control room to start of pillar |
| 885-935 | OCC Strain | Wrap around pillar counter clockwise |
| 935-965 | OCC Strain | Borehole #1 |
| 965-995 | OCC Strain | Wrap around pillar counter clockwise |
| 995-1025 | OCC Strain | Borehole #2 |
| 1025-1035 | OCC Strain | Tightly coupled, Northwest wall |
| 1035-1110 | OCC Strain | Final wrap around pillar, uncoupled |
| 1110-1200 | OCC Strain | Extra cable |
| 1200-1220 | Brugg Strain | Control room to pillar, uncoupled |
| 1220-1245 | Brugg Strain | Tightly coupled |
| 1245-1275 | Brugg Strain | Borehole #2 |
| 1275-1285 | Brugg Strain | Tightly coupled, Northwest wall |
| 1285-1335 | Brugg Strain | Uncoupled |
| 1335-1365 | Brugg Strain | Borehole #1 |
| 1365-1500 | Brugg Strain | Final wrap around pillar and back to control room/ extra cable |

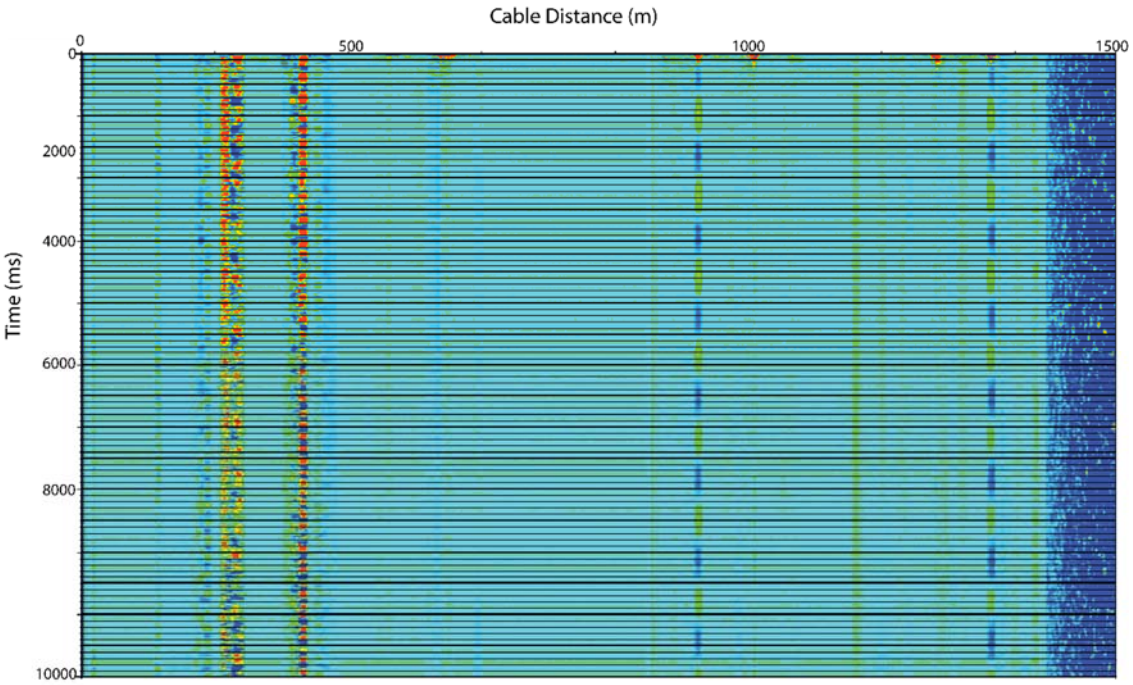


**Figure 9: An example of a full shot record of the DAS data**. All recordings were 10 s long on the y-axis. Although we only used 1500 m of fiber-optic cable, all shots recorded 1552 m to account for any discrepancies in measurement. Silixa adds padding to the beginning and end of the data to ensure the entire fiber is captured.

We secured the fiber-optic cable to the wall of the mine with epoxy and grout on certain areas of the pillar. Figure 10 highlights areas where the cable was securely coupled to the wall. Other areas did not allow for coupling to the wall, and the cable was pressed up against the wall as best as possible in these areas. Some segments of cable, the temperature cable in particular, were left intentionally uncoupled. An example of the cable on the wall of the mine can be seen in Figure 11. This coupling difference is evident in the data, with the poorly coupled areas having a much weaker signal.

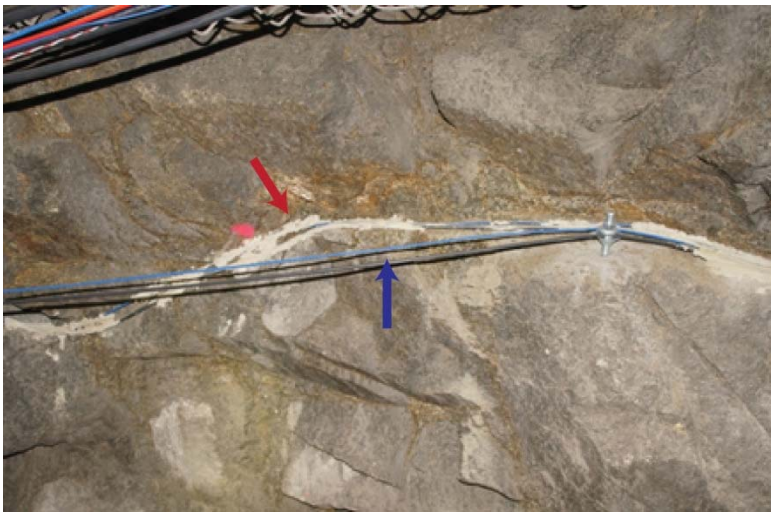

**Figure 10: An example of how the Brugg strain cable was secured to the wall of the mine using epoxy or grout.** The red arrow indicates fiber that is well coupled. The return path of the Brugg strain cable is seen that is uncoupled, highlighted with a blue arrow.

Inside of the borehole, we used a spacer to ensure the cables stayed in place inside of the borehole. We used two types of spacers: a spacer in which the cable was on the inside of the spacer, and a spacer where the cable was on the outside, pushed against the rock forming the side of the borehole. The spacers can be seen in Figures 11 and 12. The outer spacer was designed to have grooves sized for each of the cables. The purpose of the outer spacer was to tightly press the cable against the wall of the borehole and provide tight coupling between the cable and the rock. For the inner spacer, cables were zip tied to the spacer to separate them, but they were embedded in the grout filling the borehole and not in direct contact with the rock. Inside of borehole 1, the outer spacer was used for the entire borehole. For borehole 2, the outer spacer was used for the Southeast half of the borehole and the inner spacer was used for the Northwest half of the borehole.

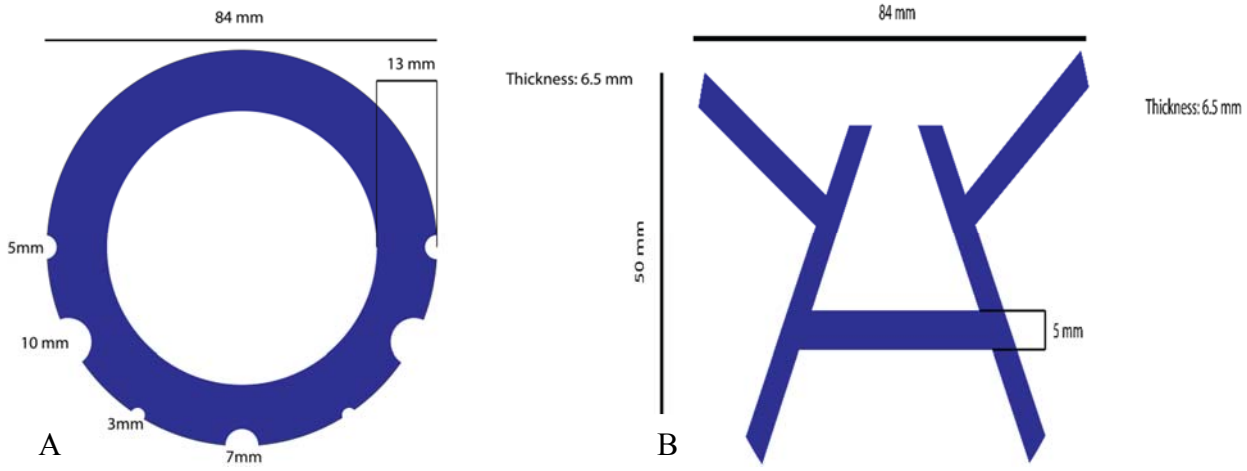


**Figure 11: Spacers used inside of borehole 2.**
(A) Diagram of the outer spacer. The OCC cable used the 5 mm groove, and the Brugg temperature and strain cables used the 3mm grooves.
(B) Diagram of the inner spacer. The cables were zip tied to the arms on the left and right. Both spacers have grooves for instrumentation wires that were not used for this project.


**Figure 12: 3D printed spacer that was used to hold the cables in place inside of the borehole.**

## 4.5 Data Collection

The data collection campaign spanned the dates of November 19 to November 21, 2016. Present at the data collection were me, in charge of geophone data collection; fellow grad student Calvin Kammerer helping with field operations; Montana Tech professors Marvin Speece, Mary MacLauglin, and Scott Rosenthal; UW-Madison personnel Neal Lord, Herb Wang, and Adam McDaniel; Pete Swanson from NIOSH Spokane Research Center; and Thomas Coleman and Taylor Martin from Silixa. Silixa provided and operated the DAS interrogator for this project. All other parties helped with equipment setup and field observations. For all data collected, a source triggered the DAS and geophone systems to start recording. The recording parameters for both systems can be seen in Table III.

**Table III: Recording Parameters**

| | DAS | Geophones |
|---|---|---|
| Live channels | 1552 | 120 |
| Sampling rate (ms) | 1 | 0.25 |
| Record Length (s) | 10 | 3 |
| Trace Spacing (m) | 1 | 3 |
| Gauge Length (m) | 10 | N/A |

The first data we collected for this project consisted of "tap testing" to help locate positions along the fiber-optic cable. Since DAS is a continuous sensor, assigning positions for specific channels is a difficult task without manually tapping on the cable and seeing where the data are observed. The positions of all of the geophones were surveyed using a total station, so we tapped on the cables as close to each geophone location as possible. This allowed us to assign locations to individual traces, and determine which traces to compare with which geophones. An example of the tap testing data can be seen in Figure 13. Due to the DAS gauge length used in this survey, taps were observed across roughly 10 channels. As stated, the gauge length is similar

to a moving average, so any gauge length that contains the tap location will produce  a trace with signal for that tap.

The second test was a series of four explosive blasts, using a 0 ms and Pentex SB Cast Boosters. We performed 2 explosions with 30 g of boosters, a third with 50 g boosters, and a blast was done with 50 g of boosters where the hole was stemmed, as seen in Table IV.

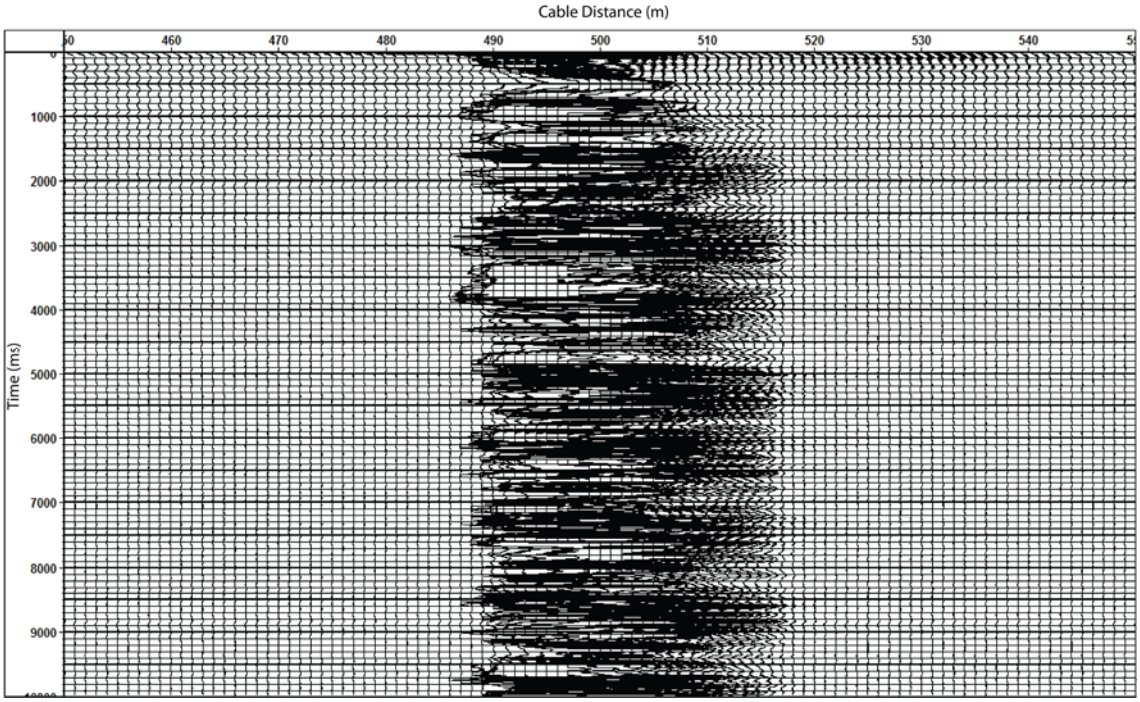


**Figure 13: Example tap testing shot at geophone station 19**. Due to the DAS using a 10-meter gauge length, the tap is observed across multiple channels. The actual location was chosen to be the center of these channels.

**Table IV: Explosive Sources**

| Blast Number | Amount of blasting caps (grams) | Stemmed? |
|---|---|---|
| 1 | 30 | No |
| 2 | 30 | No |
| 3 | 50 | No |
| 4 | 50 | Yes |

Next, we set a plate on the ground and struck it with a sledgehammer at ten different locations on the floor of the mine near surveyed pillar positions. The plate and sledgehammer can be seen in Figure 14. The plate was struck nine times at each location in order to stack out noise. We also used a sledgehammer to strike the wall of the pillar itself at two different locations. The final underground test was a “trapped miner” test, where we used a small rock hammer to tap on the wall at four locations. The purpose of tests was to compare the performance of the two different types of instrumentation for the different scenarios. The sledgehammer on a plate is an ideal scenario for exploration or controlled surveys. The sledgehammer on the wall could be used to simulate mining activity that could be monitored with these methods. The small rock hammer source experiment was used to investigate the ability of the instruments to detect the presence and/or location of a miner trapped at a location within the mine with limited tools or mobility. The location of all of the sources can be seen in Figure 15, as well as the shot locations in Table V. DAS data collection for the hammer wall hit and the trapped miner tests were unsuccessful, and so the points were not surveyed.

**Figure 14: Image of sledgehammer and steel plate used for all vertical hammer shots.**

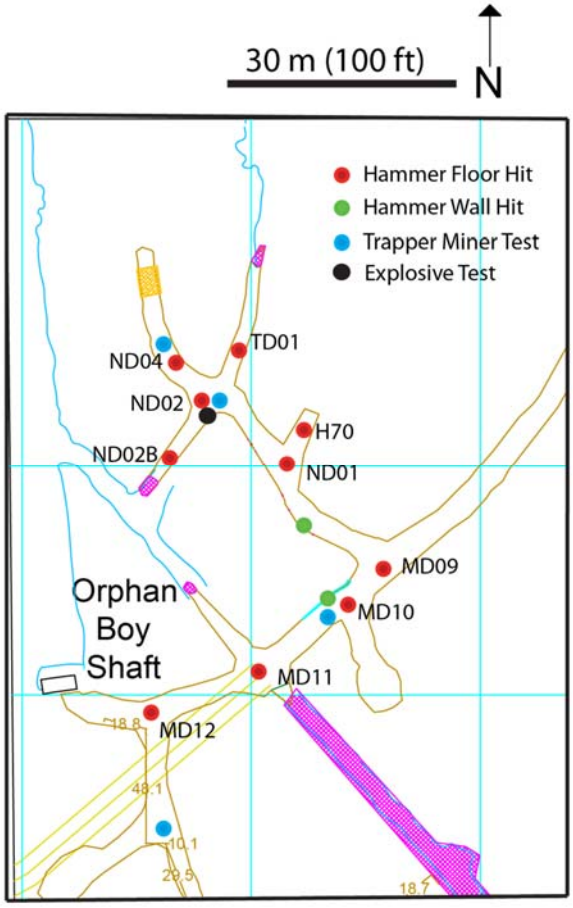


**Figure 15: Locations of all subsurface shots.**

**Table V: Hammer shot locations.** Coordinates are in UTM WGS 84 projection.

| Shot Name | X (m) | Y (m) | Elevation (m) |
|---|---|---|---|
| MD12 | 362644.0 | 200376.6 | 1707.2 |
| MD11 | 362656.7 | 200383.3 | 1708.7 |
| MD10 | 362666.2 | 200392.2 | 1709.9 |
| MD09 | 362668.9 | 200392.6 | 1711.7 |
| ND01 | 362657.7 | 200400.9 | 1709.0 |
| H70 | 362653.7 | 200408.8 | 1707.2 |
| ND02 | 362645.2 | 200417.0 | 1707.9 |
| ND02B | 362638.1 | 200409.6 | 1707.9 |
| ND04 | 362641.6 | 200419.3 | 1707.9 |
| TD01 | 362653.9 | 200424.0 | 1707.9 |

The final set of tests took place on the surface. Seven locations were chosen: in the center of the loop on the surface, in the middle of each side of the loop, and at each corner of the triangular loop. At each location, a plate was struck nine times, again to reduce noise. We also used a shear source (Figure 16) which we struck nine times oriented both North-South, and East-West at each of the locations.

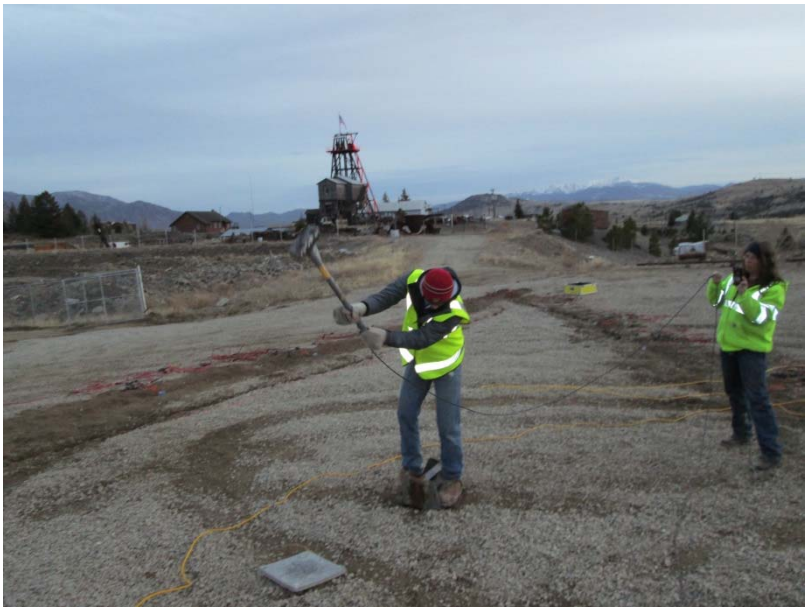

**Figure 16: Shear source oriented North-South on the surface.**

# 5. Data Processing

## 5.1. Initial Processing Steps

All data processing for the seismic data in the project was done using Vista 2013 (GEDCO VISTA Processing Manual, 2013). A similar processing flow was used for both DAS and geophone data to ensure that differences seen in the data reflected real differences in the methods, rather than simply differences in processing steps. Single traces were also exported to MATLAB for improved plotting.

The first step of data processing was to determine the geometry of the fiber-optic cable loops using the tap testing data to determine sample locations. After locations on the cable were determined, individual traces could be extracted for individual comparison. The next step in the processing flow was to filter the data. The DAS data seemed to be heavily dominated by low frequencies, and the spectrum appeared to be almost completely quiet by 200 Hz, as seen in Figure 17. For the geophones, a few small spikes can be seen in the average frequency spectrum below 60 Hz. The corner of the geophone signal appears to be at roughly 400 Hz, at which point the data appear to be dominated by noise in the higher frequencies. In order to make an accurate comparison between the two methods, I chose a bandpass filter with the same edges to apply to the data to ensure the same frequencies were represented in both methods. After testing different filters, the best compromise was determined to be a 40/50/300/400 trapezoidal bandpass filter. This filter seemed to have the highest signal to noise ratio for both methods.

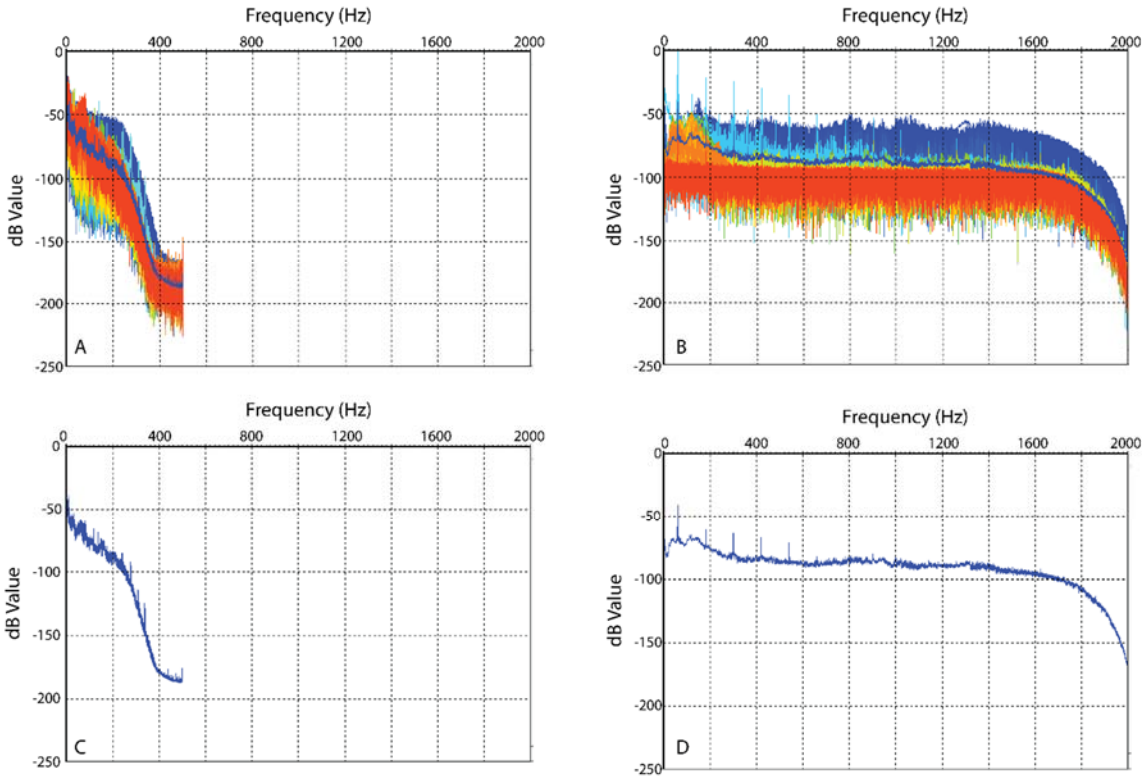


**Figure 17: Frequency content of DAS and geophone data.**
(A) The frequencies of all traces of DAS data from an explosive shot.
(B) The frequencies of all traces of geophone data from an explosive shot.
(C) The average frequency spectrum for the DAS data.
(D) The average frequency spectrum for the geophone data.
The DAS system does not record anything above 500 Hz. All of the amplitudes are on a logarithmic scale.

To pick the bandpass filter, the corners of the frequency plots above were used. The top end of the filter was set sloping down from 300 Hz to 400 Hz. Having the top cut at 400 Hz kept the high frequency data of the geophones. The low cut of the bandpass filter was set at 30 Hz to cut out some of the low frequency noise in both the DAS and the geophone data.

The next step in the processing was to convert the DAS data from strain rate to strain. In order to make this conversion, I used the equation

$$\varepsilon = g * p \int U \qquad (1)$$

where $\varepsilon$ is the strain, $g$ is the gauge length, $p$ the elongation in one radian of phase change, and $U$ is the amplitude of the signal before processing (Feigl, 2017). I used the cumulative sum in MATLAB to perform the integration.

## 5.2. Phase and Geophone rotation

Three-component geophones experience a 90-degree phase difference between the horizontal and vertical components due to the difference in their orientation. Likewise, a phase difference appears between the two horizontal components (Crampin, 1985). An example of the phase difference seen in geophones can be seen in Figure 18. Although the same energy is hitting the geophone, the peaks are not in line with each other between the three components.

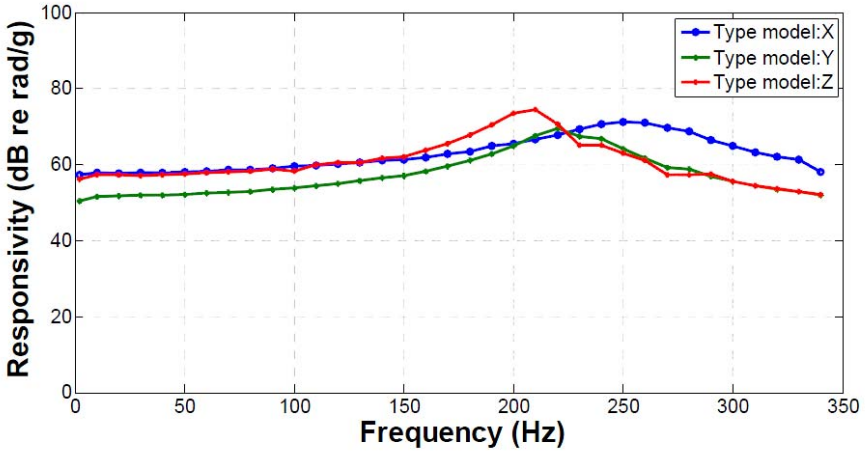


**Figure 18: Example of waves that are out of phase with each other for a 3-component geophone (Chen et al., 2016).** The plot shows the responsivity, or how sensitive a geophone is at certain frequencies, as a ratio of the phase shift in radians to the input acceleration, defined as g.

The phase difference exists not only between components of the geophone data, but also exist between the DAS and geophone data if the component of the geophone being examined is not in line with the fiber. The compression and extension of the fiber is what the DAS interrogator measures. If the direction of the compression and extension of the fiber is not in line with one of the geophone components, a phase difference will exist similar to the phase

difference between X and Y components of the geophone. The geophone components must be rotated to be parallel with the cables so that phase differences seen in the data are not due to geophone and cable orientation differences. Figure 19 shows one example of the geometric differences that must be accounted for. If a geophone has an X and Y component, a rotation can be performed to put the geophone into any desired coordinate system (Yilmaz, 2001).

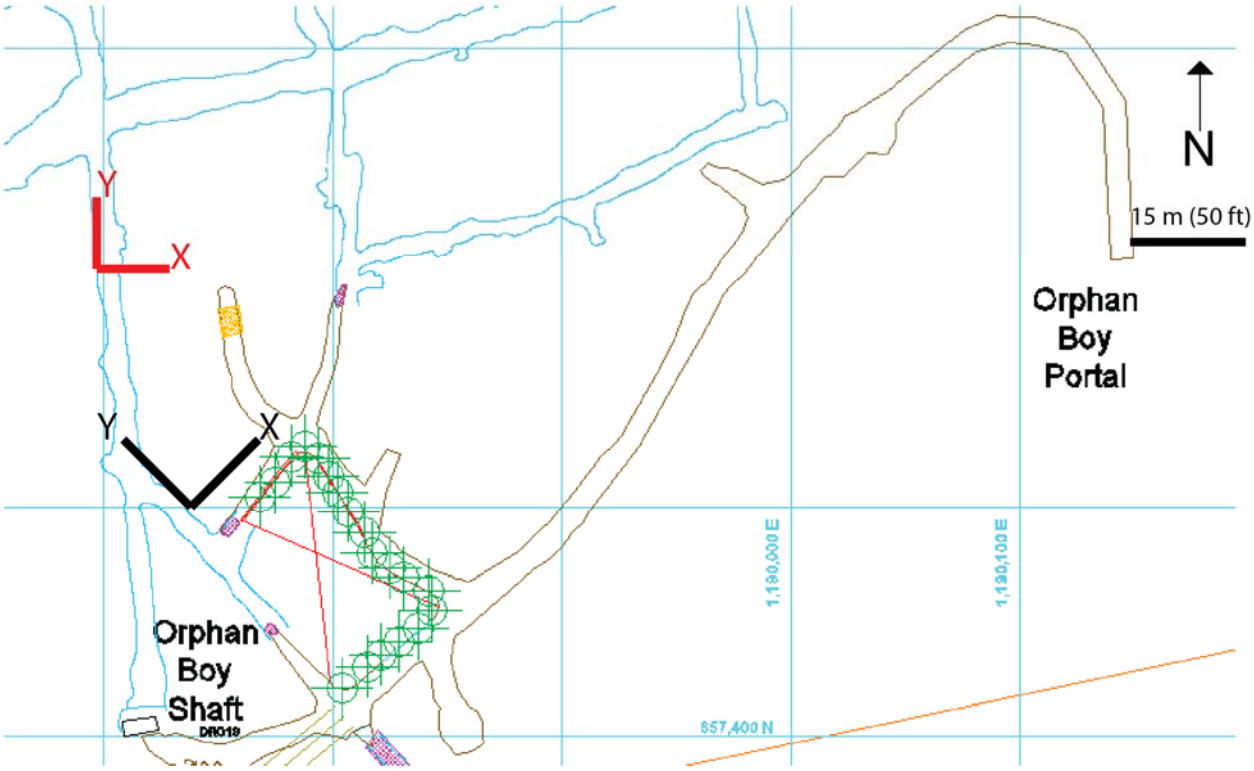


**Figure 19: Example of the coordinate system used before and after rotation.** The red coordinates show the orientation of the X and Y coordinates of the geophones. The black X and Y coordinates show the desired orientation so that the X component of the geophones is in line with the fiber-optic cable. A different rotation was done for each geophone so that there was a component in line with the fiber-optic cable.

The rotation for the data was done using built-in Vista functionality. The X and Y components of the geophone were defined, then a rotation angle was chosen, and new X' and Y' components were generated with the new rotated coordinate system. An example of a geophone X trace before and after rotation can be seen in Figure 20.

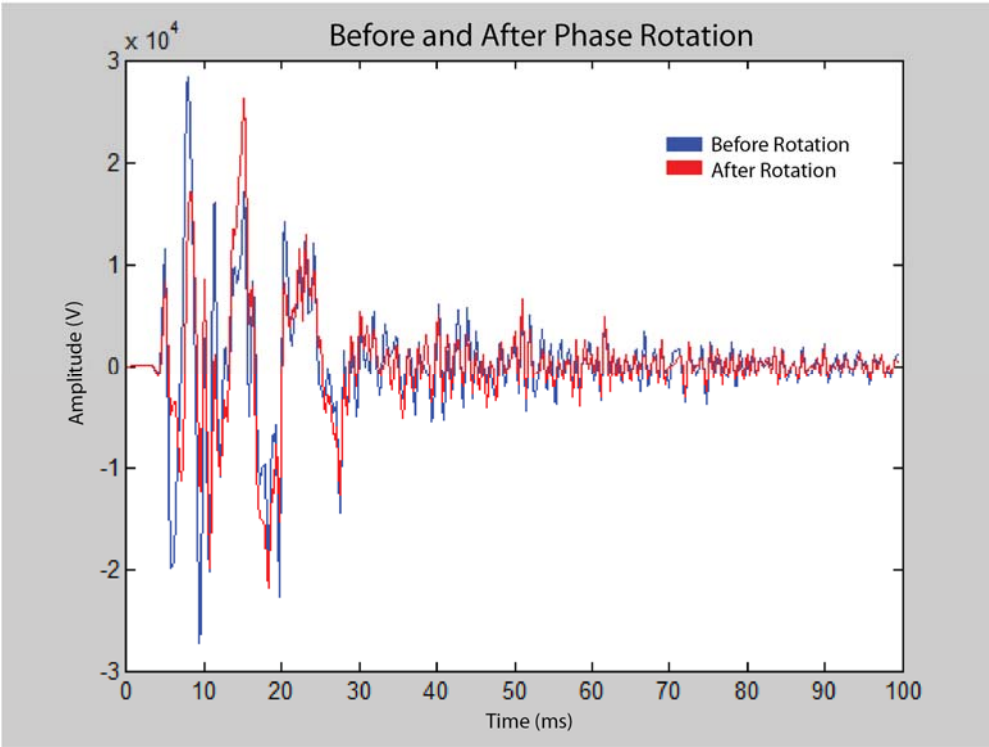


**Figure 20: One example of a rotated geophone trace**. The traces shown are taken from station 3. The blue trace is the X component before rotation, and the red trace is after a 45-degree counterclockwise rotation, which puts the component in line with the cable. A small phase difference can be seen between the two traces.

Even when the geophone and fiber are inline with each other, a phase difference can still exist between the geophones and the DAS data. The geophones essentially measure particle velocity. The magnet inside the coil of the geophone moves in the same direction as the particle velocity in the Earth. However, the fiber is sensitive to compression and extension in the cable, which means that the fiber-optic data are determined by the pressure wave, similar to a hydrophone. For a geophone, the given convention is that upward motion for a vertically oriented geophone is particle velocity, but for the fiber, an extensional force is a positive kick in energy (Brown et al, 2002). An extension in the fiber does not necessarily correspond to an upward motion in the particle velocity, which could cause a sign difference between the two instruments. In acoustic waves, a 90-degree phase difference exists between particle velocity and

pressure near the source. As the distance from the source increases, the two waves gradually become in phase (Fahy, 2003). The variable phase difference depending on distance can cause the fiber and geophone to be out of phase with one another.

For a given source, the direct arrival between the particle velocity and the pressure wave will be in phase with each other. When the wave is reflected, the phase of the pressure wave will reverse 180 degrees, whereas the particle velocity could stay constant. The sign of the reflection coefficient can also cause the sign of the particle velocity to flip. In addition, the angle at which a pressure wave strikes a receiver will cause a complex change in the phase of the wave (Barr, 1989). The result of the phase changes means that the direct arrival should be in phase between the geophones (measuring the particle velocity) and the DAS system (measuring the pressure wave). The two instruments will not necessarily be in phase for any of the energy after the first arrival. The phase difference between the two would be extremely difficult to process out without knowing the characteristics of the subsurface with detail. However, a phase-matching algorithm, such as those used to compare hydrophone and geophone data could be employed (Barr, 1992).

## 5.3. Triggering Issue

During this survey, a problem occurred with the triggering of the Silixa system. The problem occurs when the voltage of the trigger excites the optical laser. Once energy from the source reaches the fiber, the optical laser appears to operate properly. However, the early samples of the survey are compromised (T. Coleman, personal communication, 2017). The effect of this triggering issue can be seen in Figure 21. This issue cannot be processed out because the compromised data are present across all frequencies. In addition, the compromised data do not exist in a set time interval that can be muted to remove data points, as the amount of

compromised data varies from shot to shot. Consequently, the problem can not be fixed without reshooting the survey.

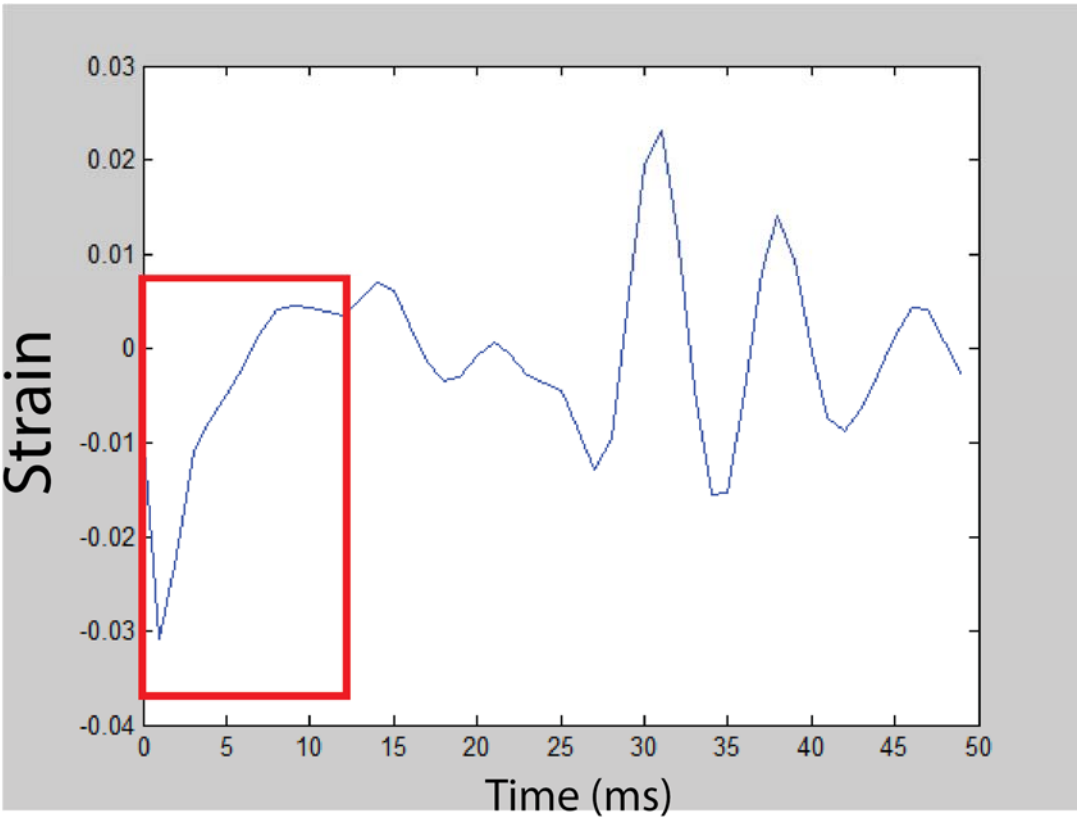


**Figure 21: An example of the compromised samples highlighted in the red box.** Ordinarily, one would expect this early part of the record to be quiet and show no strain.

Because of the triggering issue in this project, the early samples were ignored, and comparisons were made after the first break of energy in the traces. However, this is an issue that is extremely damaging to a survey, especially one where the first break times are of importance.

# 6. Results

## 6.1 Tap Tests to Confirm Cable Positions

Tap tests were used to locate all of the cable locations in relation to the geophones. Figure 22 shows an annotated tap test that depicts the different locations along one shot of the DAS data. Since the path of the cable went around the pillar multiple times, taps were seen three times at each of the underground fibers. The entirety of the tap test data can be seen in Appendix A.

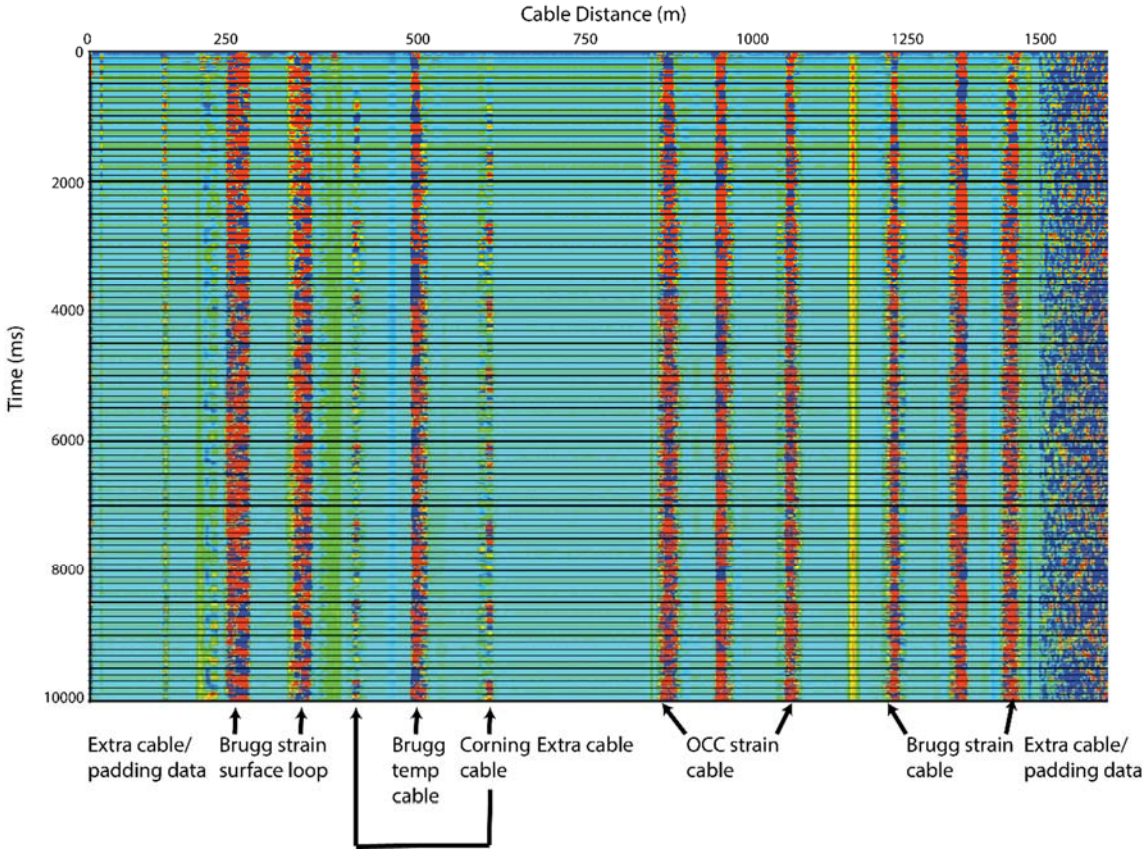


**Figure 22: Tap test taken at geophone station 19.** The surface cable is bound by areas of wind where the cable is not buried. Taps for the underground stations show up three times for each cable due to the path around the pillar.

Table VI shows the results of the underground and surface tap tests. The station number indicates which geophone station we tapped near. Due to gauge length, the taps were observed over a number of traces. The trace(s) listed in the table were the middle of the range of traces that

responded to each tap. Due to the path of the underground cable loop, some of the strain cables showed up across multiple traces. the cables had multiple traces. Also, due to noise or low amount of signal, the tap at station 17 could not be picked.

**Table VI: Underground (Stations 1-19) and Surface (Stations 20-40) Tap Tests**

| Station | Brugg Temp | OCC Strain | Brugg Strain | Station | Brugg Surface |
|---|---|---|---|---|---|
| 1 | 558 | 1010 | 1279 | 20 | 306 |
| 2 | 560 | 1015 | 1285 | 21 | 302 |
| 3 | 549 | 1009 | 1281 | 22 | 295 |
| 4 | 461, 539 | 925, 1003 | 1286, 1367 | 23 | 292 |
| 5 | 458, 541 | 922, 1004 | 1289, 1367 | 24 | 289 |
| 6 | 458, 532 | 917, 1001 | 1294, 1375 | 25 | 285 |
| 7 | 504, 542 | 926, 1007 | 1328, 1404 | 26 | 281 |
| 8 | 434, 526 | 916, 996 | 1294, 1378 | 27 | 278 |
| 9 | 431, 527 | 911, 990 | 1307, 1385 | 28 | 275 |
| 10 | 441, 529, 600 | 913, 993, 1054 | 1242, 1302, 1383 | 29 | 272 |
| 11 | 429, 529 | 913, 985 | 1313, 1377 | 30 | 268 |
| 12 | 433, 520, 592 | 911, 985, 1053 | 1243,1302, 1389 | 31 | 266 |
| 13 | 431,523, 596 | 907, 985, 1054 | 1239, 1305, 1388 | 32 | 264 |
| 14 | 422, 512, 597 | 895, 976, 1050 | 1236, 1316, 1400 | 33 | 263 |
| 15 | 422, 508, 599 | 893, 969, 1061 | 1242, 1321,1392 | 34 | 261 |
| 16 | 504 | 963, 1065 | 1236, 1319, 1397 | 35 | 259 |
| 17 | Not visible | Not visible | 1323 | 36 | 255 |
| 18 | 414, 502, 602 | 891, 965, 1070 | 1228, 1320, 1405 | 37 | 251 |
| 19 | 410, 505, 612 | 886, 963, 1069 | 1220,1323, 1405 | 38 | 249 |
| | | | | 39 | 248 |
| | | | | 40 | 246 |

The underground tap tests show that some of the trace locations are unreliable. Although the locations of the taps were a consistent (but nominal) 3 m apart, the taps do not always show up 3 m from each other. The gauge length combined with inconsistencies in taps (how hard the

cable was gripped, how hard the hammer was swung, etc.) lead to some uncertainty in the trace locations.

## 6.2 Data Sets from Surface Hammer Sources

One set of tests for this project was done using a sledgehammer on the ground surface. Figure 23 shows a vertical hammer shot observed at the geophone and DAS trace location on the North wall of the pillar. The data appear to match well. Figure 24 shows the results at the same location, but for a North-South oriented shear source. The geophone component chosen in both Figure 23 and 24 is the component that is in line with the cable. In both Figure 23 and 24, the first break of energy appears to line up in the geophone and the DAS data. The data also appear to be in phase for most of the trace in the North-South shot of Figure 24.

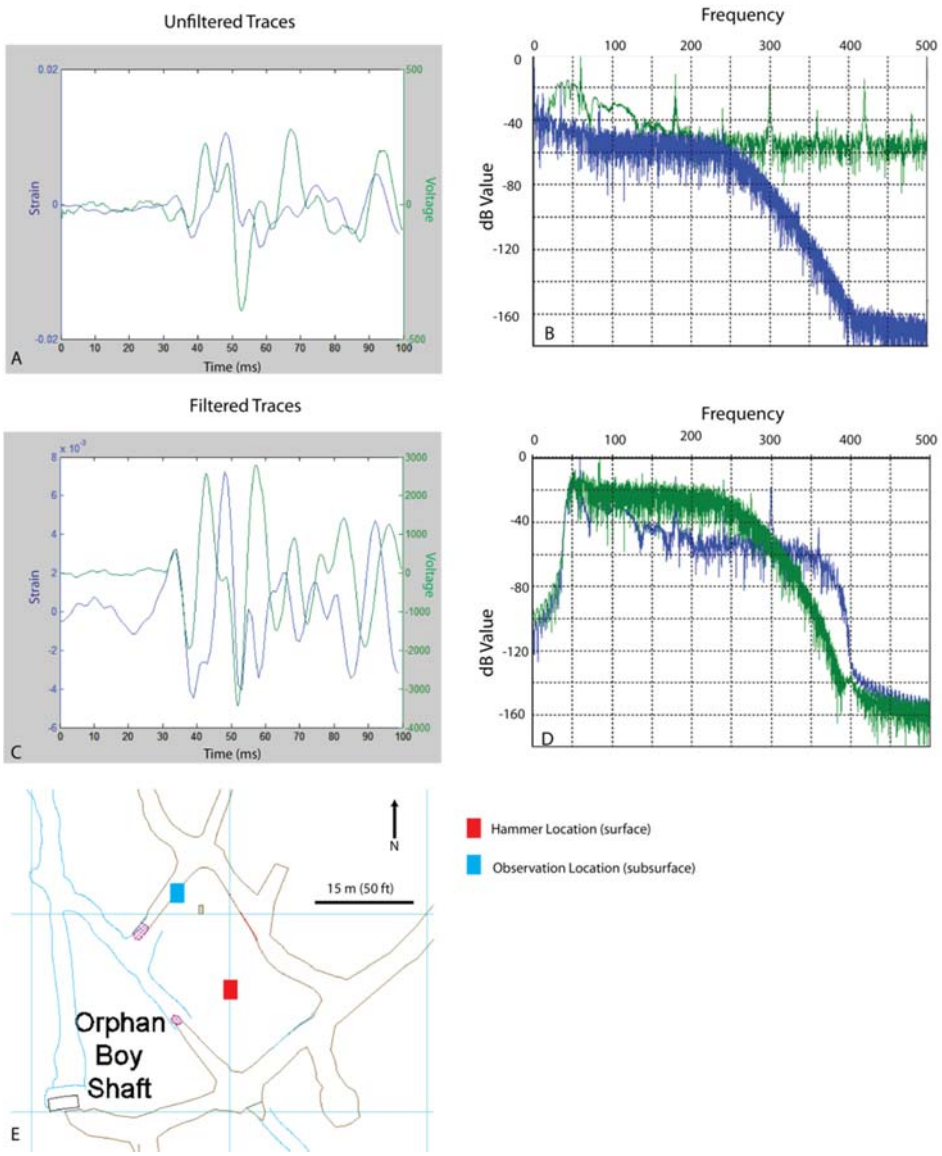


**Figure 23: Single trace comparison of the DAS (blue) and geophone data (green) from a vertical shot. The geophone trace is the X component rotation 45 degrees counter clockwise to be in line with the fiber.**
(A) The geophone and DAS traces before a filter was applied.
(B) Frequency content of the DAS and geophone before a filter was applied.
(C) The geophone and DAS traces after a filter was applied.
(D) The frequency content after a bandpass filter had been applied.
(E) The hammer location on the surface and the observation location in the subsurface. The geophone trace is the X component rotation 45 degrees counter clockwise to be in line with the cable.

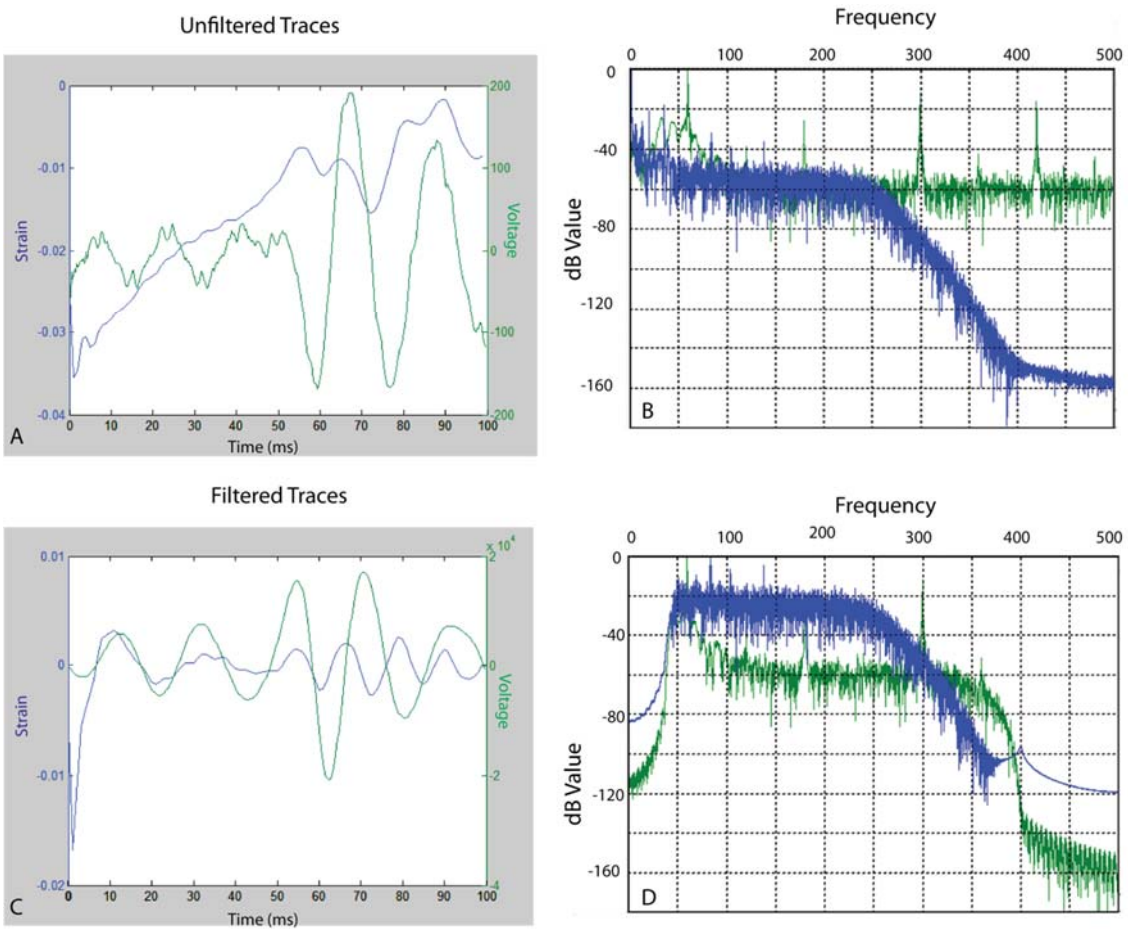


Figure 24: **Single trace comparison of the DAS (blue) and geophone data (green) from a North-South shear shot. The X component of the geophone was used and rotated 45 degrees to be in line with the fiber. The shot and observation locations are the same as in Figure 23E.**
(A) The geophone and DAS traces before a filter had been applied.
(B) The frequency content of the DAS and geophone data before a filter was applied.
(C) The geophone and DAS traces after a filter had been applied.
(D) The frequency content of the DAS and the geophone data after a filter had been applied.

According to the field data represented in Table I, the weathered granite rock present at the UMEC site has an average P-wave velocity between 1100-2000 m/s and an average S-wave velocity of roughly 600 m/s. The distance from the surface shots to the north wall observation point was roughly 35 m. In Figure 23, the first arrival of energy is at 32 ms, which would make the average velocity roughly 1100 m/s. The arrival seen in Figure 23 is possibly a P-wave arrival, which would make sense due to the strike being vertical. Vertical shots send P-waves into the

subsurface, which allows us to see strong P-wave arrivals. In Figure 24, the first arrival time is 45 ms and this corresponds to an average velocity of 777 m/s. This velocity is much closer to the average S-wave velocity for the rock in the mine, which means the first arrival seen in Figure 24 is most likely S-wave arrival, particularly since the data presented were generated using a shear wave source.

The data suggest that fiber-optic cable used in DAS is most sensitive to strain in line with the cable as seen in the difference between Figure 23 and Figure 24. The shots for these two figures were in the same location, however the shot in Figure 23 was vertical, and the shot it Figure 24 was oriented North-South, roughly in line with the cable. The DAS data aligns much more closely with the geophone data in Figure 24 where the cable is in line with the S-wave source.

The experimental layout of the fiber-optic cable deployed at the UMEC pillar was designed to host other experiments in addition to the DAS data collection campaign, and consequently, the design included significant segments of cable that were not coupled to the rock. The DAS data traces chosen to compare with the geophones were from areas on the northwest wall of the pillar, where the cable was well-coupled to the wall. In areas where the cable was uncoupled, the data was essentially not usable. Figure 25 shows an example of a poorly coupled section next to the well-coupled section. The areas with uncoupled cable show a clear decrease in amplitude as well as quality of data, underlining the fact that good coupling of the cable to the rock is extremely important for the collection of DAS data.

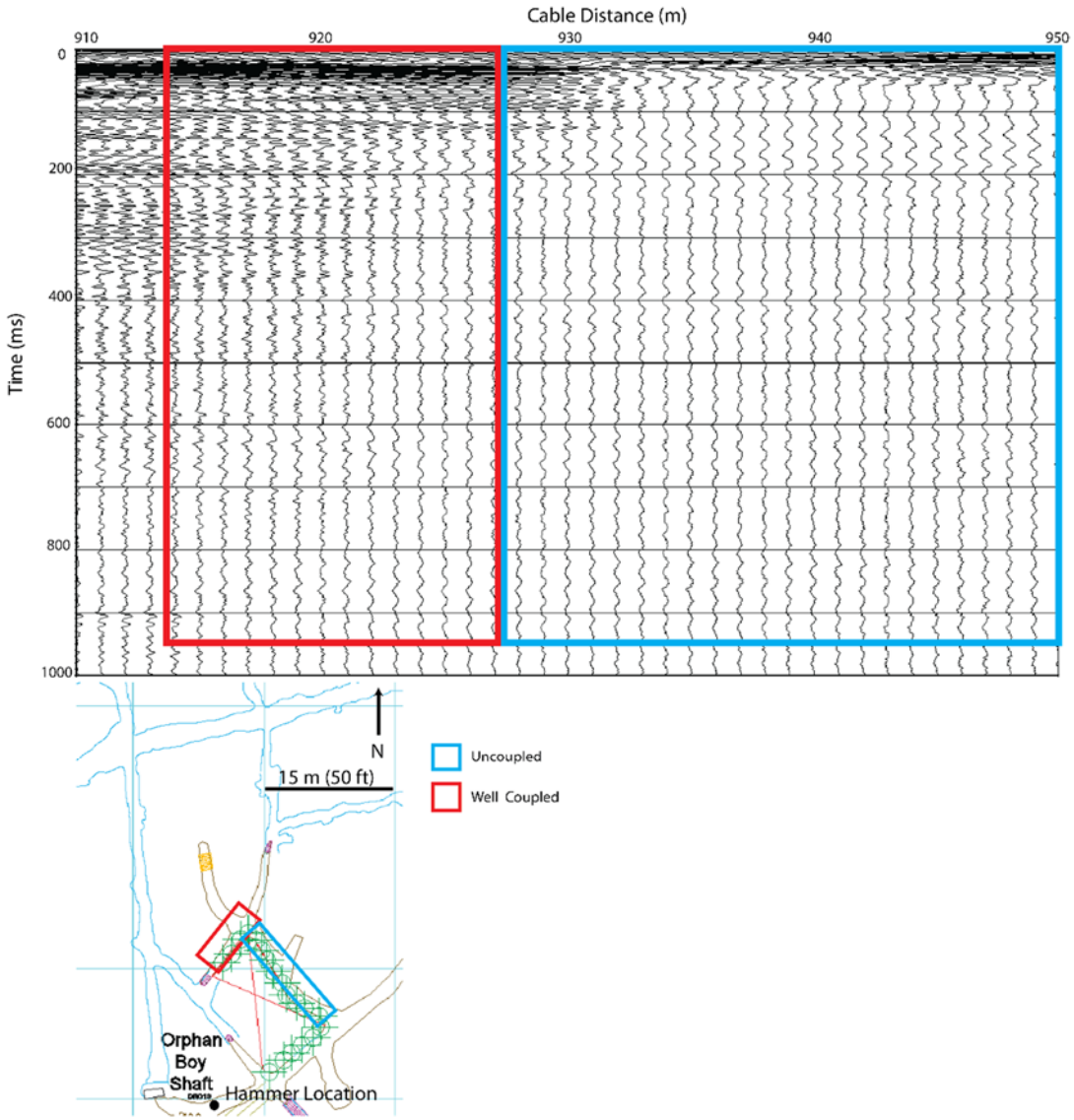


**Figure 25: Hammer shot with the well-coupled section highlighted in red and the uncoupled section highlighted in blue.** The data clearly drop in quality between the two sections.

## 6.3 Surface Loop Comparison

Vertical and shear oriented shots were performed on the surface. Shots were taken at the center of the loop, the corners of the triangle, and the center of each side of the triangle. All shots were taken nine times and the data were stacked. The surface loop had one side oriented East-West, one side oriented North-South, and the final side oriented diagonally connecting the two

other sides. We numbered the sides as shown in Figure 26. We chose the observation location of each side to be in the center of the side to account for the 10-meter gauge length. With the observation location in the center, only traces from each side would be averaged in the gauge length for the chosen location. Side 1 contained geophones 20 to 24 and fiber traces 306 to 288. Side 2 contained geophones 25 to 32 and fiber traces 287 to 264. Side 3 contained geophones 33 to 40, and fiber traces 263 to 246.

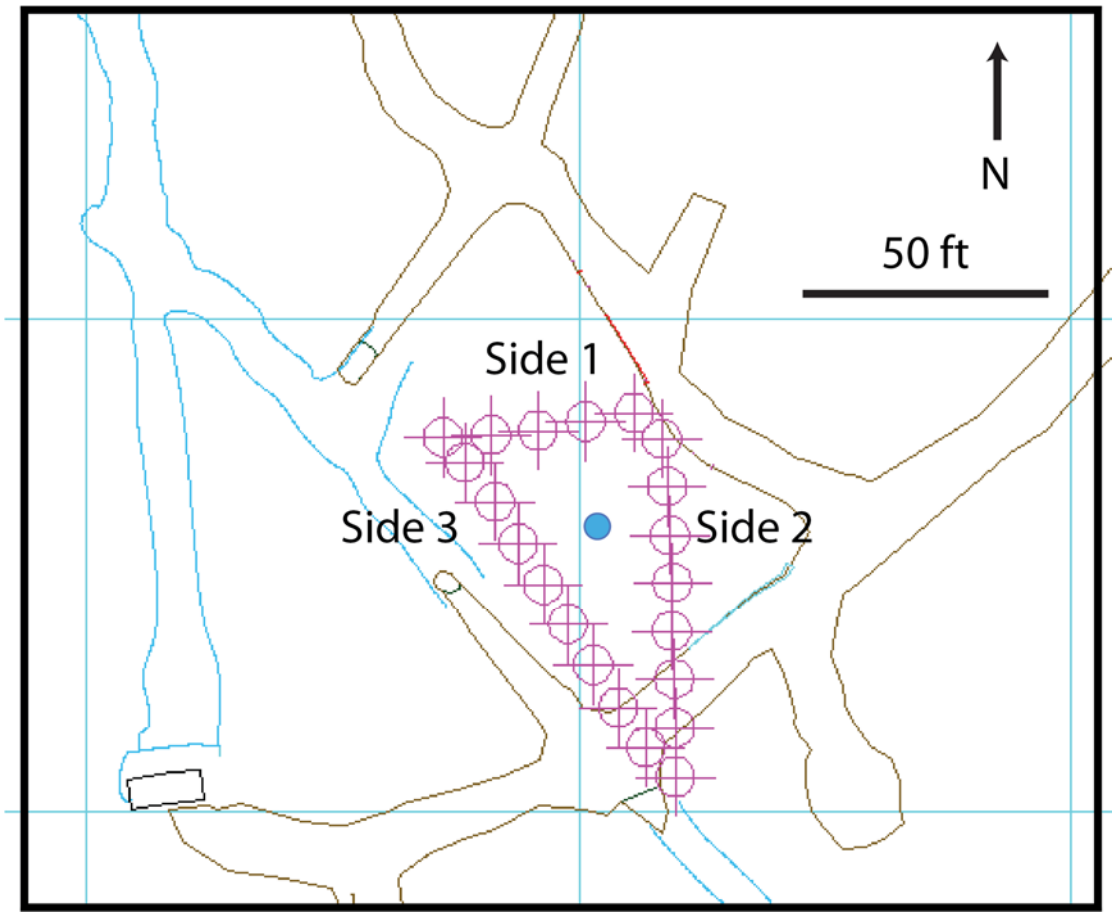


**Figure 26: Surface geophones overlain on the map of the mine.** Each side was labeled in order to keep track of data. The blue dot in the center was the location of the source for the surface tests.

To examine the effect of the orientation of the fiber in relation to the source location, data were collected corresponding with a vertical, North-South horizontal, and East-West horizontal sources located in the center of the triangle. The results from these tests can be seen in Figure 27,

Figure 28, and Figure 29 respectively. The shots shown have the same bandpass filter as in the previous examples. Although the shot in Figure 27 is a vertical shot, the vertical trace of the geophone is not shown due to the fact that a vertically oriented fiber was not used in the test.

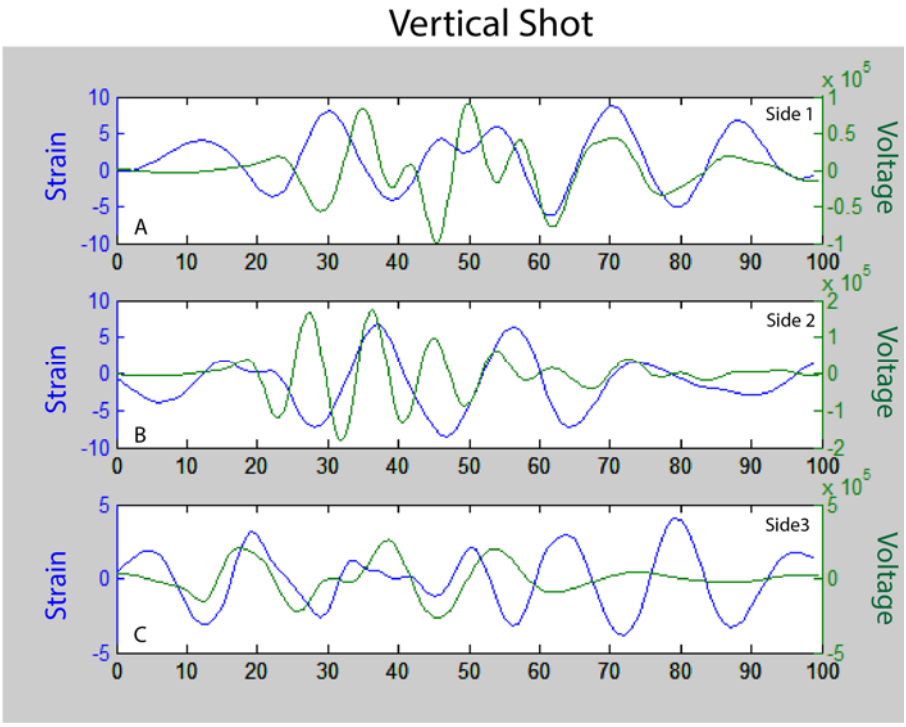


**Figure 27: Vertical surface shot.**
(A) Side 1 of the vertical surface shot using the x component of the geophone.
(B) Side 2 of the vertical surface shot using the y component of the geophone.
(C) Side 3 of the vertical surface shot using the y component of the geophone rotated 45 degrees.

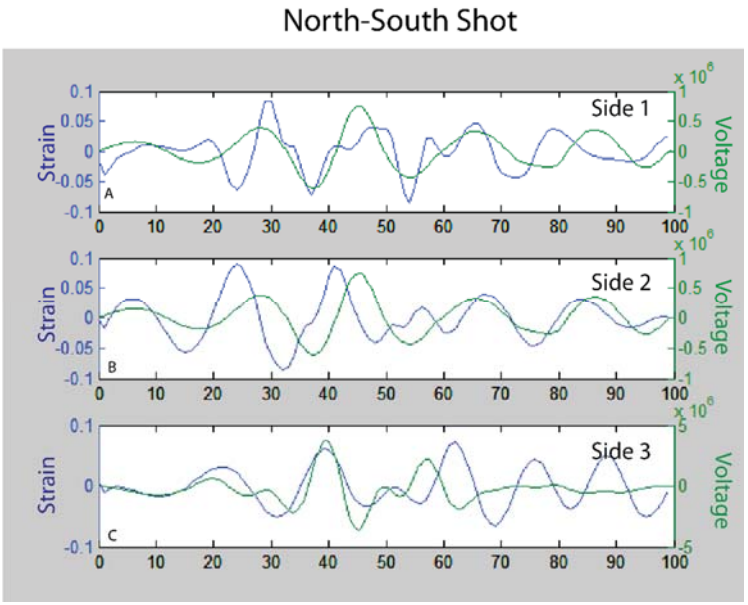


**Figure 28: North-South shear surface shot.**
(A) Side 1 of the North-South surface shot using the x component of the geophone.
(B) Side 2 of the North- South surface shot using the y component of the geophone.
(C) Side 3 of the North-South surface shot using the y component of the geophone rotated 45 degrees.

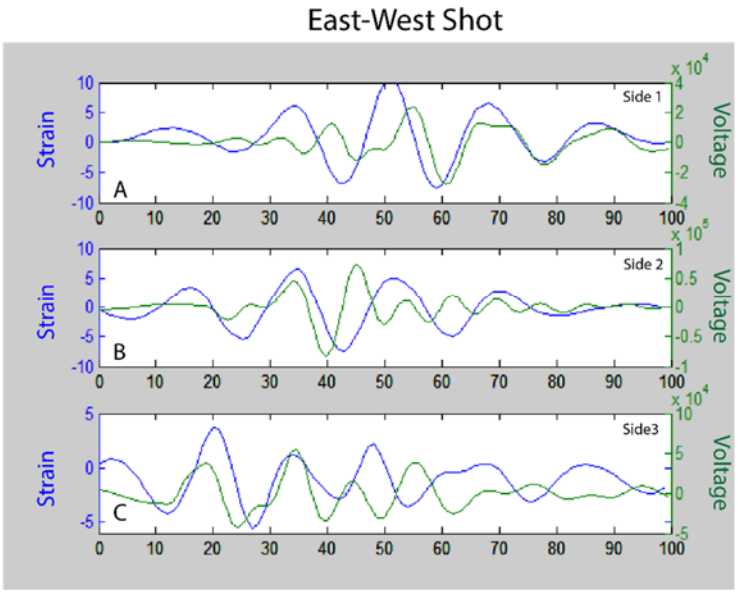


**Figure 29: East-West shear surface shot.**
(A) Side 1 of the East-West surface shot using the x component of the geophone.
(B) Side 2 of the East-West surface shot using the y component of the geophone.
(C) Side 3 of the East-West surface shot using the y component of the geophone rotated 45 degrees.

All shots taken on the surface seem to have some agreement between the data from DAS and the aligned geophone. The traces produced using the two different types of instrumentation have roughly the same shape and timing of events, but there are small phase differences between the traces. For example, Figure 28A shows the two traces in phase with each other, whereas Figure 28B shows the traces with a 90-degree phase difference. The shear-oriented shots have a high degree of agreement, especially on the side that is in line with the shot. This effect is seen clearly in side 2 of the East-West shot (Figure 29). From the previous work done by the senior design students, the S-wave velocity was determined to be between 500 and 1500 m/s. These velocities were taken from the subsurface rock, which would have a higher velocity than the surface materials. Material on the surface, which is often times largely made of loose sediment, typically has a lower velocity than crystalline rock seen in the subsurface. From the center of the triangle to any side is roughly 10 m. The S-wave arrivals should be roughly 5 to 15 ms given this dimension. The first arrivals can be seen around 20 ms in the geophones, specifically in side 3 of the East-West shot. However, the first arrivals are not clear enough in the DAS data due to the triggering issue, which makes picking S-wave arrivals difficult.

## 6.4 Data Sets from Subsurface Hammer Sources

The next data set examined was associated the subsurface hammer shot sources. The first comparison that was made was on the north face of the pillar, because this was one section of the cable that was well coupled to the rock. Figure 30 shows a comparison of DAS and geophone traces located on the north wall. The geophone traces were rotated to be in line with the cable. Figure 30 shows that once a bandpass filter has been applied to both sets of data, the geophone and DAS data traces appear to line up with each other and be in phase. The triggering issue has a

large effect on the DAS data, but after 20 ms, the DAS and geophone traces line up with each other.

The data in the subsurface hammer shots appear to have slightly less agreement between the geophones and DAS, which suggests that when the source is underground, the underground source has a negative effect on the data. One explanation for the negative effect of an underground source could be the ringing of the source on the walls of the mine. The DAS data collected when the source is outside of the mine appear to line up with the geophone data more closely. Another possible explanation is that in the subsurface, more reflection of the waves from the sides of the tunnels causes phase differences between the DAS and the geophones.

The subsurface hammer shots were also examined at surface locations. An example can be seen in Figure 31. Before the data have been filtered, the fiber and the geophone traces do not line up with one another at all. The fiber data seem to be dominated by low frequency noise. Once the data have been filtered, however, the two methods appear in phase with each other for most of the measurement period.

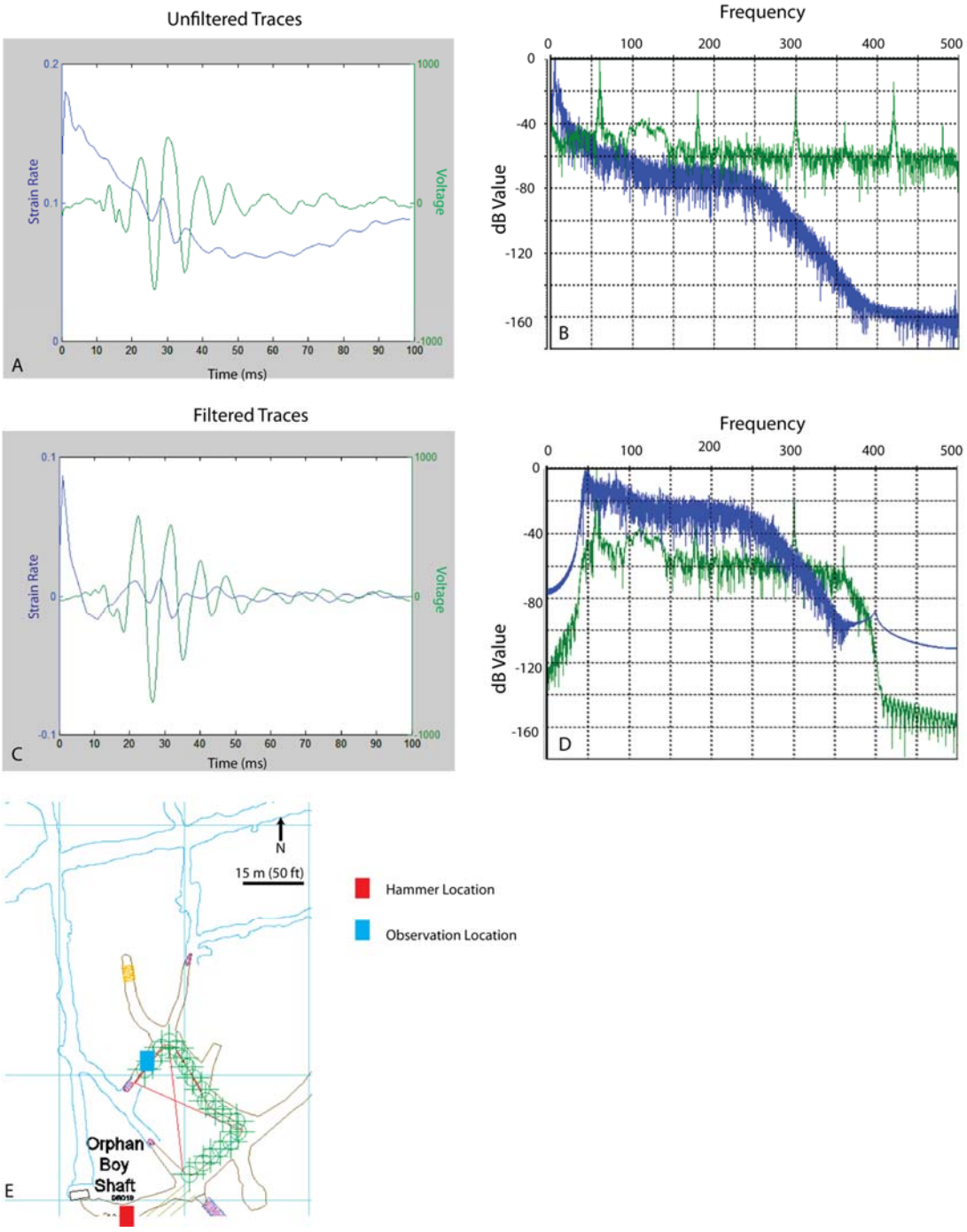


**Figure 30: Single trace comparison of the DAS (blue) and geophone data (green) from a vertical shot in the subsurface. The X component of the geophone has been rotated 45 degrees to be in line with the cable.**
(A) The geophone and DAS traces before a bandpass filter had been applied.
(B) The frequency content of the DAS and geophones before a filter has been applied.
(C) The geophone and DAS traces after a bandpass filter had been applied.
(D) The frequency content of the DAS and geophone after a filter had been applied.
(E) The shot and observation location for the traces shown. The observations location was the well-coupled section on the northwest face of the pillar.

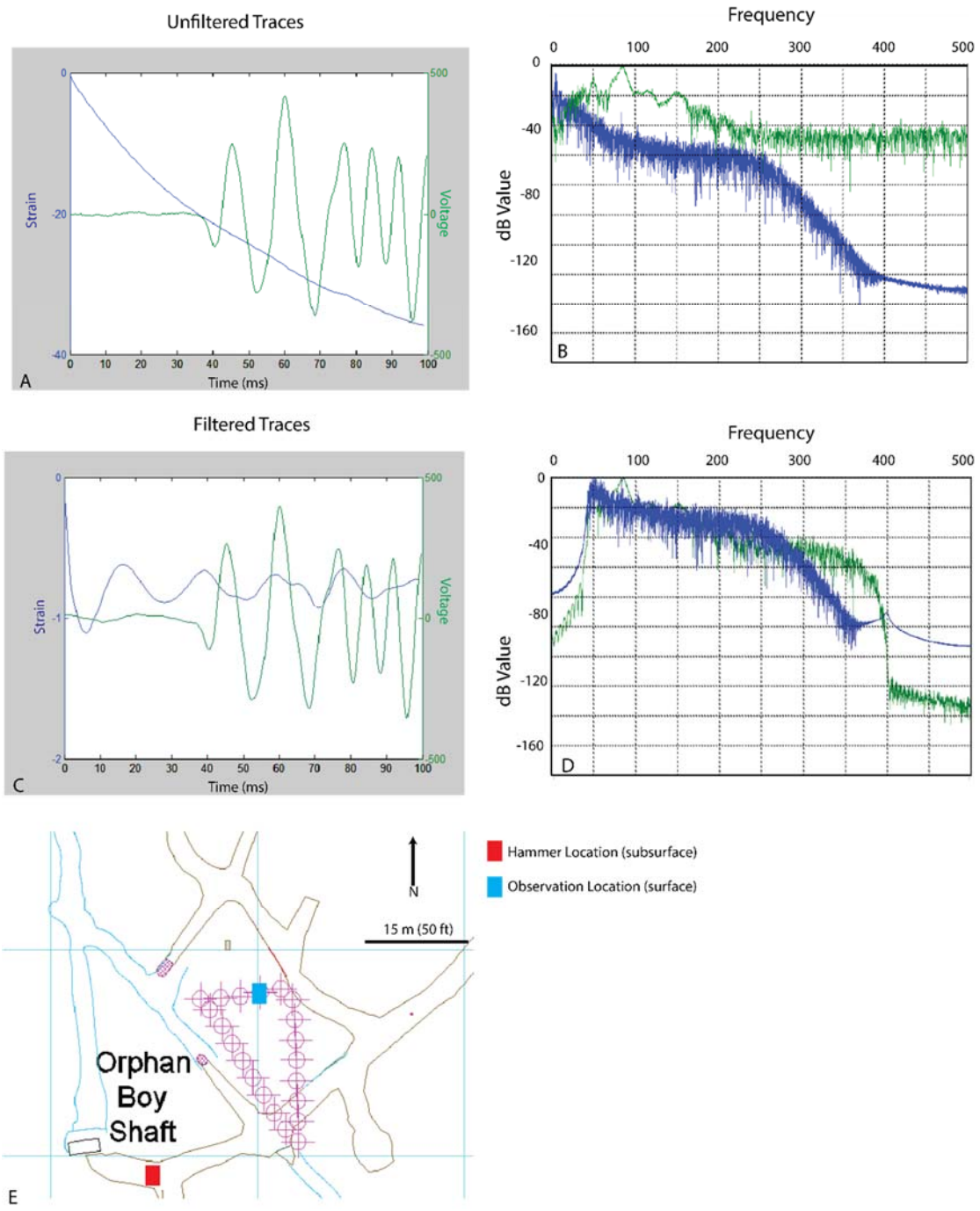


**Figure 31: Single trace comparison of the DAS (blue) and geophone data (green) from a vertical shot in the subsurface observed on the surface. The X component of the geophone has been rotated 45 degrees to be in line with the cable.**
(A) The geophone and DAS traces before a filter was applied.
(B) The frequency content of the DAS and geophone before a filter was applied.
(C) The geophone and DAS traces after a filter was applied.
(D) The frequency content of the DAS and geophone after a filter was applied.
(E) The location of the hammer in the subsurface and the observation location on the surface.

## 6.5 Cable Comparison

Three different types of fiber-optic cable were used for this project: a Brugg temperature cable, a Brugg strain cable, and an OCC Strain cable. The main difference between these types of cables is the coupling of the fiber to the cable jacket. The strain cables have the fiber tightly coupled to the jacket, whereas the temperature cable has a gap between the fiber and the cable jacket in order to allow the fiber to move freely. An unfiltered comparison can be seen in Figure 32.

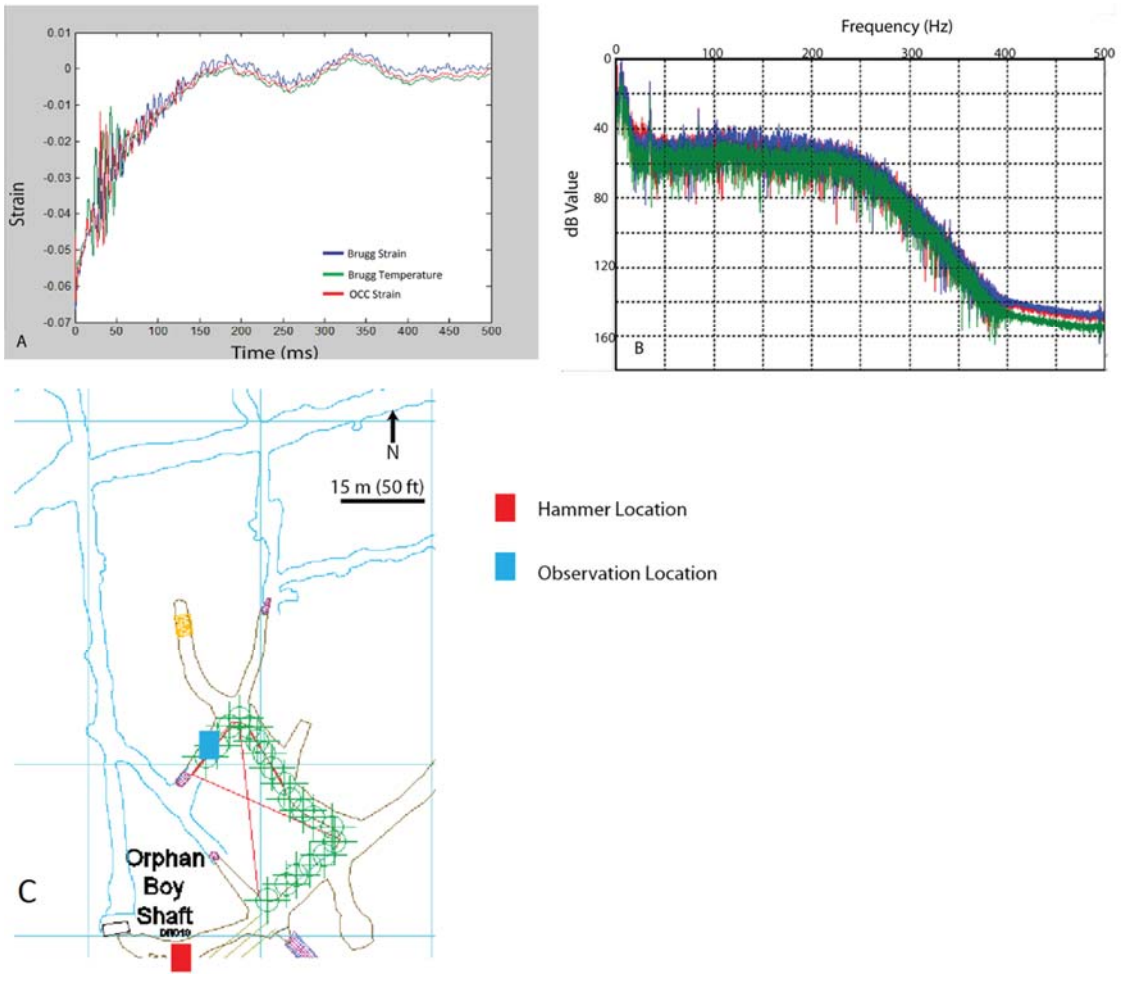


**Figure 32: Unfiltered comparison of the three cables used.**
(A) Traces taken from all three types of the fiber-optic cables that were used in the experiment.
(B) Average frequency content of all three types of cable.
(C) Location of hammer shot and cable observation locations. All three cables were embedded in concrete in order to improve coupling to the rock.

While the three cables have a similar wave shape, a noticeable phase difference exists between the Brugg temperature cable and the other two cables. In terms of frequency content, the OCC has a spike at very low frequency, below 5 Hz, that the other cables do not have. The Brugg strain falls off slightly quicker in the higher frequencies in comparison to the other cables. A bandpass filter was applied to the cables and this can be seen in Figure 33.

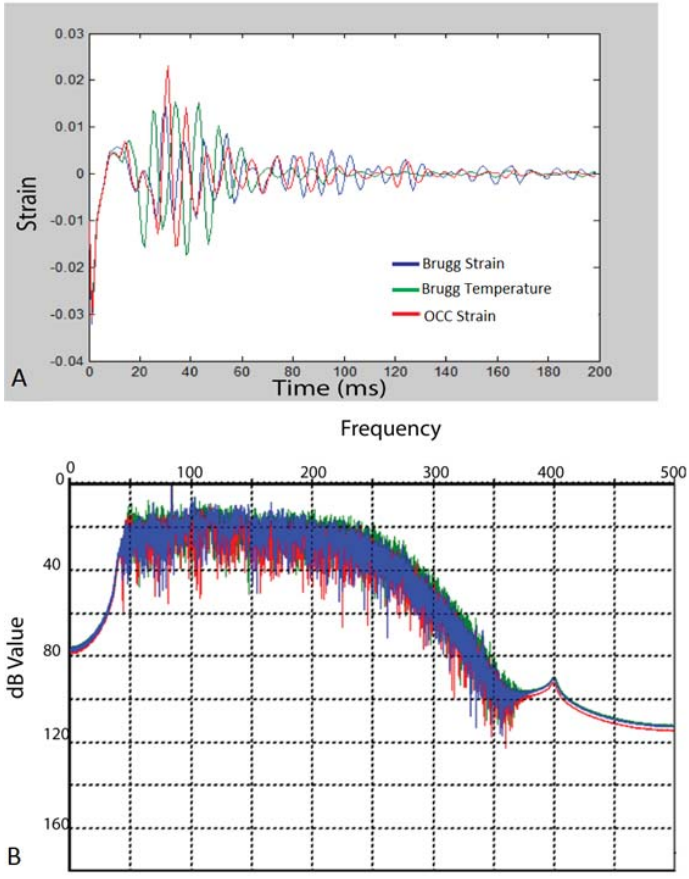


**Figure 33: Filtered comparison of the three cables used.**
(A) Three traces from the underground cable along the northwest wall of the pillar during a hammer shot after a 40/50/300/400 bandpass filter was applied.
(B) The frequency content of the three cable after the bandpass filter was applied. The amplitude is on a logarithmic scale.

Since the same filter was applied to all three of the cables, the frequency content is very similar between all of the cables. The Brugg temperature cable appears to be out of phase by 180 degrees with the other two cables, and the OCC strain has a slightly higher amplitude than the Brugg cables. The cables showed very similar results between all sources and receivers. Surprisingly, the strain cables do not seem to outperform the temperature cable, even with the tight jacket coupling. The results show that none of the cables have a significant advantage over another, and the brand of cable does not need to be a factor of great concern when designing a DAS survey.

However, a noticeable phase difference exists between the Brugg temperature and the other two cables. One possible explanation for this difference is that although they are all taken from the same location, the distances along each given cable might be different. The distance along the cable could have an effect on phase, however more lab testing would need to be done to determine if this was definitely the cause. Another possible cause of the difference in the Brugg temperature cable could be its loose tube design, in contrast to the tightly jacketed strain-sensing cables.

## 6.6 Spacer Comparison

Borehole #2 was examined in the subsurface shot to see if a difference was apparent between the inner and outer spacers inside the borehole, which can be seen in Figure 34. For the hammer shot, the difference between the fiber spacer interactions seems to be very clear. The first half of the dataset corresponds to the cable being pressed against the borehole wall, and the second half of the dataset corresponds to the cable being embedded in the grout filling the borehole. Stronger signal is observed for the first half of the data where the cable is well-coupled to the rock. The second half of the data, with the fiber on the inside of the spacer, is quieter.

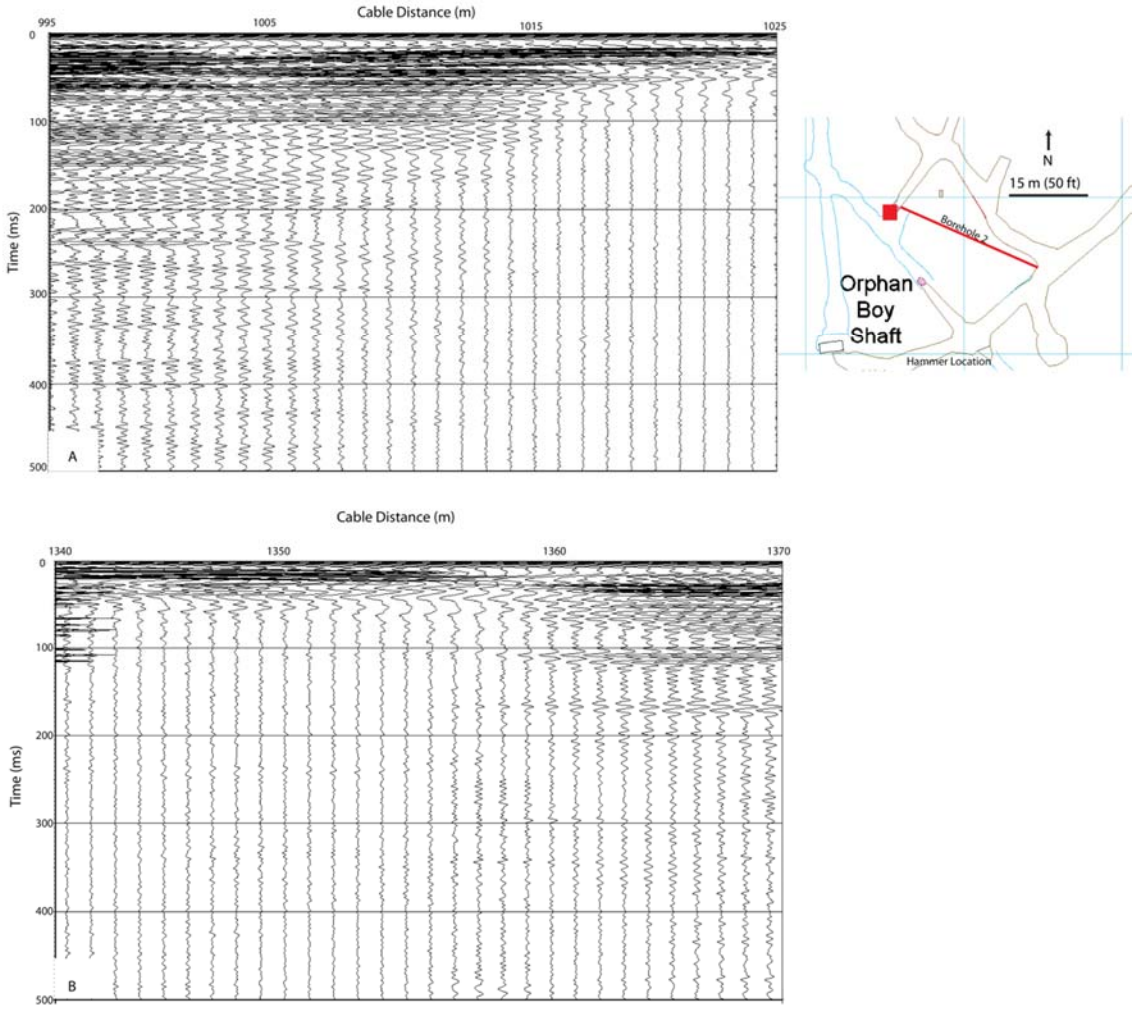


**Figure 34: Vertical hammer shot (location seen on the right) and a view of Borehole #2 on the OCC cable and Borehole #1 on the Brugg Strain.**
(A) The first half of the borehole uses the outside spacer and the second half of the borehole uses the inside spacer.
(B) Data from borehole #1 which used the outer space for the entirety of the borehole. The quality of data stays relatively constant throughout the entire borehole.

## 6.7 Subsurface Explosive Source Experiments

The subsurface explosive experiments conducted for this project were unsuccessful. Figure 35 shows response of the entire OCC fiber cable to the first explosive shot. The DAS data for this cable have a high amplitude burst of energy that does not seem to decrease in amplitude in most places. The data stay noisy in many locations for the entire 10 s recording window. The energy also seems to arrive across large segments of cable at the same time, rather than moving

along the fiber as a wave. The dataset also has large segments with almost no signal, likely due to the fact that long portions of the cable that were not coupled to the rock. Similar issues with the DAS data can be seen in Figure 36, which shows the data from the OCC cable from the fourth explosion. The OCC cable dataset contains a gap of no data in roughly the first 5 ms. Similar to the first explosion, energy arrives at large segments of the cable at the same time, regardless the distance between a trace and the explosion. Figure 37 shows a single trace of the DAS and geophone data from a location on the Northwest wall of the pillar where the cable was tightly coupled to the rock. While some peaks line up with each other between the two traces, the

DAS trace is dominated by noise, even after a filter had been applied. The DAS trace does not line up with the geophone trace.

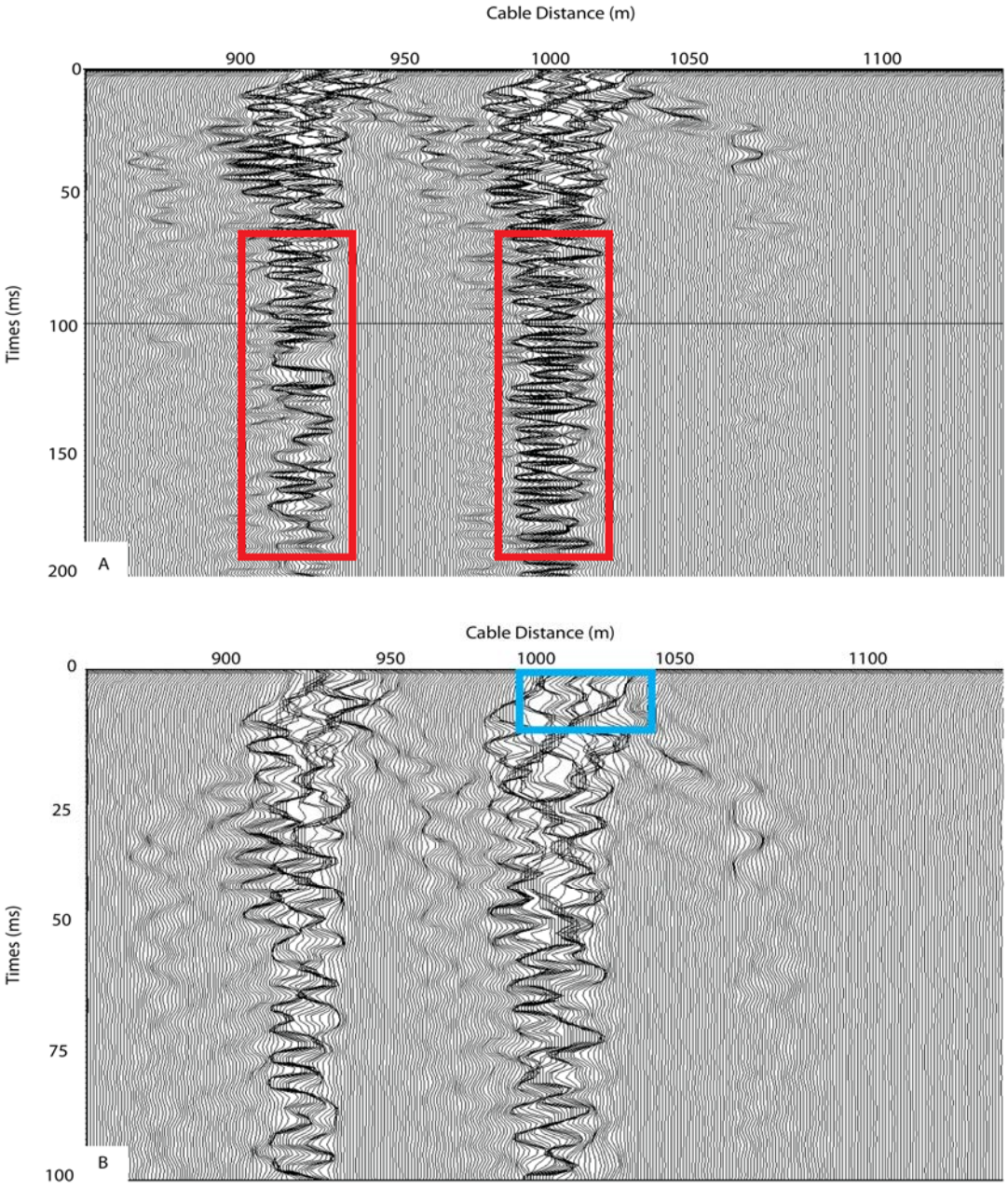


**Figure 35: OCC fiber during the first explosion.**
(A) First 200 ms of data from the OCC cable during the first explosion. The red box highlights areas that had high amplitude energy for the entirety of the shot.
(B) First 100 ms of data from the OCC cable during the first explosion. The blue box highlights and area where multiple traces had very similar arrival times, regardless of their distance from the explosion.

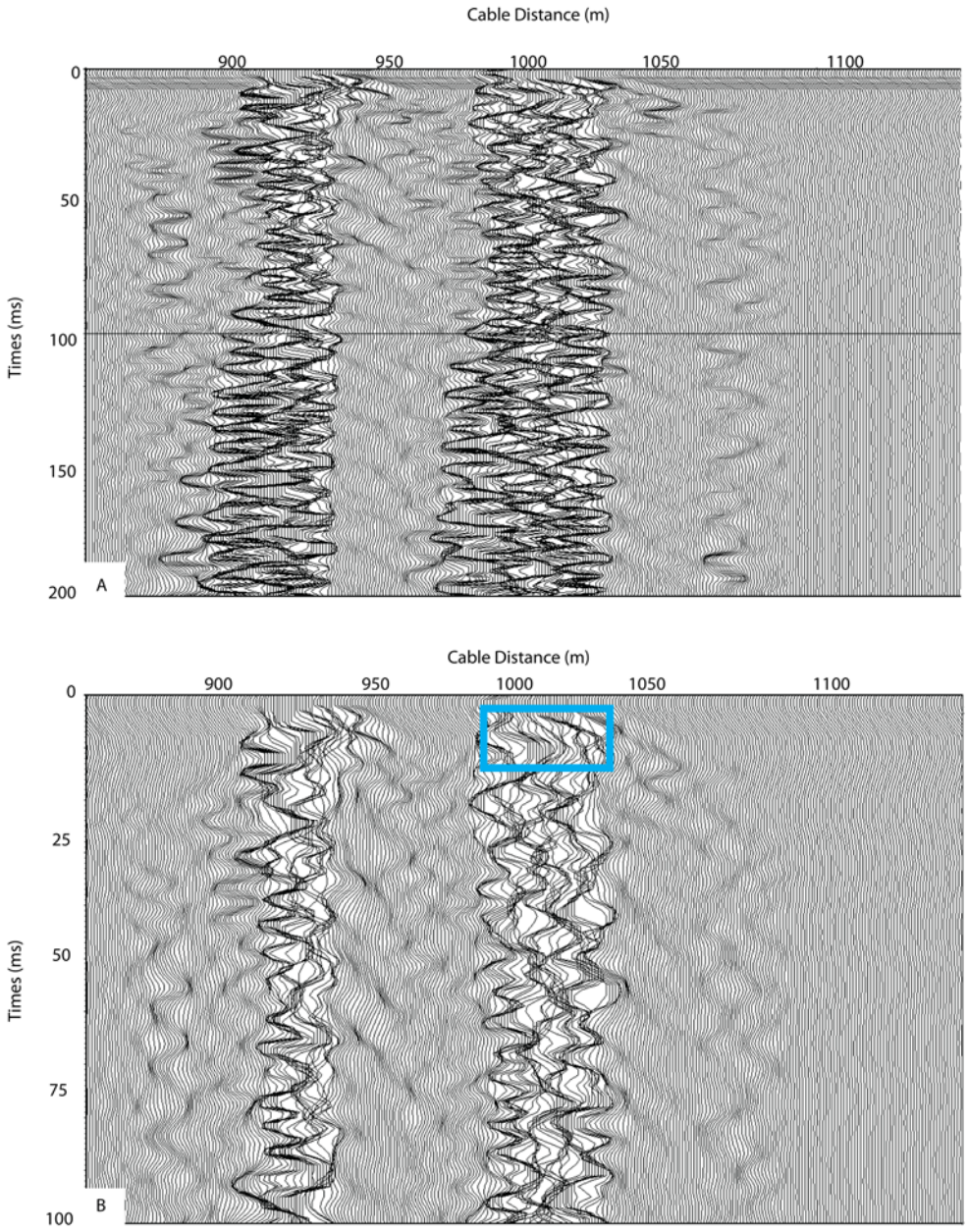


**Figure 36: OCC fiber during the fourth explosion.**
(A) First 200 ms of data from the OCC cable during the fourth explosion. Large area can be seen that stayed noisy for the entirety of the shot. A ~5 ms gap can be seen at the top of the data. (B) First 100 ms of data from the OCC cable during the fourth explosion. The blue square highlights large areas that had very similar traces regardless of distance from the source. The gap in the top of data can also be seen.

One possible explanation for traces with continuous large amplitude energy and a high amount of noise from the explosive shot could be the airwave of the explosion. With a large blast in the mining setting, the airwave could cause noise in the parts of the cable cemented around the

pillar as the air traveled through the mine. However, if the airwave were the cause of the noise, the traces inside of the boreholes would not experience the same problems due to the cable being securely cemented inside the borehole. Figure 38 shows traces from inside borehole 1. Borehole 1 would be mostly in line with the explosion, and should therefore be able to accurately show the increasing arrival time as the distance from the explosion increased. Instead, we see a very similar pattern across all 20 traces of the borehole, highlighted with a red box, which suggests a problem with the entire underground section of the loop. We found that the blast compromised the loop for an unknown reason, and caused the data to be unusable from the explosive shots, even inside of the boreholes.

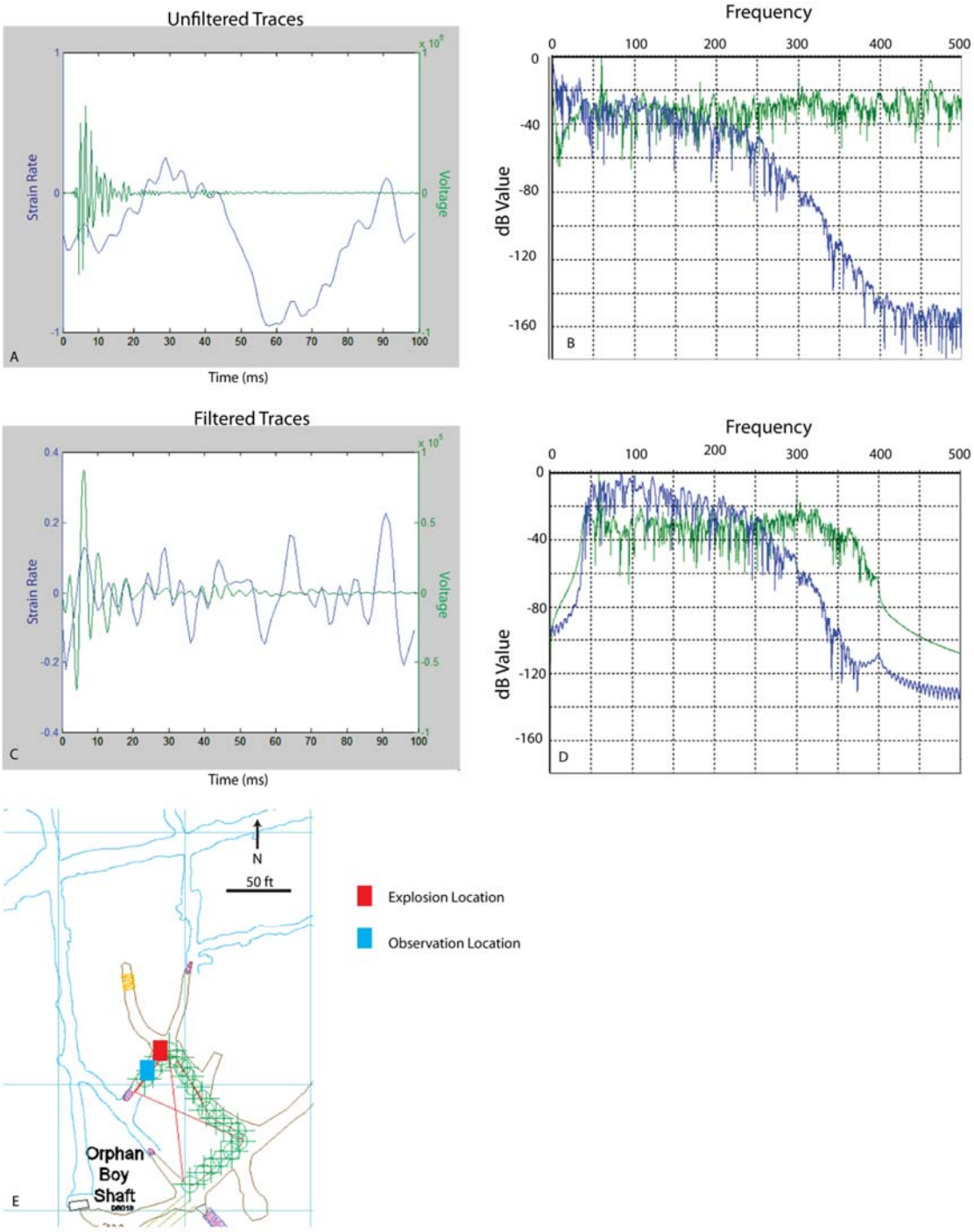


**Figure 37: Single trace comparison of the DAS (blue) and geophone data (green) from the fourth explosion.**

(A) Unfiltered traces from the rotated X component geophone and the OCC cable.
(B) Frequency spectrum for the geophone and DAS data before a filter was applied.
(C) Filtered traces from the rotated X component geophone and the OCC cable.
(D) Frequency spectrum after a bandpass filter had been applied.
(E) Map of shot and receiver location.

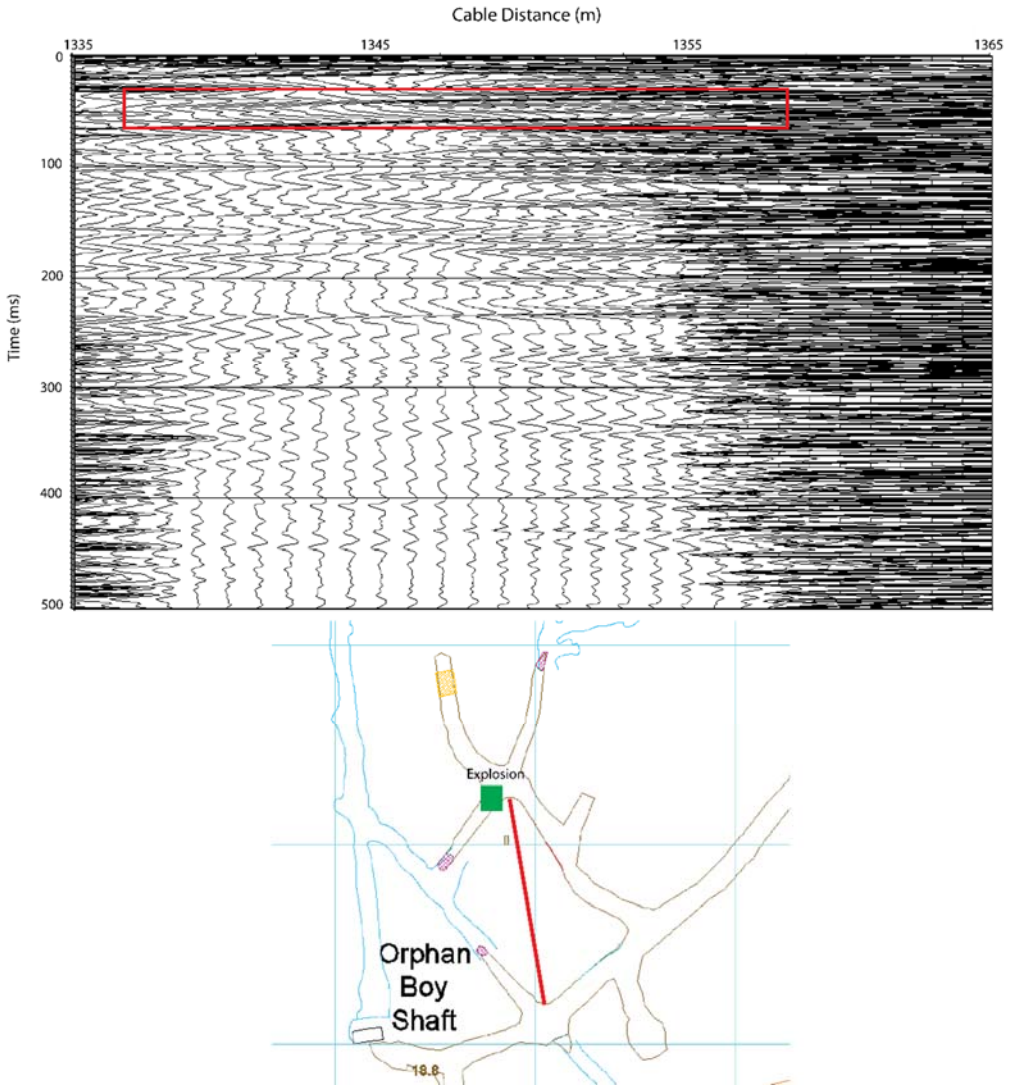


**Figure 38: Data from the fourth explosion inside the borehole on the Brugg strain cable.**
(A) The fiber traces from inside of the borehole on the Brugg strain cable. The red box highlights areas where traces are very similar regardless of their distance from the explosion.
(B) The location of the explosion and the borehole being examined.

The final comparison done using the explosive data was to examine data measured on the ground surface. These data were separated from the explosions by 30 meters of rock, meaning the data should not have been affected by any kind of airwave in the mine. Figure 39 shows the comparison of a location on the North side of the surface loop during the fourth explosion that seems to suffer from the same problems of noise in the DAS data as the underground loop during the explosion.

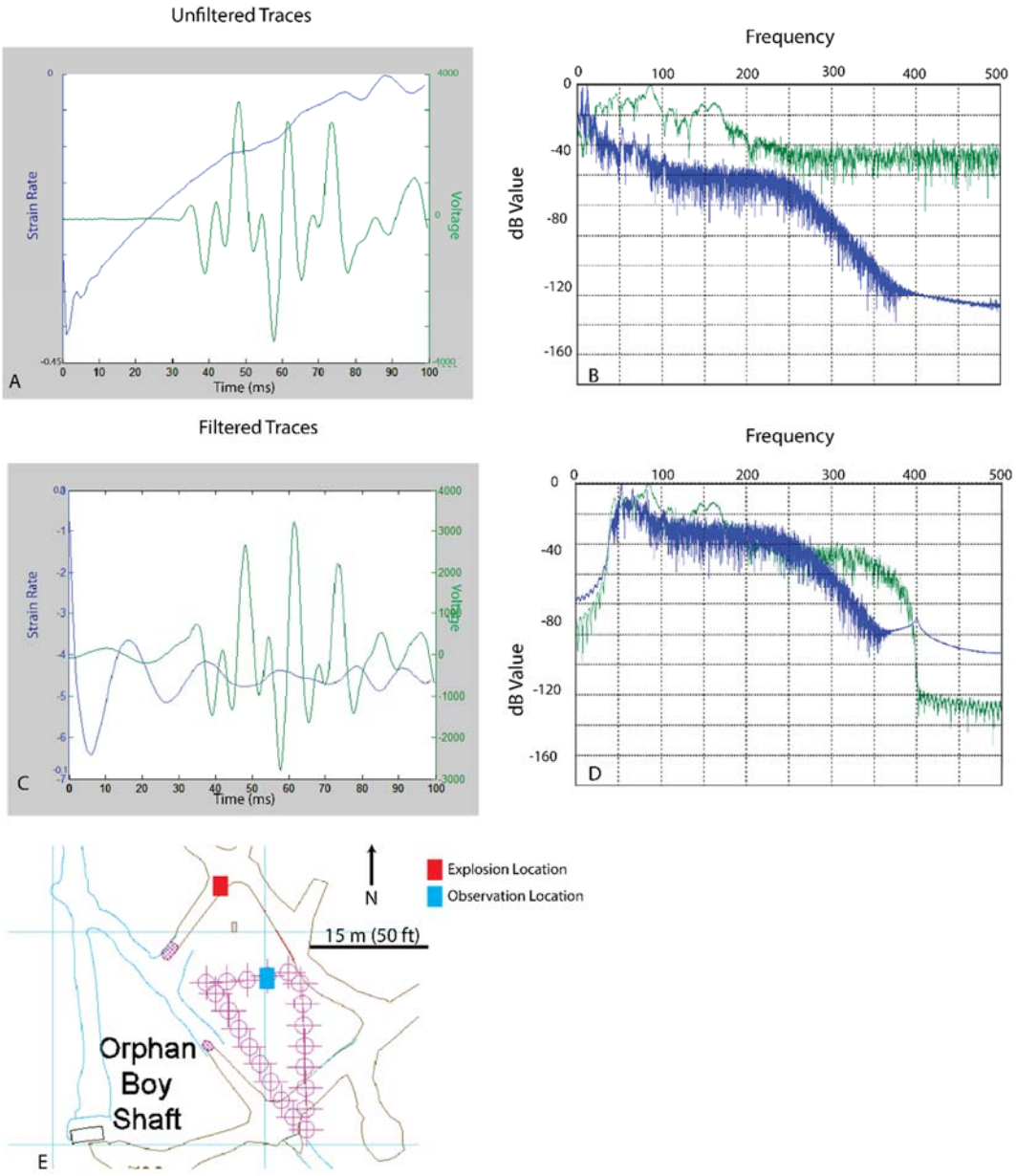


**Figure 39: Single trace comparison of the fiber (blue) and geophone data (green) from the fourth explosion observed on the surface using the Brugg strain cable and the X component of the geophones.**

(A) Unfiltered traces of the DAS data and the geophone before a filter was applied.
(B) Frequency of the geophone and DAS data before a filter was applied.
(C) Filtered traces from the geophone and DAS data from the surface during the fourth explosion. Similar to the subsurface traces, the traces do not agree with each other for the most part. However, after 80 ms, the traces seem to line up with a 180° phase shift
(D) Frequency content of the geophone and DAS data after a bandpass filter had been applied
(E) The location of the explosion, which was underground, and the observation location, which was on the surface.

Although the geophone and fiber optic cable data from the surface locations do not line up in the early part of the traces, they do seem to align near 80 ms with a 180° phase shift. This might suggest that the surface loop handled the explosion better than the underground fiber optic cable, but the evidence is not conclusive.

A possible explanation for the poor performance of the explosive source could involve the reference loop inside of the DAS interrogator. The interrogator used a reference loop in order to acquire a baseline reading of the background noise. The reference loop was possibly compromised by the size of the source. However, this explanation is not very likely, due to the improved performance of the surface portion of the loop, which were the first traces recorded. All four cables were monitored using a single channel in the interrogator, which means if the reference loop was compromised, all cables would likely see the effect.

## 6.8 Trapped Miner Testing and Wall Hits

The original goal of both the trapped miner tests as well as the shots that involved hitting the wall instead of a plate was to see if DAS data could be used to find a source location. Locating a source by measuring acoustic data is extremely dependent on time, and even small differences in arrival times can lead to very different source location solutions. In order to perform triangulation, one would need to pick both P- and S-wave arrivals. Picking both P- and S-wave arrivals was not possible with this data set, which inhibited this experiment. Figure 40 shows an example of a trapped miner shot. Some energy can be seen, and the experiment shows promise for future tests, but source location could not be determined from these tests.

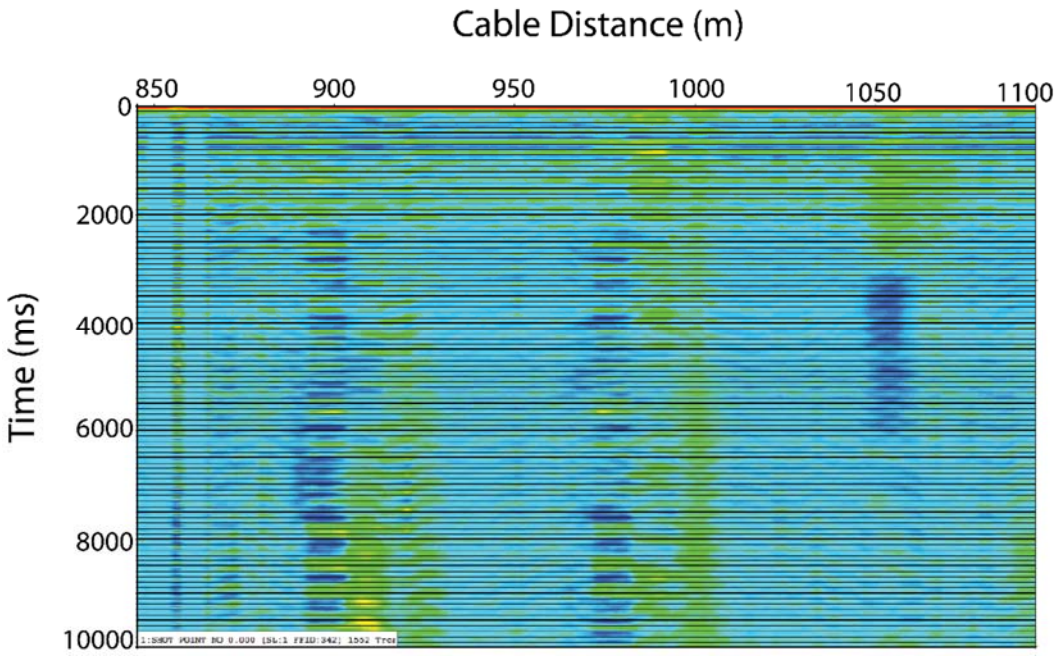


**Figure 40: Example of a trapped miner shot on the OCC strain cable.** The dark blue spots are possibly signal from the trapped miner taps.

# 7. Conclusions

Geophones and DAS are both types of instrumentation that can accurately capture seismic data. However, the two methods both have their strengths and weaknesses. At the current time and with the system used for this study, DAS does not seem like a method that is suitable for high frequency data. The frequency spectra examined for this project showed that DAS recording frequencies dropped in amplitude much quicker than the recording frequencies of geophones. This project would also suggest that DAS is not suited for large sources that are extremely close to the fiber-optic network; however, this could be due to the setup of the cable in this specific case. The explosive source did not provide a significant amount of usable data. All of the subsurface traces showed almost no alignment between DAS and geophone data. The surface traces did show slight agreement, which suggests that the cable that was further from the source could be usable. The cause of the poor data in the subsurface could not be determined from this study. Relatively good agreement was seen in hammer datasets, specifically using the shear sources.

The type of fiber-optic cable does not have a significant effect on the quality of data from DAS. All three types of cable that were in the mine appeared to have very similar results, and one brand did not clearly outperform the others. Instead, the coupling of the cable to the rock appears to be the most important factor. The importance of coupling was also seen inside the borehole, where the outside spacer with the cable pressed up against the rock outperformed the spacer with the cables on the inside. A 180-degree phase difference did appear between the Brugg temperature and both types of strain cables. We were not able to determine if this phase difference negatively affected the dataset. DAS also performs best when the particle motion

produced by a source is in line with the orientation of the cable, seen in the comparisons between vertical and shear sources.

DAS is extremely reliant on the setup of the survey. Areas in this project that were poorly coupled did not provide usable data. The setup of the DAS for this specific project also led to the previously unknown triggering problem that compromised the early samples of the DAS traces and first break times of all of the shots.

One area where DAS out performs three component geophones is station spacing and the amount of data from a given area. The geophones in this project were spaced every three meters. The DAS is essentially a continuous sensor with traces sampled out every one meter. Although the DAS system does have a gauge length associated with recording, the gauge length operates as a moving average and provides a unique data point at each meter. The increased resolution could be useful in a mine setting where it was essential to capture small rock bursts. Although the DAS system was set up for a 10 m gauge length for this project, the increased amount of data from a smaller station spacing could allow for better monitoring of a mine. For future projects, a smaller or larger gauge length could be discussed to better suit the project needs.

Our geophone system was designed to start recording for a small amount of time after a trigger. Seismometers can be permanently installed that continuously record, but are typically more expensive than our system, which makes it difficult to have close station spacing through a mine. DAS is designed for continuous recording, which allows DAS systems to be a great choice for extended monitoring of a mine.

## 8. References

Barfoot, D.A., 2013, Efficient vertical seismic profiling using fiber-optic distributed acoustic sensing and real-time processing: Second EAGE Workshop on Borehole Geophysics.

Barr. F, and J. Sanders, 1989, Attenuation of water-column reverberations using pressure and velocity detectors in a water-bottom cable: SEG Technical Program Expanded Abstracts 1989, 653-656.

Barr, F. and J. Sanders, Method for correcting impulse response differences of hydrophones and geophones as well as geophone coupling to the water-bottom in dual-sensor, bottom-cable seismic operations: E.S. Patent 5163028A.

Brown, J. R., R. Stewart, and D. Lawton, 2002, A proposed polarity standard for multicomponent seismic data: Geophysics, **67 (4)**, 1028-1037.

Cannon, R. T., and F. Aminzadeh, 2013, Distributed acoustic sensing: state of the art: SPE Digital Energy Conference.

Carpenter, C., 2017, Fiber-Optic Leak-Detection Project: Society of Petroleum Engineers **69 (4).**

Castongia, E., H. Wang, N. Lord, D. Fratta, M. Mondanos, and A. Chalari, 2017, An experimental investigation of distributed acoustic sensing (DAS) on lake ice: Journal of Environmental & Engineering Geophysics, **22 (2),** 167-176.

Chen, J., T. Chang, Q. Fu, J. Lang, W. Gao, Z. Wang, M. Yu, Y. Zhang, and H. Cui, 2016, A fiber-optic interferometric tri-component geophone for ocean floor seismic monitoring: Sensors.**17(1),** 47-59.

Crampin, S. 1985, Evaluation of anisotropy by shear-wave splitting: Geophysics, **50,** 142-152.

Daley, T. M., D. E. Miller, K. Dodds, P. Cook, and Freifeld, B. M., 2015, Field testing of modular borehole monitoring with simultaneous distributed acoustic sensing and

geophone vertical seismic profiles at Citronelle, Alabama: Geophysical Prospecting, **64**, 1318-1334.

Daley, T. M., B. M. Freifeld, J. Ajo-Franklin, S. Dou, R. Pevzner, V. Shulakova, and S. Lueth, 2013, Field testing of fiber-optic distributed acoustic sensing (DAS) for subsurface seismic monitoring: The Leading Edge, **32**, 699-706.

Dean, T., T. Cuny, and A. Hartog, 2016, The effect of gauge length on axially incident P-waves measure using fibre optic distributed vibration sensing: Geophysical Prospecting, **65,** 184-193.

Fahy, F.J., 2003, Some applications of the reciprocity principle in experimental vibroacoustics: Acoutical Physics, **48(2),** 217-229.

Feigl, K. L., and P. Team, 2017, Overview and Preliminary Results from the PoroTomo Project at Brady Hot Springs, Nevada: Poroelastic Tomography by Adjoint Inverse Modeling of Data from Seismology, Geodesy, and Hydrology: Proceedings, 42nd Workshop on Geothermal Reservoir Engineering, 1-15.

Goodman, R. E., 1993, Engineering Geology: Rock in Engineering Construction: John Wiley & Sons, Inc.

Hornby, B., F. Bostick, B. Williams, K. Lewis, and P. Garossino, 2004, Field test of a permanent in-well fiber-optic seismic system: Geophysics, **70 (4),** E11-E19.

Kendall, R., 2014, A comparison of trenched distributed acoustic sensing (DAS) to trenched and surface 3C geophones – Daly, Manitoba, Canada: SEG Technical Program Expanded Abstracts 2014, 5183.

Kuvshinov, B. N., 2016, Interaction of helically wound fibre-optic cables with plane seismic waves, interaction of fibre-optic cables: Geophysical Prospecting, **64 (3)**, 671-688.

Lancelle, C., 2016, Distributed acoustic sensing for imaging near-surface geology and monitoring traffic at Garner Valley, California: Ph. D dissertation, The University of Wisconsin – Madison.

Liu, X, B. Jin, Q. Bai, Y. Wang, D. Wang, and Y. Wang, 2016, Distributed fiber-optic sensors for vibration detection: Sensors, **16 (8)**, 1164-1195.

Mateeva, A., J. Mestayer, B. Cox, D. Kiyaschenko, P. Wilis, J. Lopez, S. Grandi, K. Hornman, P. Lumens, A. Franzen, D. Hill, and J. Roy, 2012, Advances in distributed acoustic sensing (DAS) for VSP: SEG Technical Program Expanded Abstracts 2012, 4609.

Mestayer, J., B. Cox, P. Wills, D. Kiyashchenko, J. Lopez, M. Costello, S. Bourne, G. Ugueto, R. Lupton, G. Solano, D. Hill, and A. Lewis, 2011, Field trials of distributed acoustic sensing for geophysical monitoring: SEG Technical Program Expanded Abstracts 2011, 4253-4257.

Parker, T., S. Shatalin, and M. Farhadiroushan, 2014, Distributed Acoustic Sensing – a new tool for seismic applications: First Break, **32,** 61-69.

Poczęsny, T., K. Prokopczuk, P. L. Makowski, and A. W. Domański, 2011, Optical fiber macro-bend seismic sensor for real-time vibration monitoring in harsh industrial environment: SPIE Proceedings, 8082.

Rose, E., 2017, Characterization of granite and subsequent ground control management plan at Orphan Boy Mine-Butte, Montana: M.S. thesis, Montana Tech of the University of Montana.

Tanimola, F., and D. Hill, 2009, Distributed fibre optic sensors for pipeline protection: Journal of Natural Gas Science and Engineering, **1**, 134-143.

Wu, H., W. Wong, Z. Yang, P. Wills, J. Lopez, Y. Li, B. Blonk, B. Hewett, and A. Mateeva, 2015, Dual-well 3D vertical seismic profile enabled by distributed acoustic sensing in deepwater Gulf of Mexico: Interpretation, **5**, SW11-SW25.

Yilmaz, Ö., 2001, Seismic Data Analysis: Processing, Inversion, and Interpretation of Seismic data: Society of Exploration Geophysicists.

# 9. Appendix: Tap Tests

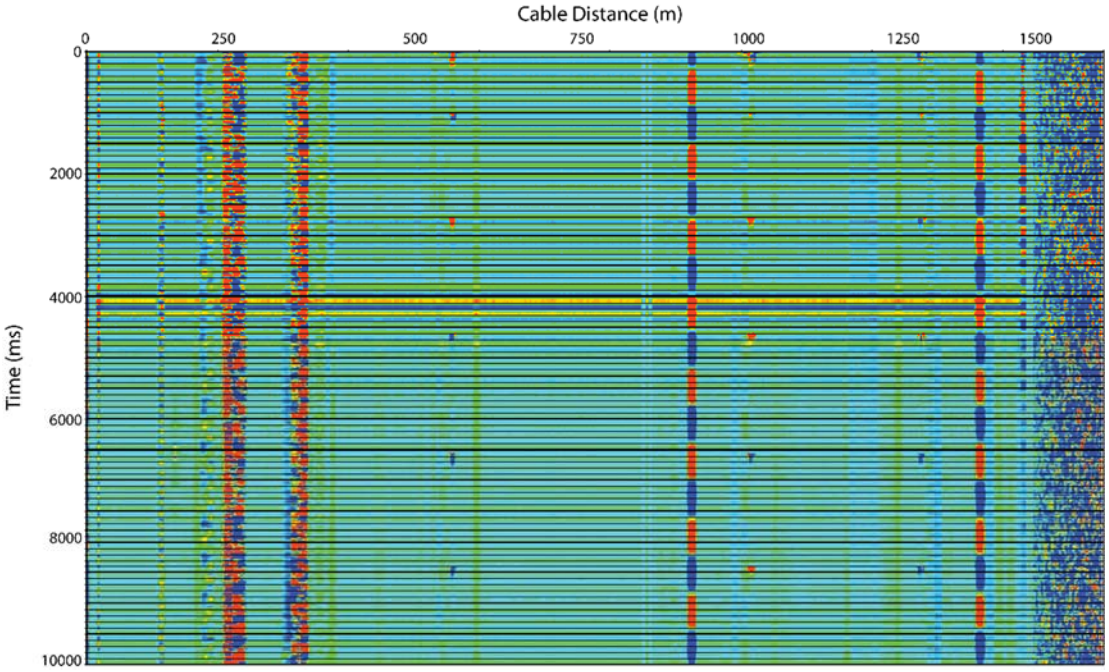


**Figure 41: Tap test at geophone station 1.** Taps were picked at 558, 1010, and 1279 m.

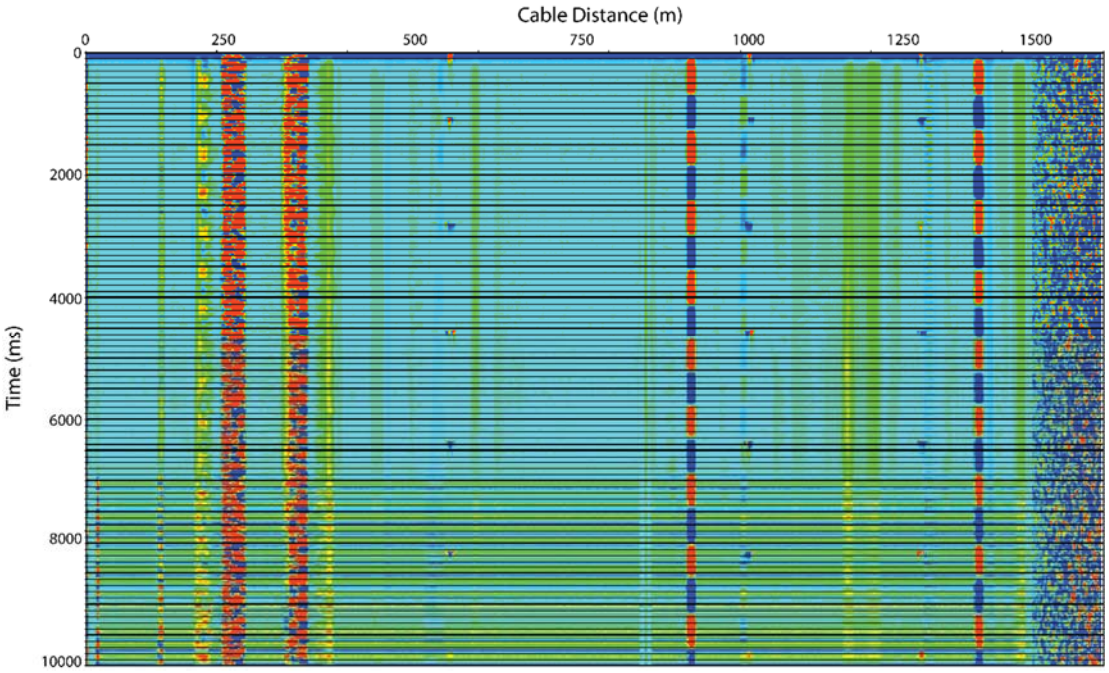


**Figure 42: Tap test at geophone station 2.** Taps were picked at 560, 1015, and 1285 m.

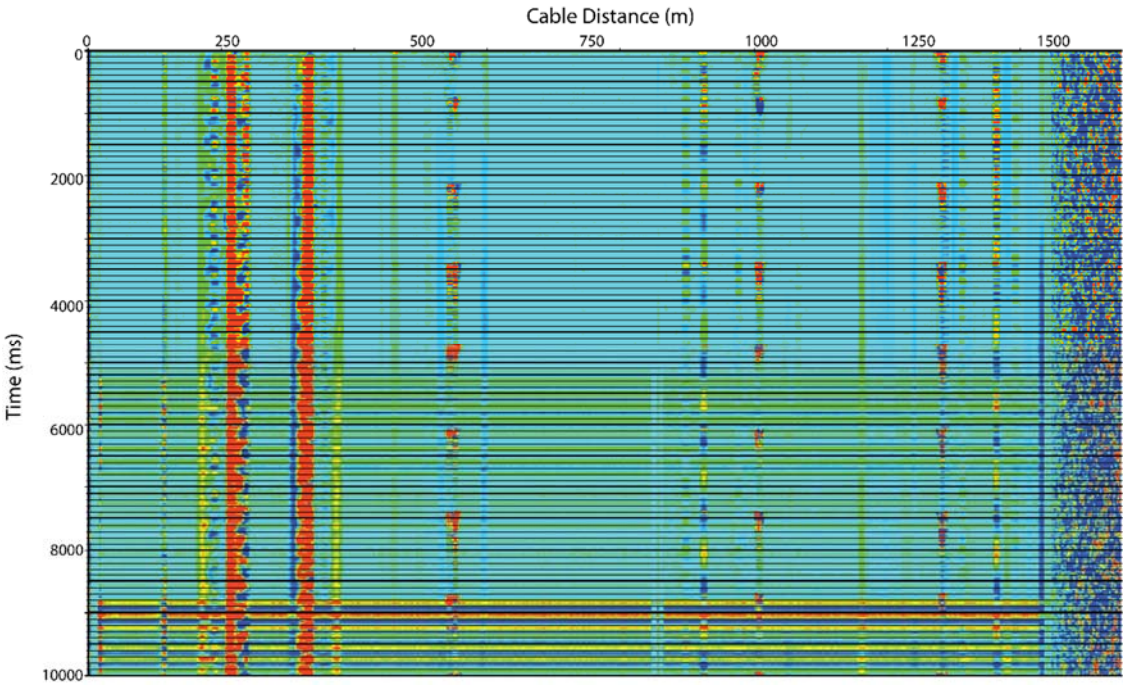


**Figure 43: Tap test at geophone station 3.** Taps were picked at 549, 1009, and 1281 m.

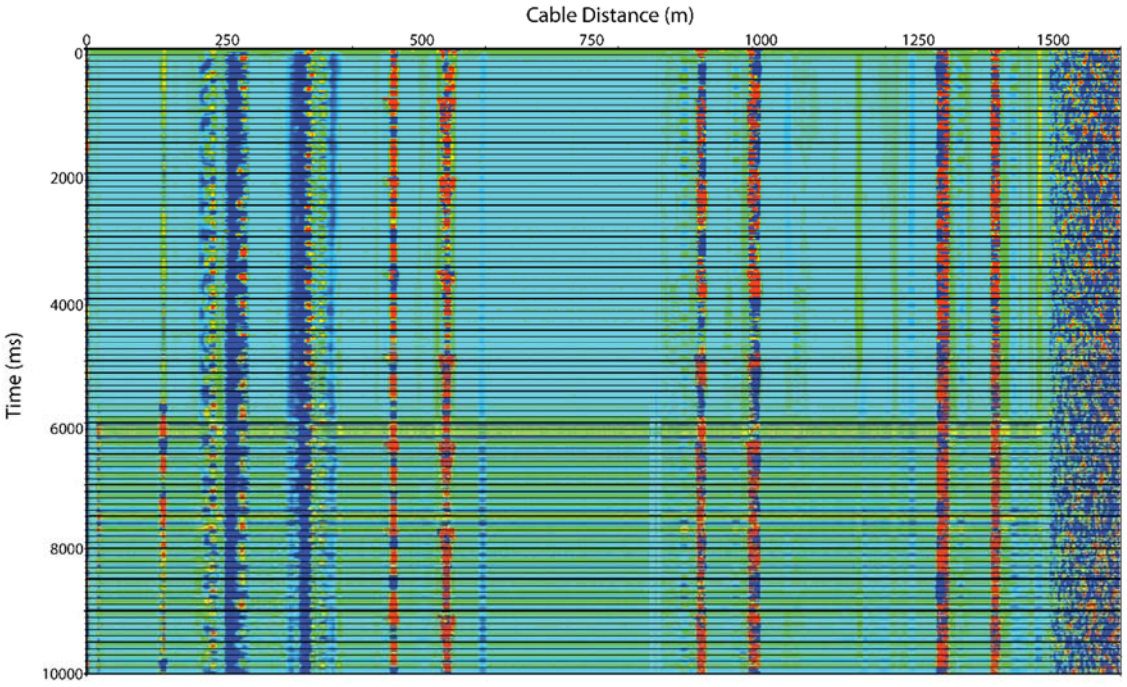


**Figure 44: Tap test at geophone station 4.** Taps were picked at 461, 539, 925, 1003, 1286, and 1367 m.

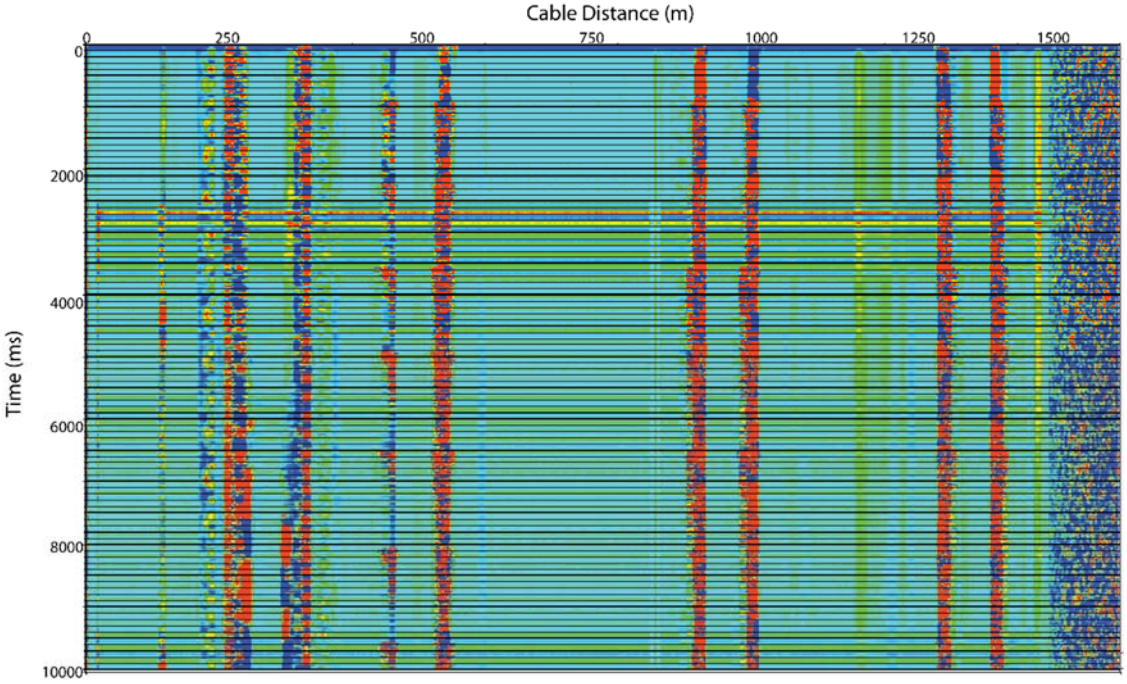


**Figure 45: Tap test at geophone station 5.** Taps were picked at 458, 541, 922, 1004, 1289, and 1367 m.

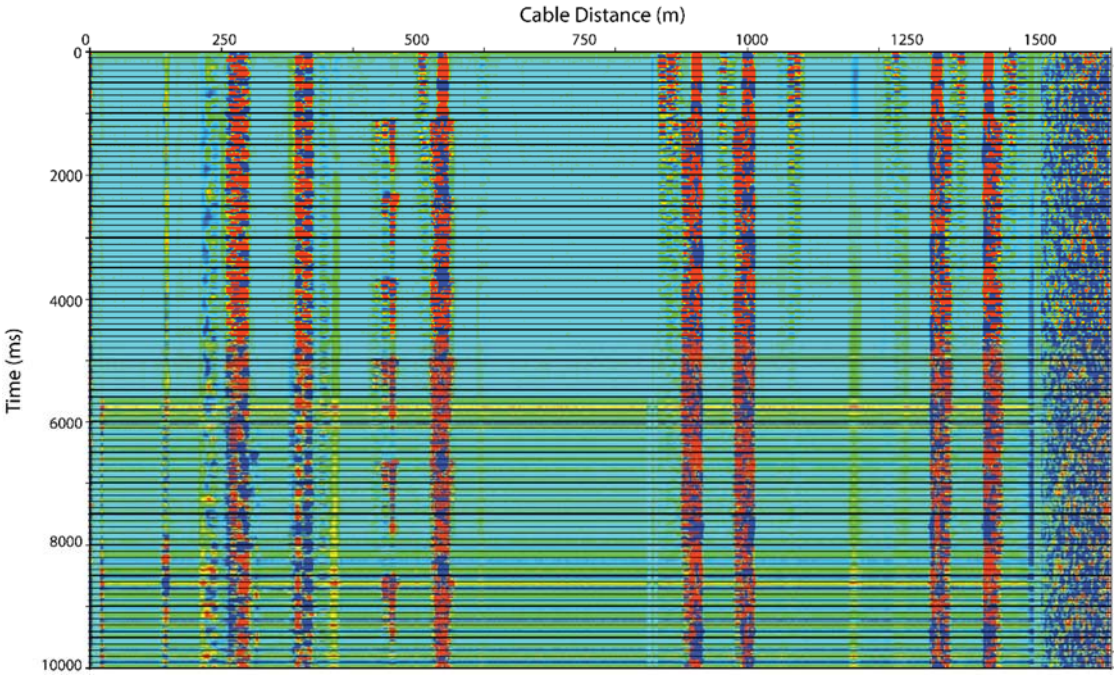


**Figure 46: Tap test at geophone station 6.** Taps were picked at 458, 541, 922, 1001, 1294, and 1378 m.

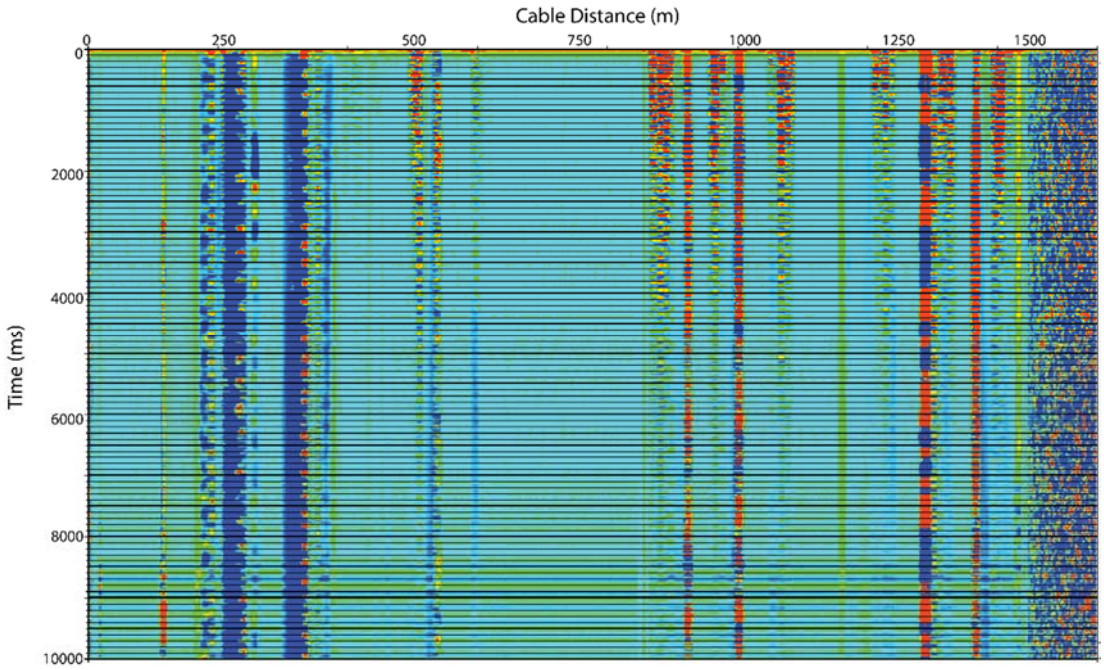


**Figure 47: Tap test at geophone station 7.** Taps were picked at 504, 542, 926, 1007, 1328, and 1404 m.

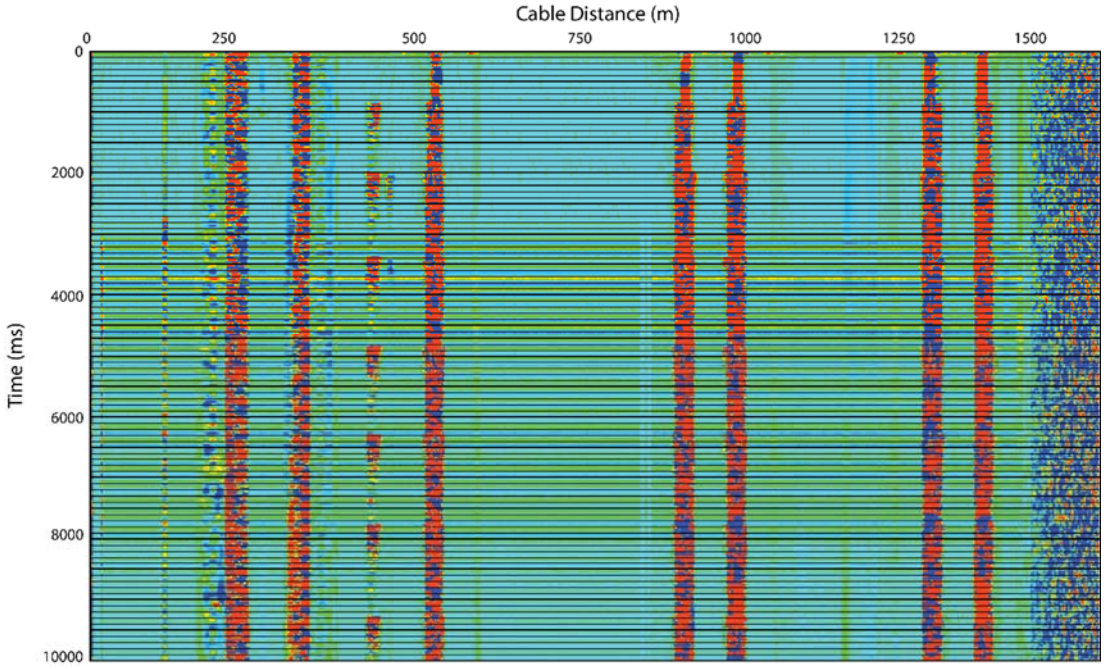


**Figure 48: Tap test at geophone station 8.** Taps were picked at 434, 526, 916, 996, 1294, and 1378 m.

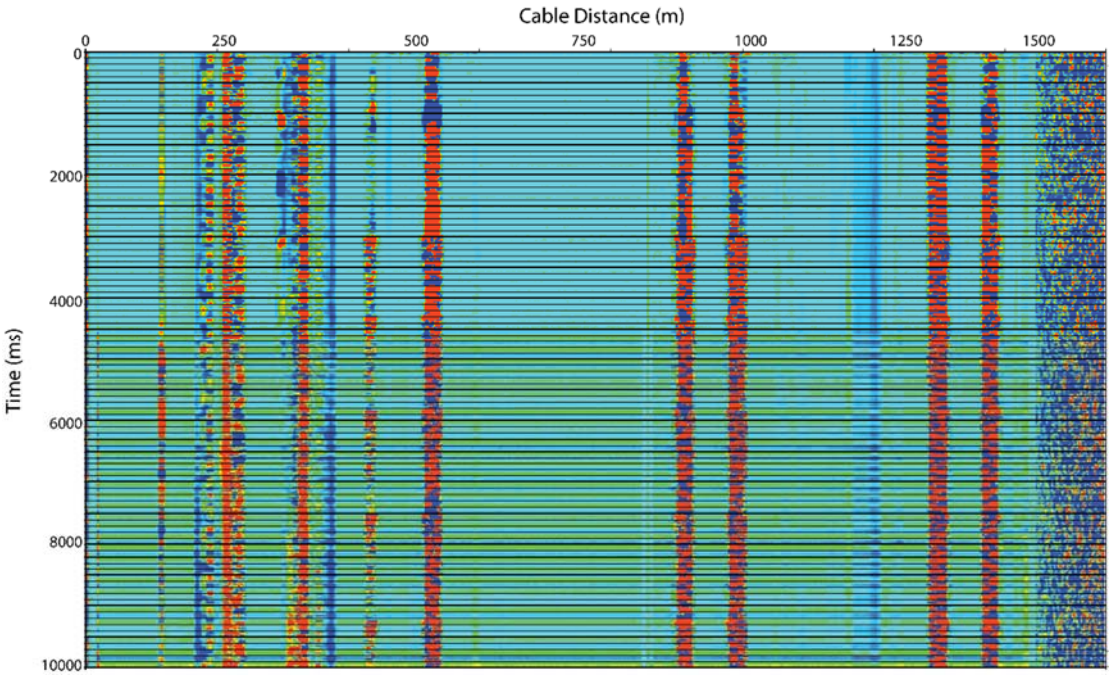


**Figure 49: Tap test at geophone station 9.** Taps were picked at 431, 527, 911, 990, 1307, and 1385 m.

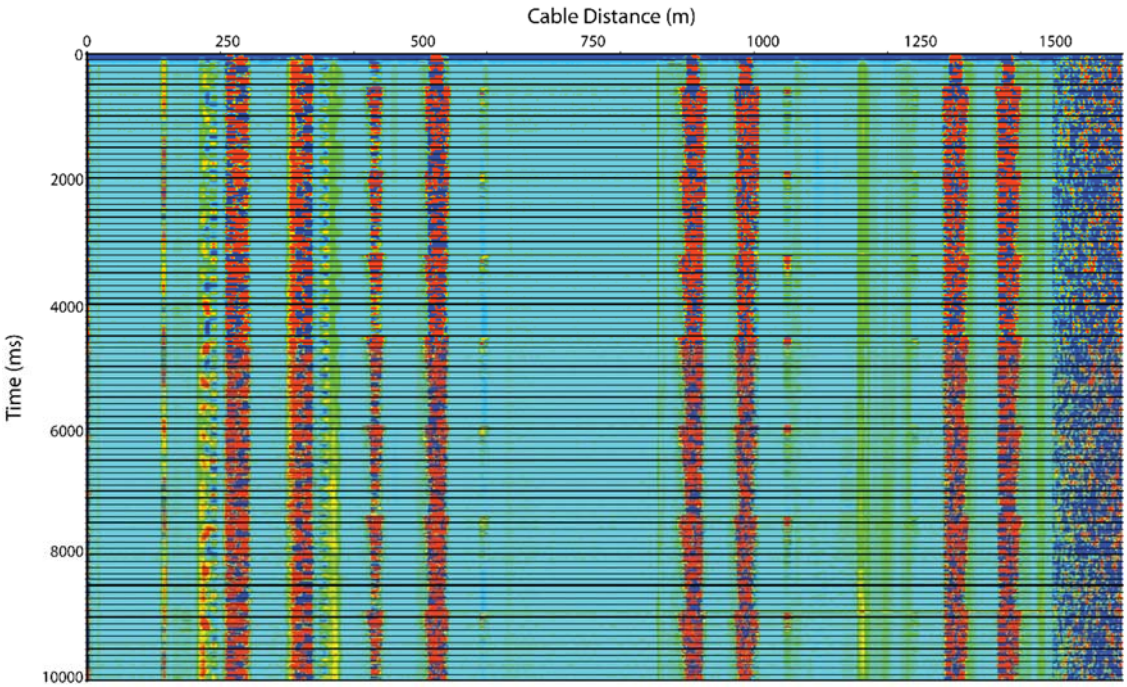


**Figure 50: Tap test at geophone station 10.** Taps were picked at 441, 529, 600, 913, 993, 1054, 1242, 1302, and 1383 m.

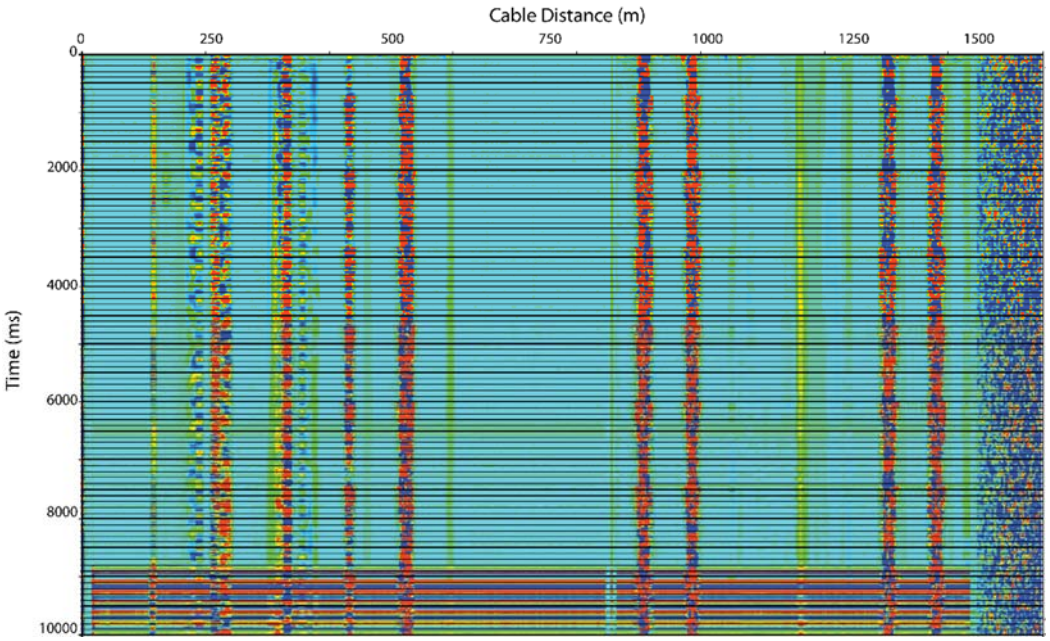


**Figure 51: Tap test at geophone station 11.** Taps were picked at 429, 529, 913, 985, 1313, and 1377 m.

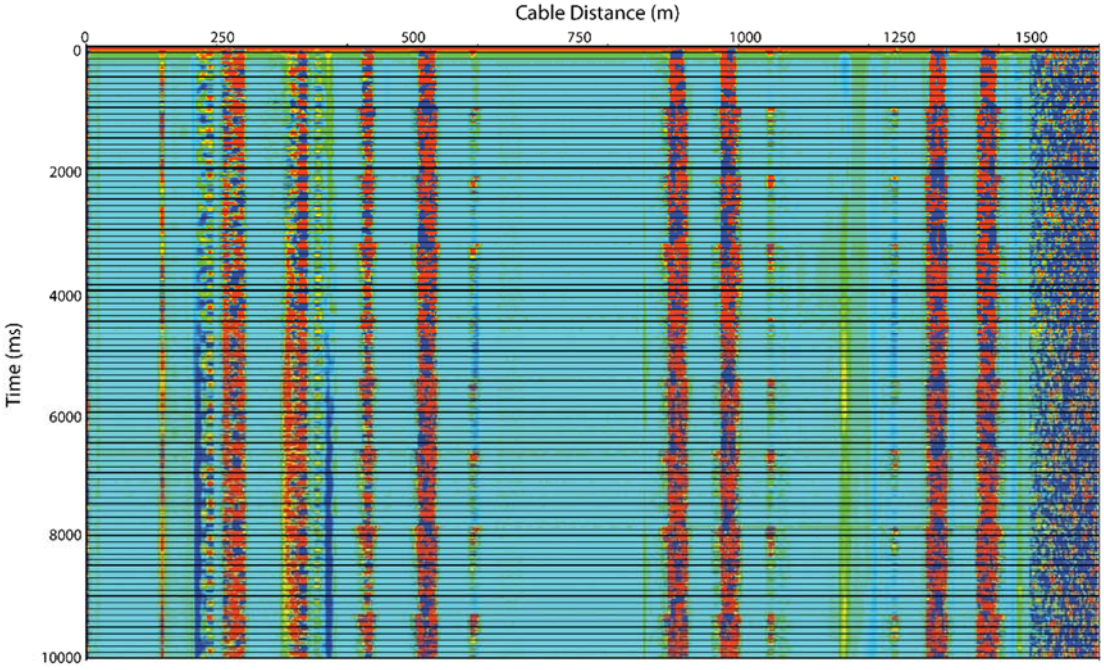


**Figure 52: Tap test at geophone station 12.** Taps were picked at 433, 520, 592, 911, 985, 1053, 1243, 1302, and 1389 m.

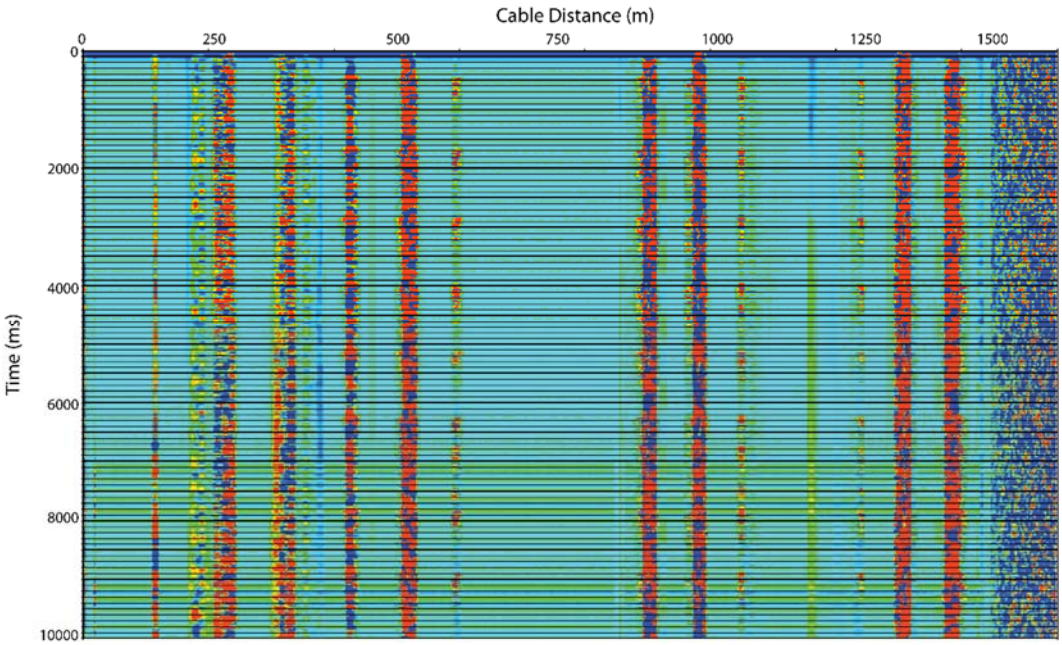


**Figure 53: Tap test at geophone station 13.** Taps were picked at 431, 523, 596, 907, 985, 1054, 1239, 1305, and 1388 m.

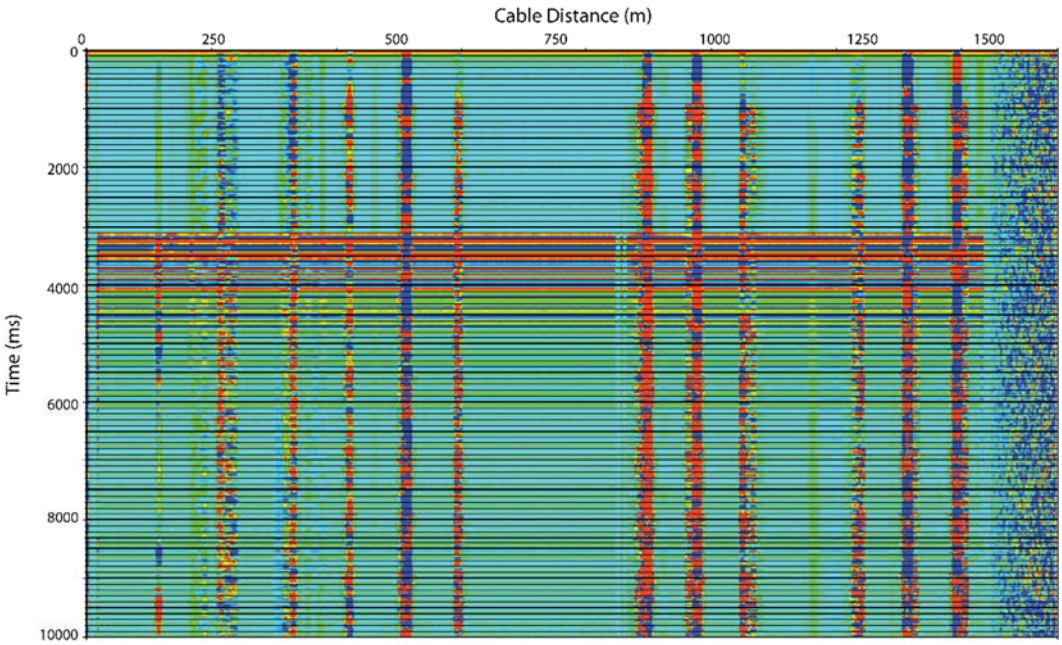


**Figure 54: Tap test at geophone station 14.** Taps were picked at 422, 512, 597, 895, 976, 1050, 1236, 1316, and 1400 m.

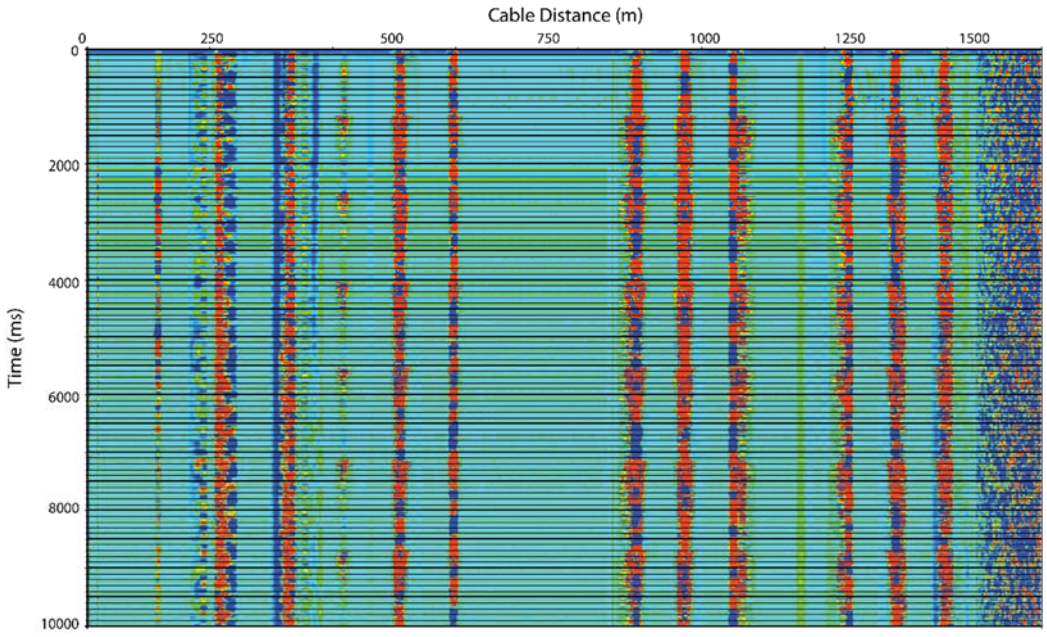


**Figure 55: Tap test at geophone station 15.** Taps were picked at 422, 508, 599, 893, 969, 1061, 1242, 1321, and 1392 m.

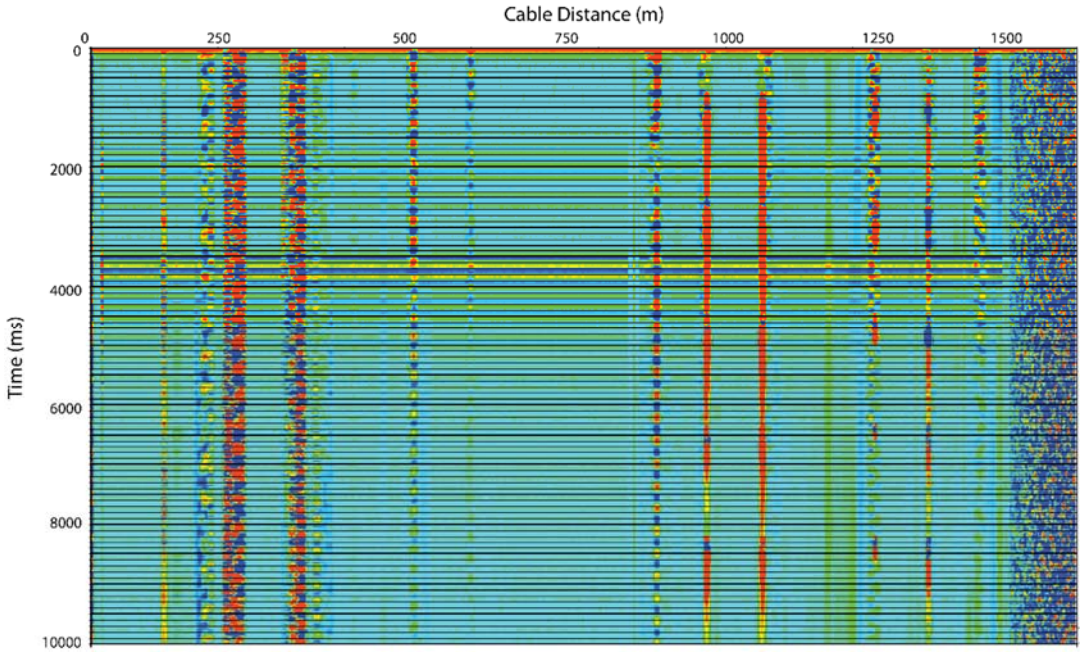


**Figure 56: Tap test at geophone station 16.** Taps were picked at 504, 963, 1065, 1236, 1319, and 1397 m.

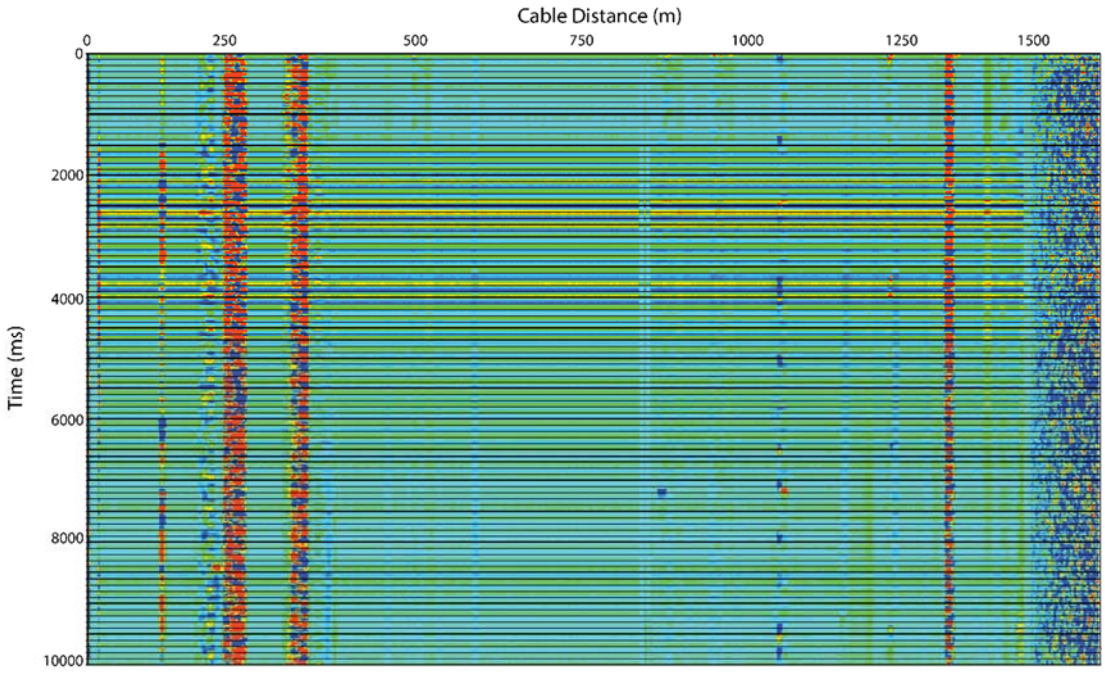


**Figure 57: Tap test at geophone station 17.** One tap was picked at 1323 m.

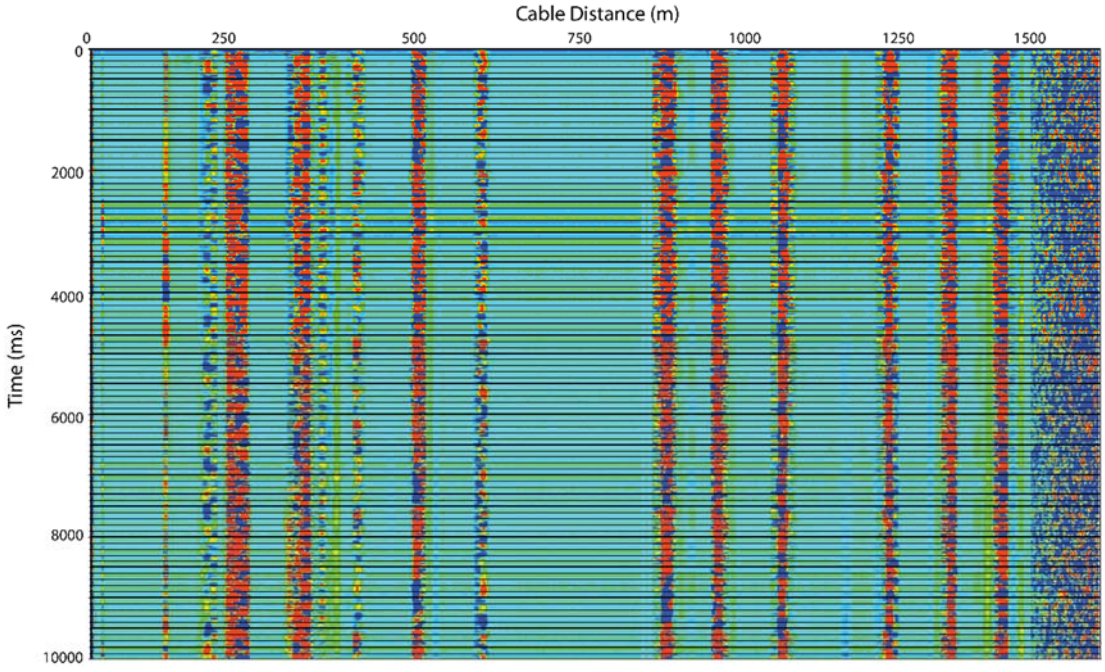


**Figure 58: Tap test at geophone station 18.** Taps were picked at 414, 502, 602, 981, 965, 1070, 1228, 1320, and 1405 m.

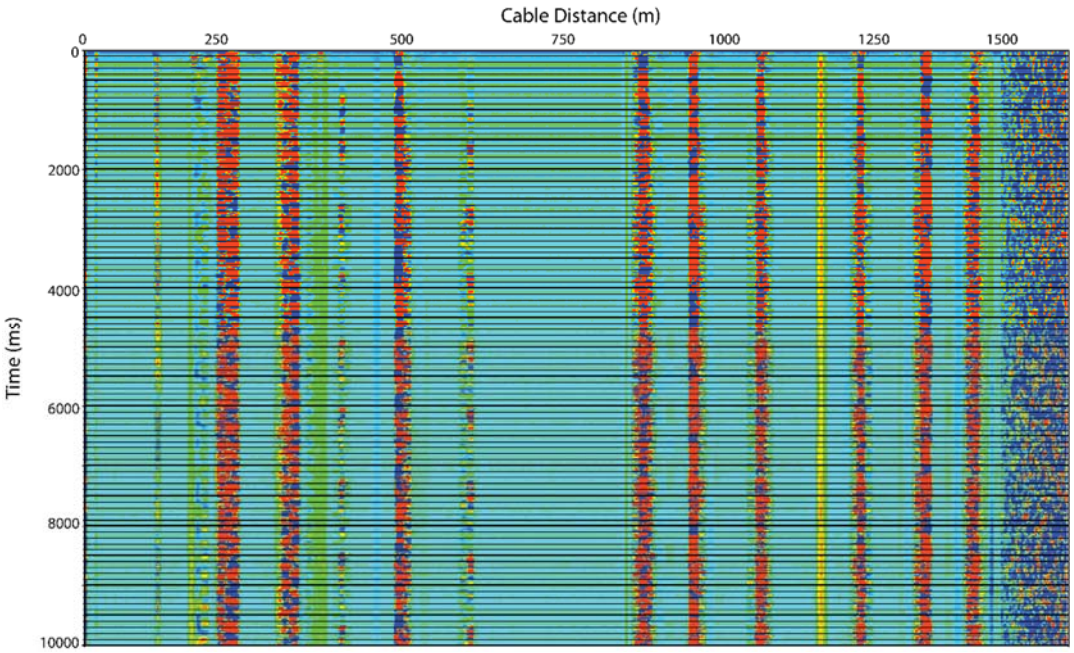


**Figure 59: Tap test at geophone station 19.** Taps were picked at 410, 505, 612, 886, 963, 1069, 1220, 1323, and 1405 m.

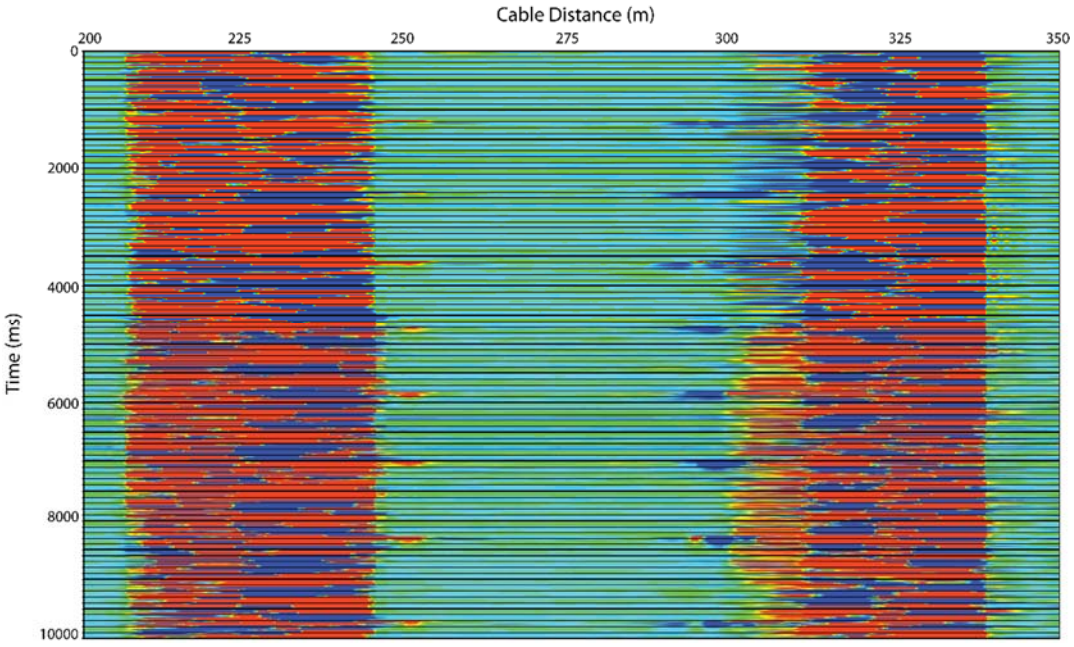


**Figure 60: Tap test at geophone station 20.** A tap was picked at 306 m. This station is at the northwest corner of the surface loop.

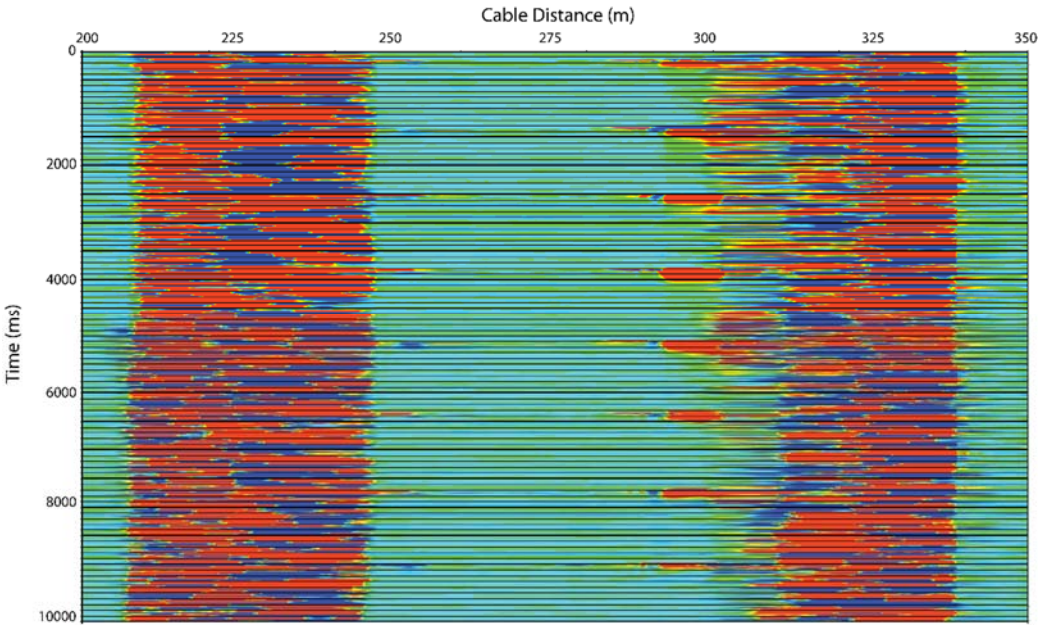


**Figure 61: Tap test at geophone station 21**. A tap was picked at 302 m.

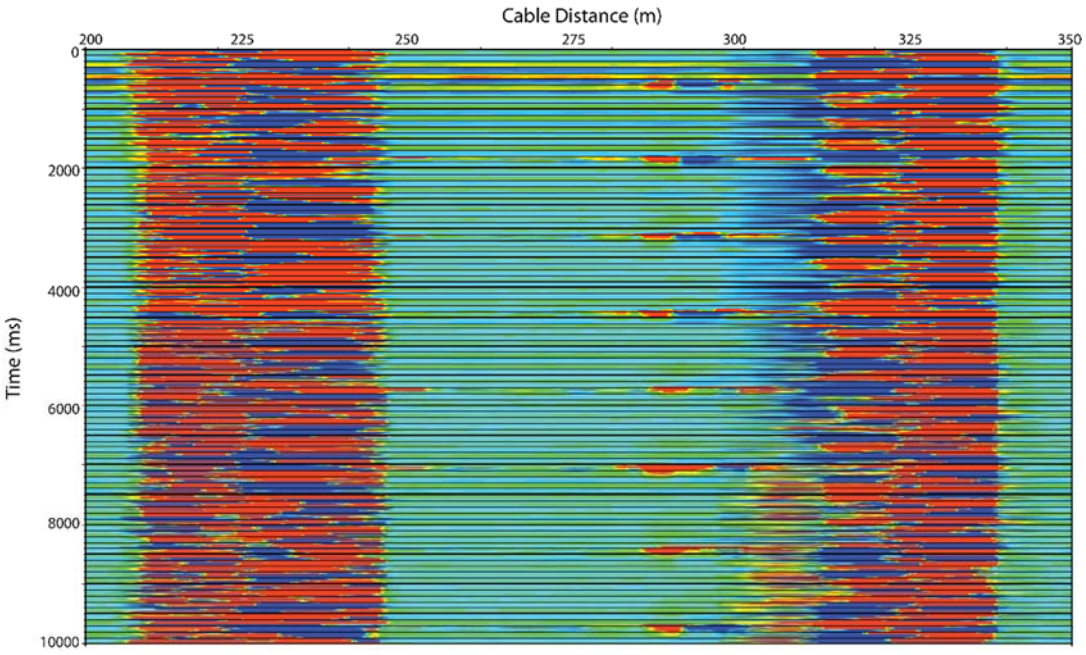


**Figure 62: Tap test at geophone station 22.** A tap was picked at 295 m.

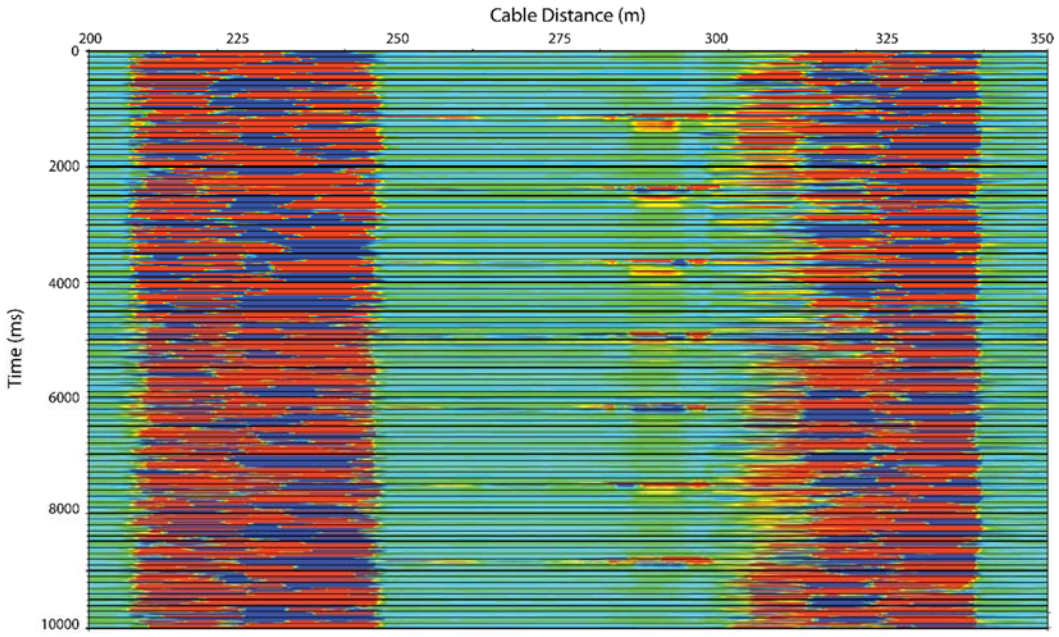


**Figure 63: Tap test at geophone station 23.** A tap was picked at 292 m.

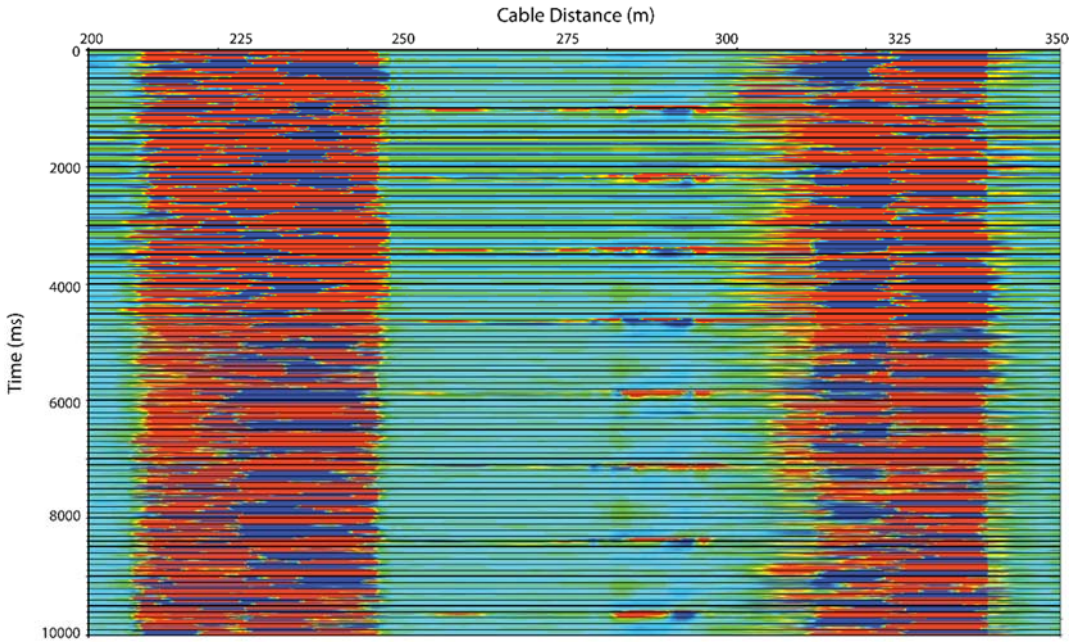


**Figure 64: Tap test at geophone station 24.** A tap was picked at 289 m. This station is at the northeast corner of the surface loop.

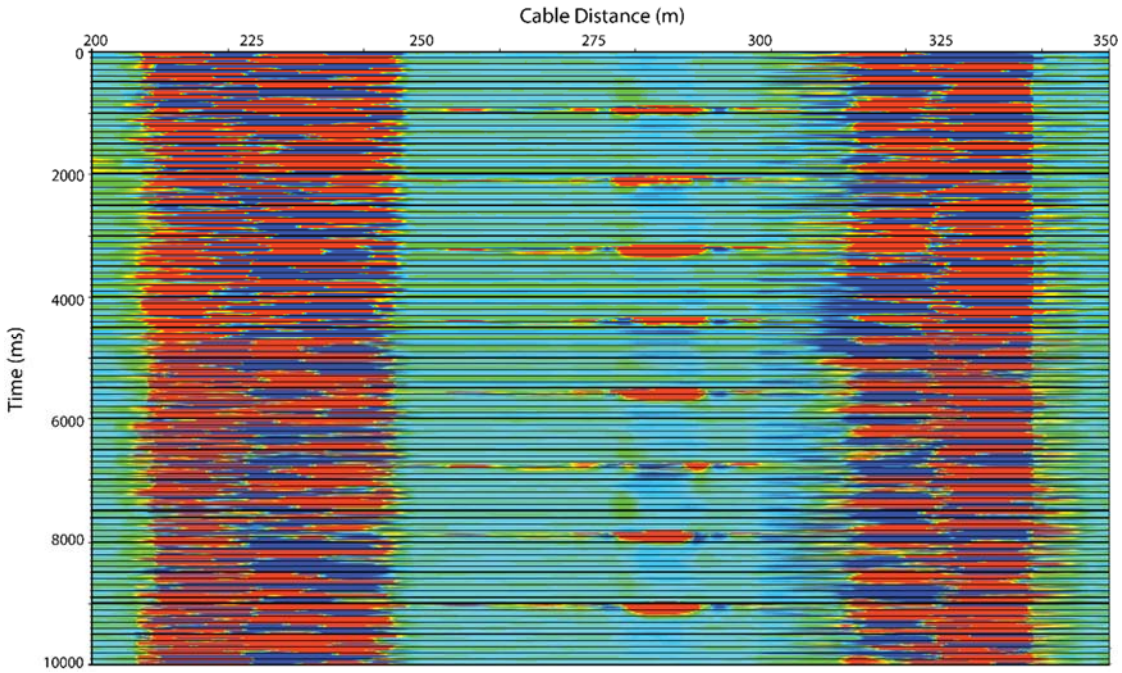


**Figure 65: Tap test at geophone station 25.** A tap was picked at 285 m.

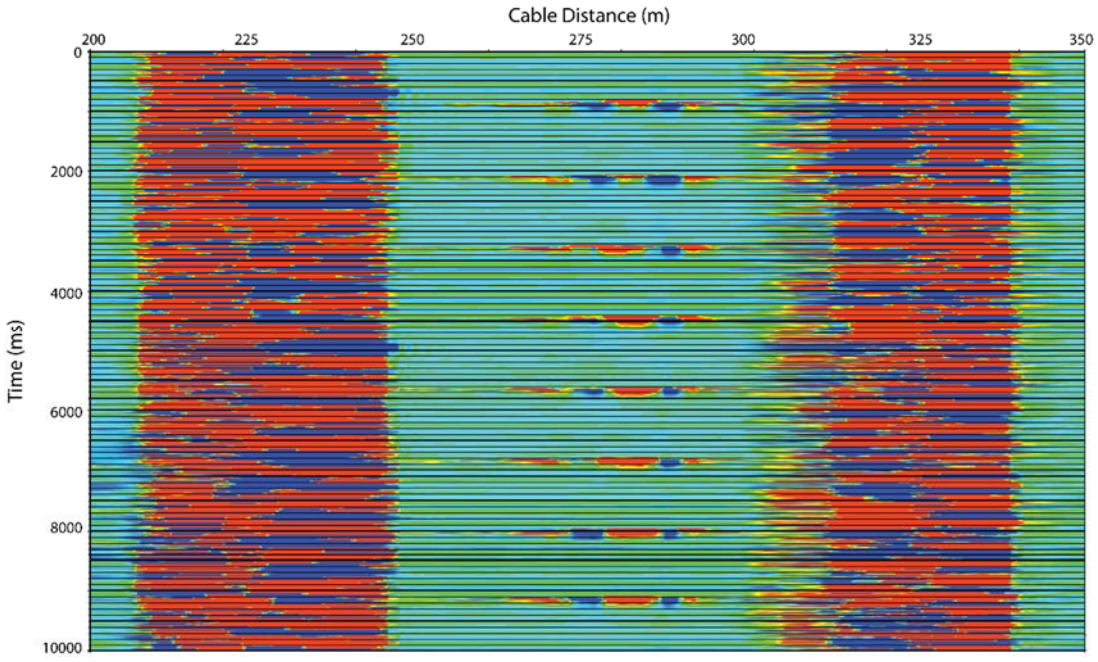


**Figure 66: Tap test at geophone station 26.** A tap was picked at 281 m.

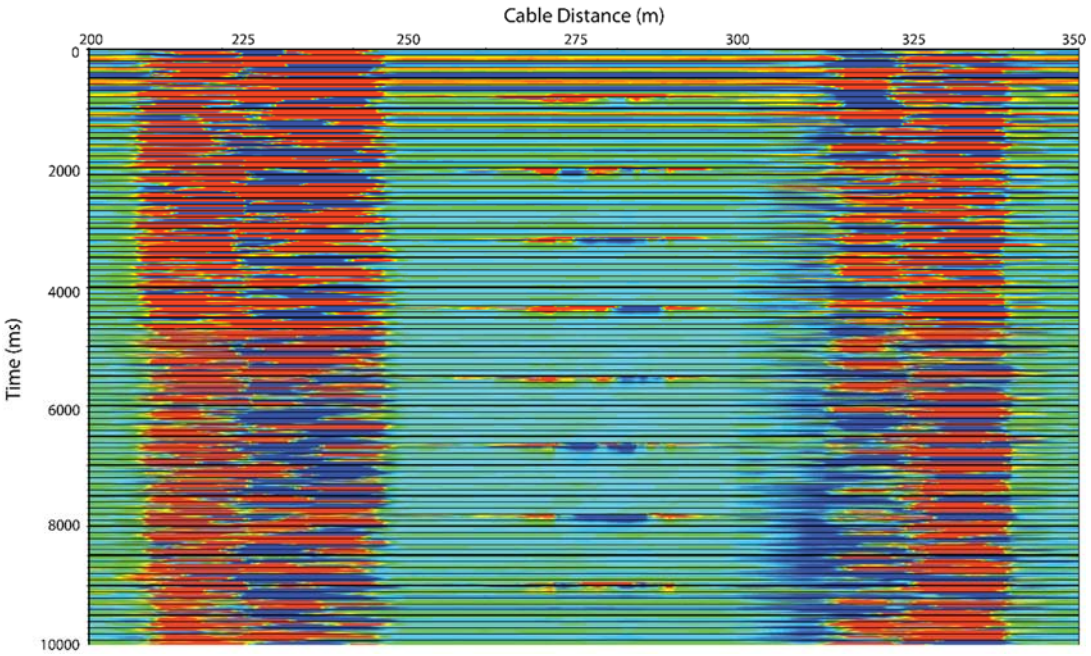


**Figure 67: Tap test at geophone station 27.** A tap was picked at 278 m.

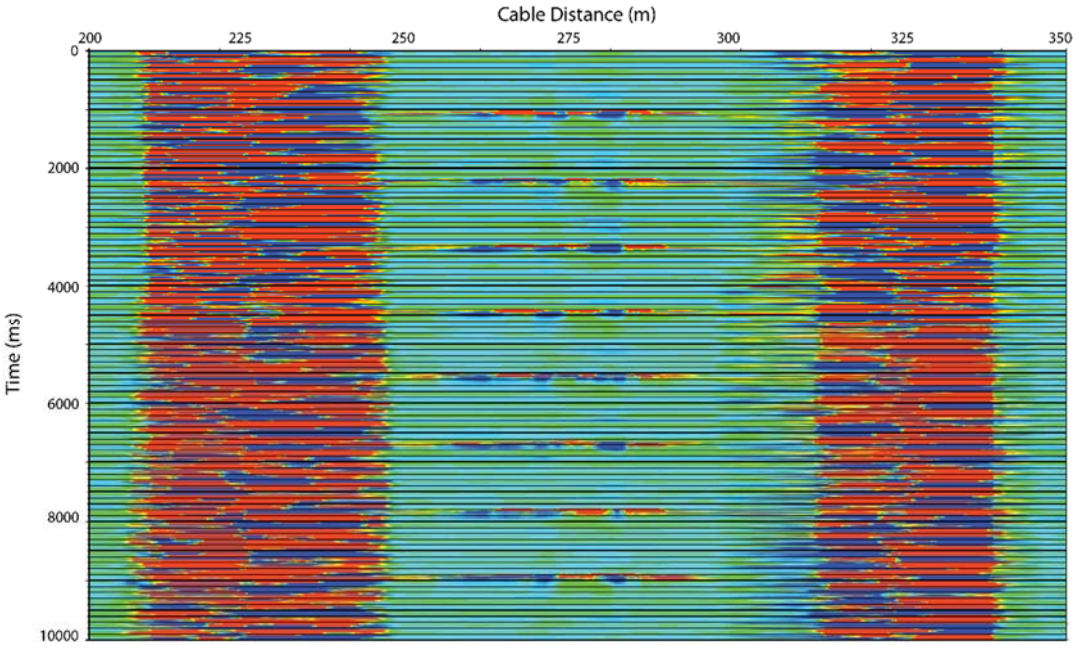


**Figure 68: Tap test at geophone station 28.** A tap was picked at 275 m.

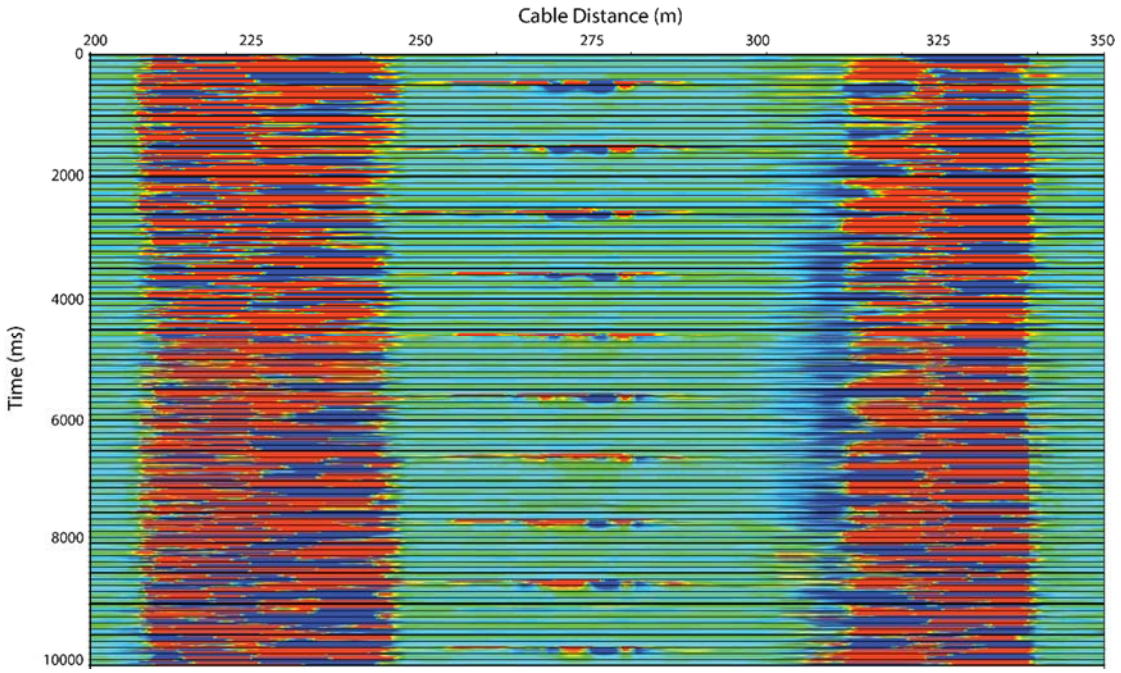


**Figure 69: Tap test at geophone station 29.** A tap was picked at 272 m.

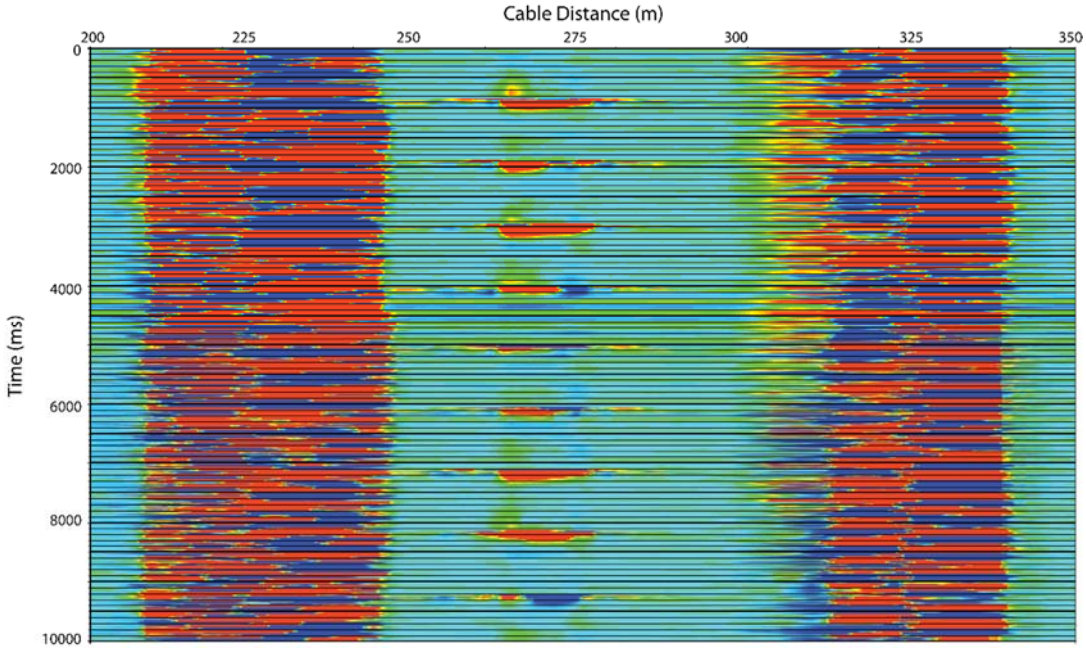


**Figure 70: Tap test at geophone station 30.** A tap was picked at 268 m.

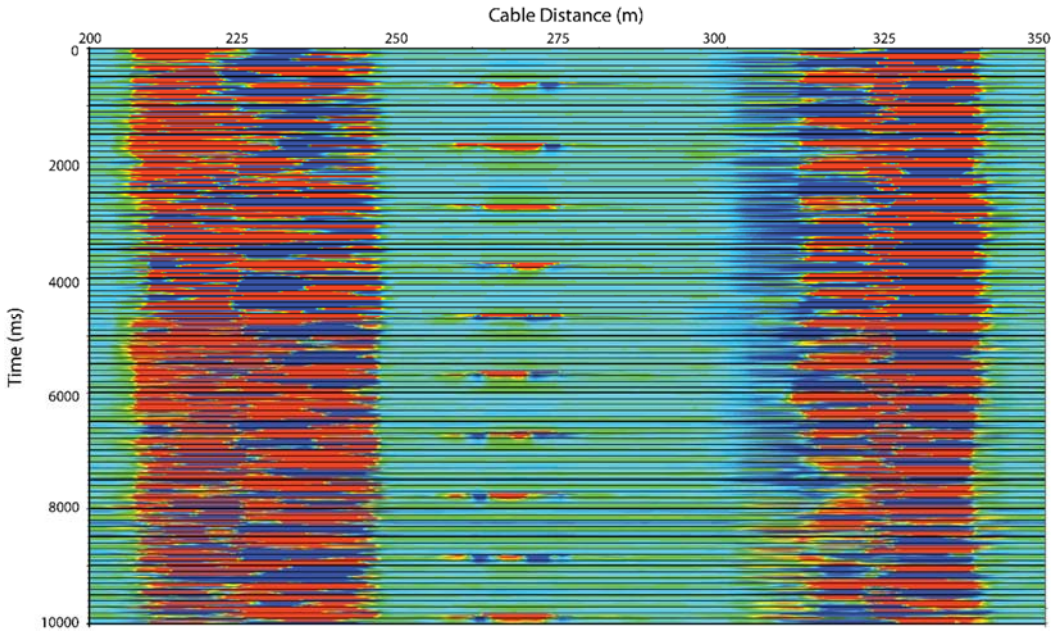


**Figure 71: Tap test at geophone station 31**. A tap was picked at 266 m.

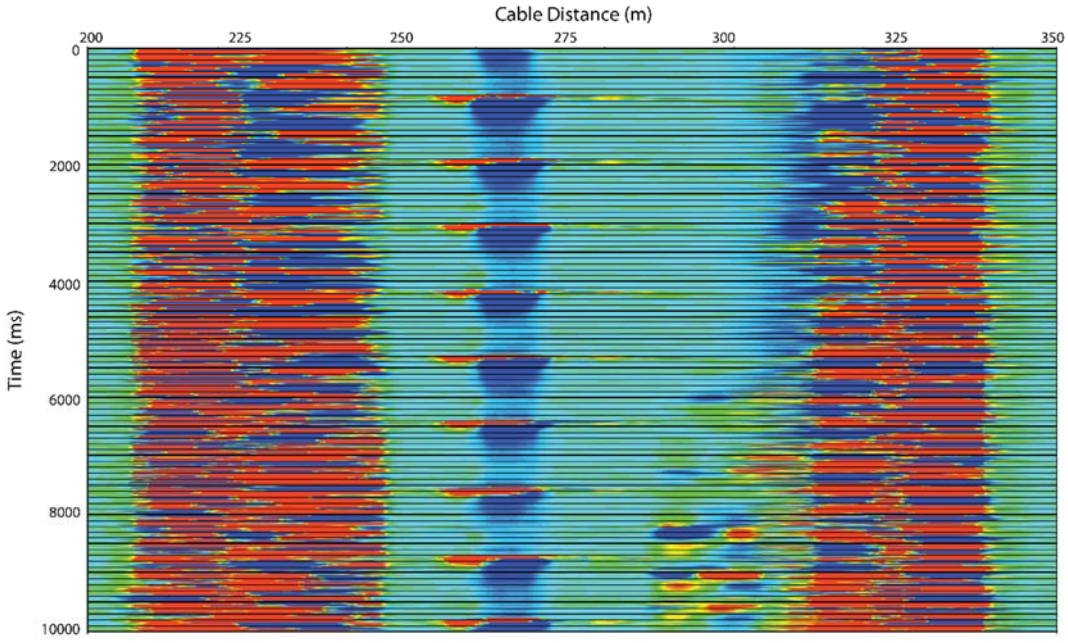


**Figure 72: Tap test at geophone station 32.** A tap was picked at 264 m. This station is at the southeast corner of the surface loop.

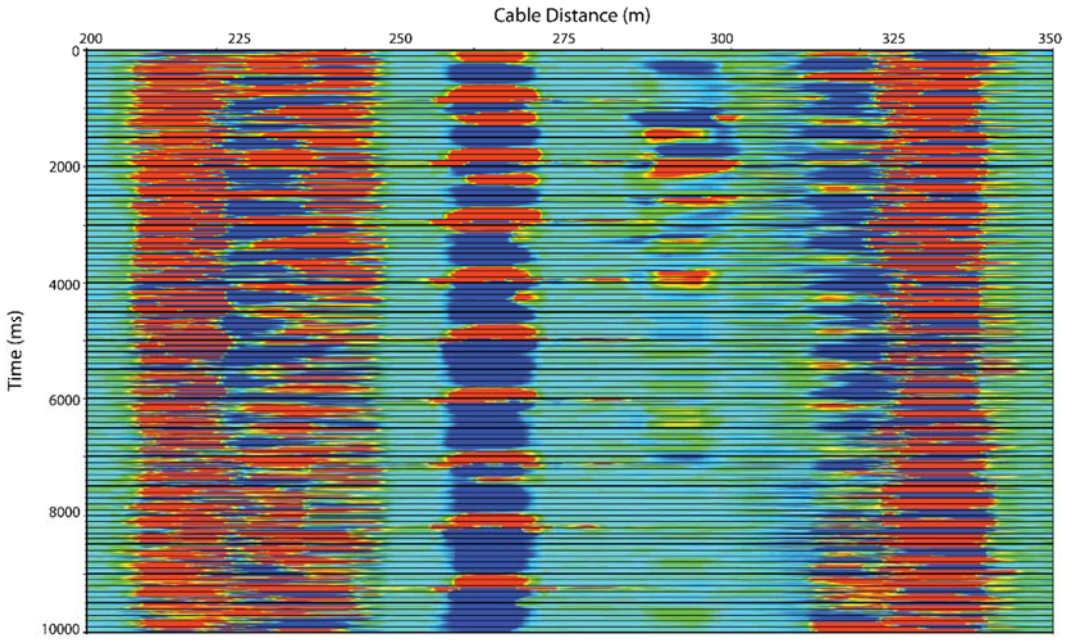


**Figure 73: Tap test at geophone station 33.** A tap was picked at 263 m.

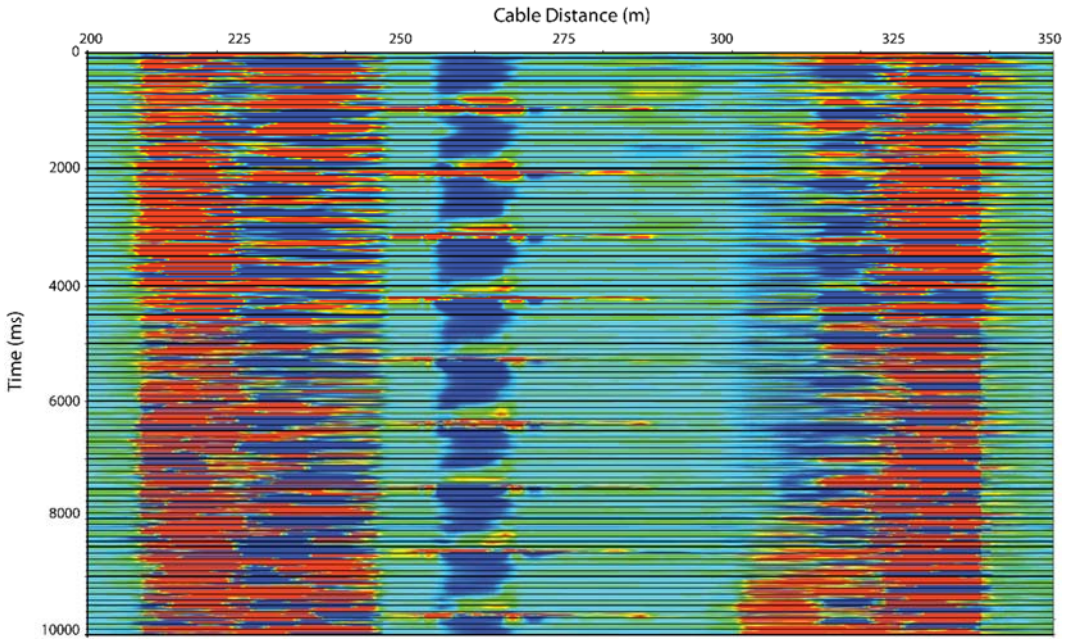


**Figure 74: Tap test at geophone station 34**. A tap was picked at 261 m.

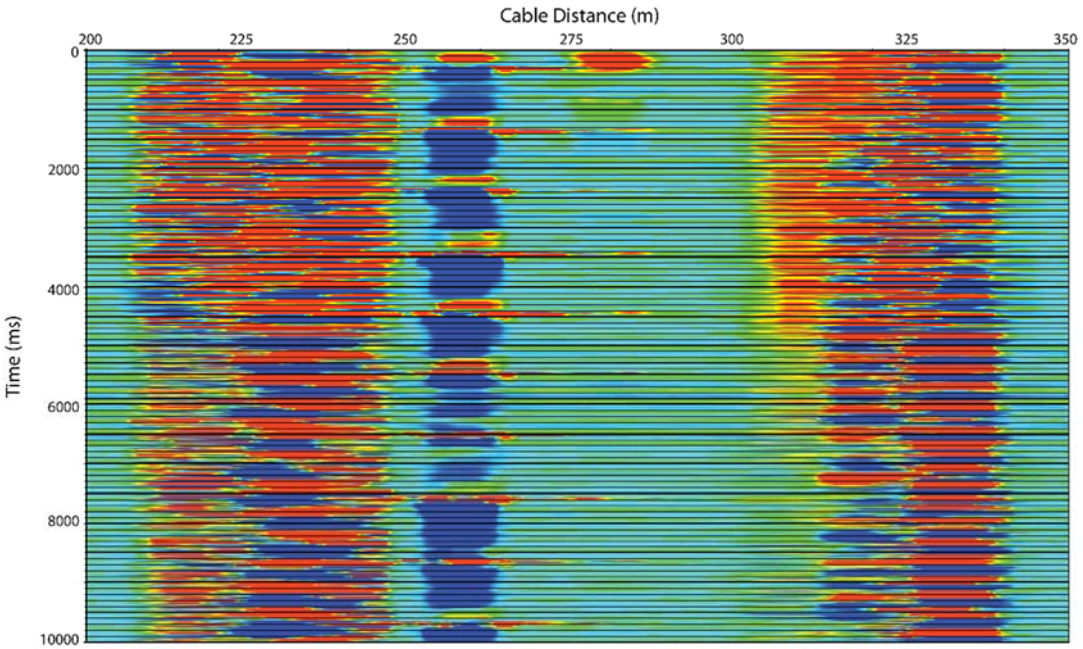


**Figure 75: Tap test at geophone station 35.** A tap was picked at 259 m.

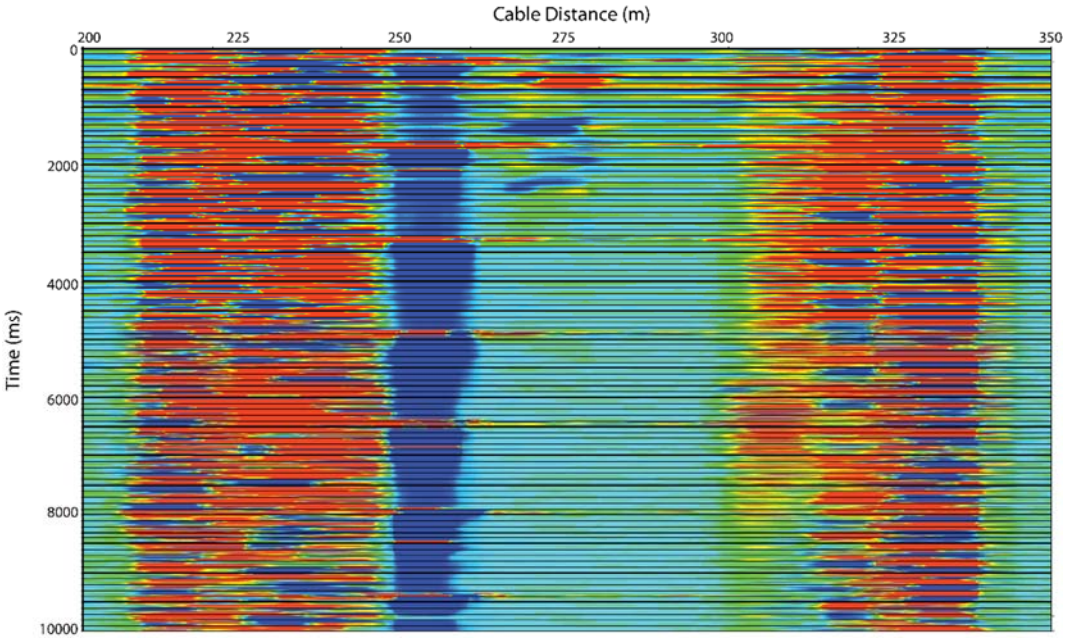


**Figure 76: Tap test at geophone station 36.** A tap was picked at 255 m.

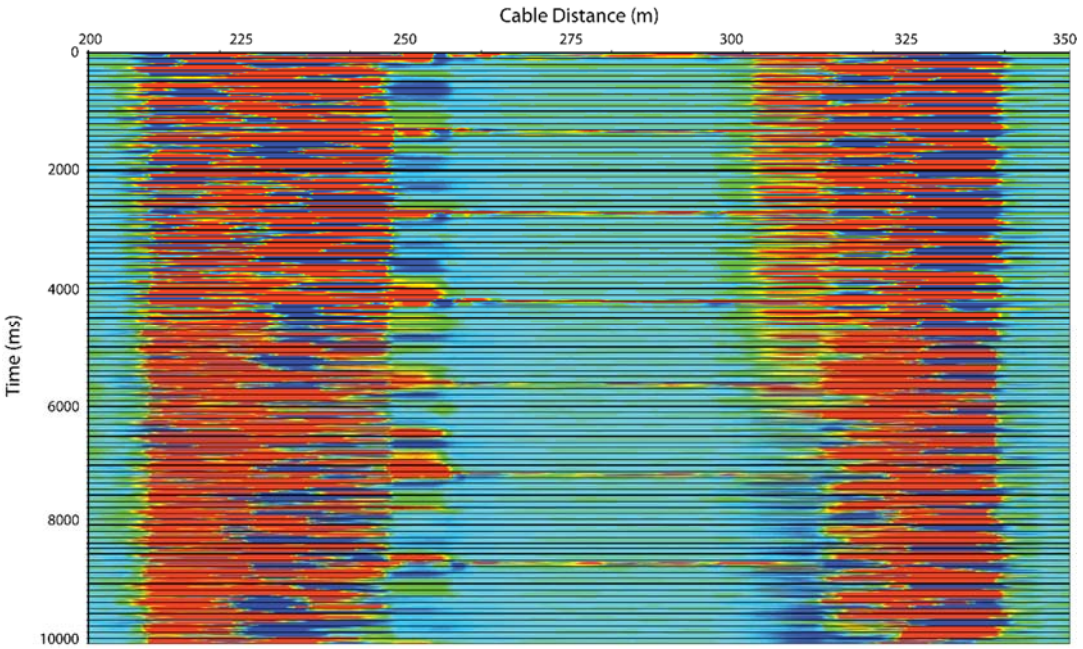


**Figure 77: Tap test at geophone station 37.** A tap was picked at 251 m.

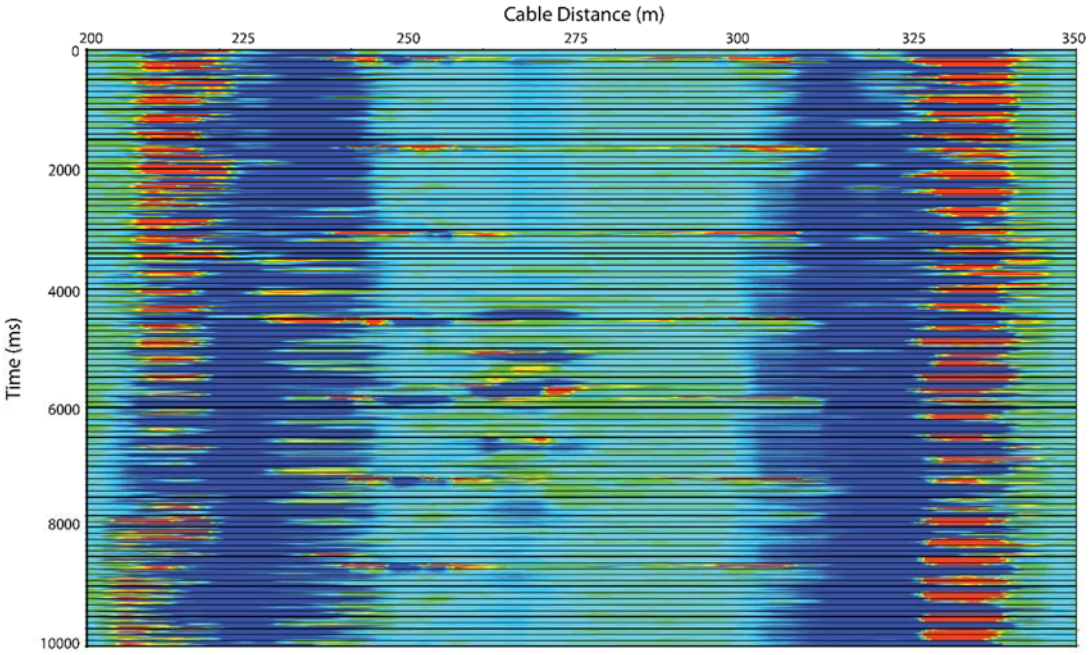


**Figure 78: Tap test at geophone station 38.** A tap was picked at 249 m.

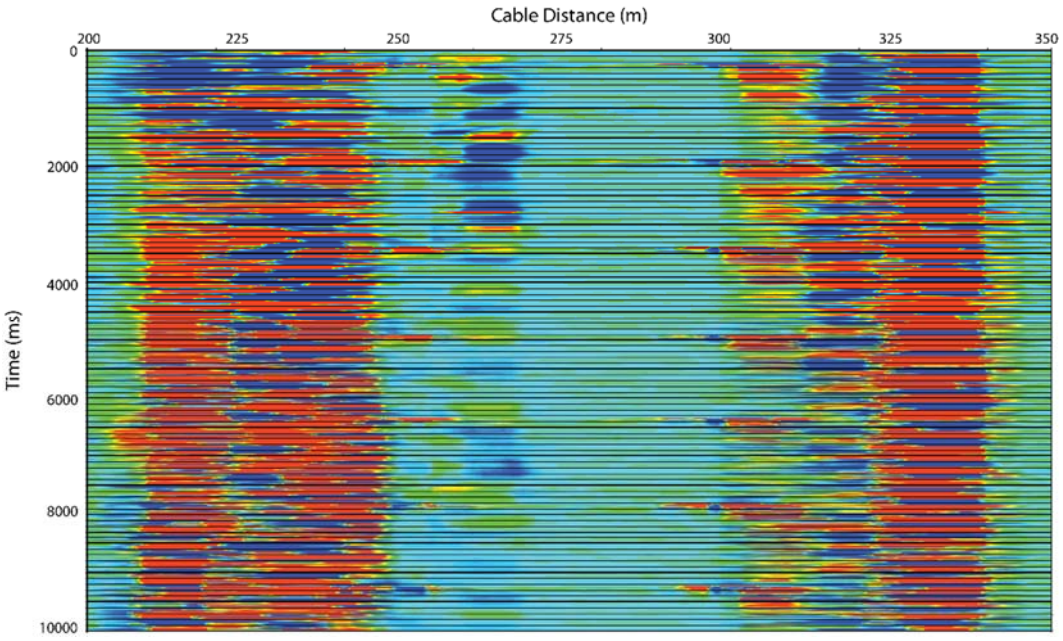


**Figure 79: Tap test at geophone station 39.** A tap was picked at 248 m.

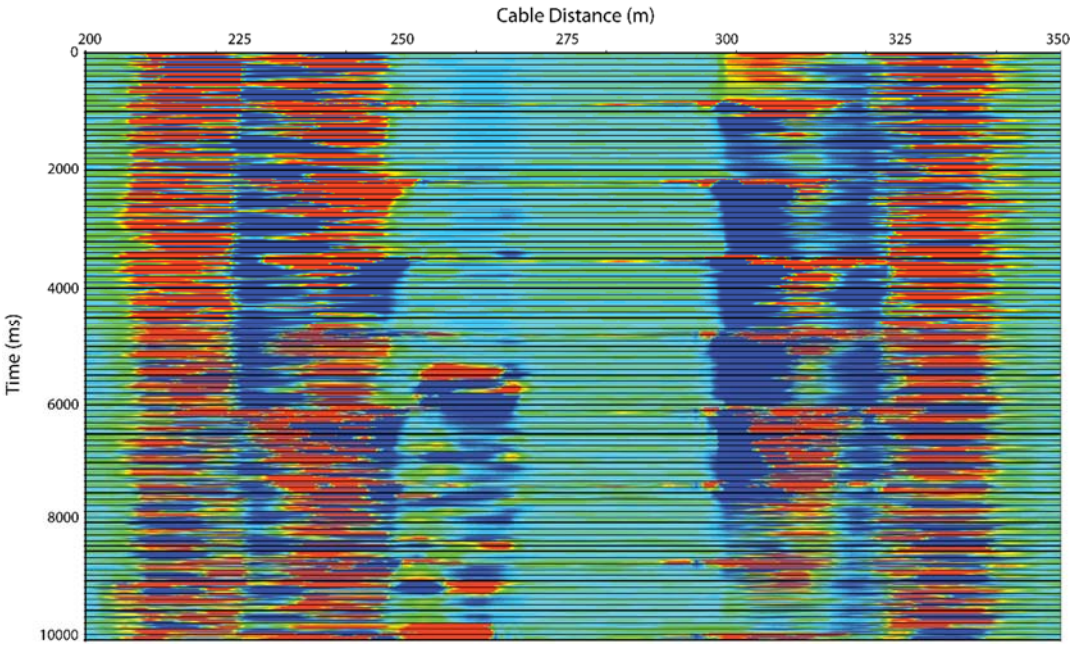


**Figure 80: Tap test at geophone station 40.** A tap was picked at 246 m. This station is at the northwest corner of the surface loop.

## SIGNATURE PAGE

This is to certify that the thesis prepared by Nikolas Nesladek entitled "Comparing Distributed Acoustic Sensing to Three-Component Geophones in an Underground Mine" has been examined and approved for acceptance by the Department of Geophysical Engineering, Montana Tech of The University of Montana, on this 14th day of June, 2017.

Marvin Speece, PhD, Professor and Department Head
Department of Geophysics
Chair, Examination Committee

Mary MacLaughlin, PhD, Professor
Department of Geological Engineering
Member, Examination Committee

Khalid Miah, PhD, Assistant Professor
Department of Geophysical Engineering
Member, Examination Committee

Scott Rosenthal, MS, Assistant Professor and Department Chair
Department of Mining Engineering
Member, Examination Committee